Dosimetry for Small and Nonstandard Fields

by

Stephanie L. Junell

A dissertation submitted in partial fulfillment of

the requirements for the degree of

Doctor of Philosophy

(Medical Physics)

at the

University of Wisconsin-Madison

2013

Date of final oral examination: 5/24/2013

The dissertation is approved by the following members of the Final Oral Committee:

Larry A. DeWerd, Professor (CHS), Medical Physics
Bryan Bednarz, Assistant Professor, Medical Physics
Edward Bender, Assistant Professor, Human Oncology
Michael W. Kissick, Assistant Professor, Medical Physics
T. Rockwell Mackie, Emeritus Professor, Medical Physics
Bhudatt R. Paliwal, Professor, Medical Physics

Abstract

The proposed small and non-standard field dosimetry protocol from the joint International Atomic Energy Agency (IAEA) and American Association of Physicist in Medicine working group[2] introduces new reference field conditions for ionization chamber based reference dosimetry. Absorbed dose beam quality conversion factors (k_Q factors) corresponding to this formalism were determined for three different models of ionization chambers: a Farmer-type ionization chamber, a thimble ionization chamber, and a small volume ionization chamber. Beam quality correction factor measurements were made in a specially developed cylindrical polymethyl methacrylate (PMMA) phantom and a water phantom using thermoluminescent dosimeters (TLDs) and alanine dosimeters to determine dose to water. The TLD system for absorbed dose to water determination in high energy photon and electron beams was fully characterized as part of this dissertation. The behavior of the beam quality correction factor was observed as it transfers the calibration coefficient from the University of Wisconsin Accredited Dosimetry Calibration Laboratory (UWADCL) ^{60}Co reference beam to the small field calibration conditions of the small field formalism.

TLD-determined beam quality correction factors for the calibration conditions investigated ranged from 0.97 to 1.30 and had associated standard deviations from 1% to 3%. The alanine-determined beam quality correction factors ranged from 0.996 to 1.293. Volume averaging effects were observed with the Farmer-type ionization chamber in the small static field conditions. The proposed small and non-

standard field dosimetry protocols new composite-field reference condition demonstrated its potential to reduce or remove ionization chamber volume dependancies, but the measured beam quality correction factors were not equal to the standard CoP's k_Q, indicating a change in beam quality in the small and non-standard field dosimetry protocols new composite-field reference condition relative to the standard broad beam reference conditions. The TLD- and alanine-determined beam quality correction factors in the composite-field reference conditions were approximately 3% greater and differed by more than one standard deviation from the published TG-51 k_Q values for all three chambers .

The characterization of multiple calibration conditions provides an improved understanding of how the ^{60}Co ionization chamber absorbed dose to water calibration coefficient from an ADCL can optimally be applied to small and nonstandard field calibrations to reduce the associated dose uncertainty. The developed methodology will contribute to future research of other small field radiotherapy modalities and measurements of even smaller field sizes. The resulting database provides support for future recommendations on the implementation of small and non-standard field calibration protocols.

Acknowledgments

I would like to take this opportunity to express my immense gratitude to all the people who have given their invaluable support and assistance. In particular, I would like to thank my advisor Dr. Larry DeWerd whose generosity, patience and guidance created an ideal atmosphere for performing research. I am grateful to all the staff and students in the calibration lab, especially John Micka, whose expertise and feedback made this work possible. I would like to thank my thesis committee Dr. Paul DeLuca, Dr. Rock Mackie, Dr. Michael Kissick, Dr. Ed Bender, Dr. Paliwal, Dr. Bednarz, and Dr. Doug Henderson for their guidance. I would especially like to thank Dr. Rock Mackie who proposed the topic of this thesis and provided me with collaborations that made this work possible. Many thanks to my collaborators who helped at various stages of this work including Dr. Hugo Palmans and Peter Sharpe at the National Physical Laboratory, Brian Hooten at Standard Imaging Inc., Dr. Desrosiers at the National Institute of Standards and Technology, and Dr. Saiful Huq at the University Pittsburg Medical Center. I would also like to thank the UW Radiation Calibration Lab customers for their ongoing support of student research. And finally, but not least, many thanks to my parents and Dr. Benjamin Burwitz who have been an important and indispensable source of support and sanity.

Content

List of Figures

List of Tables

Chapter 1

Introduction

1.1 Overview

Radiation therapy is an effective and integral component of curative and palliative cancer therapy for primary and metastatic cancers. The primary objective of radiation therapy is the sparing of healthy tissue and critical organs from damaging doses, while locally depositing the amount of radiation energy necessary to treat the cancerous tissue. Technological advances have helped meet this objective through delivery optimization and dose conformality. The precise nature of advanced radiation therapy requires stringent verification for the technology to be fully utilized.

Governing and professional organizations are responsible for maintaining a level of quality and reproducibility in clinical radiation therapy treatments through the establishment of measurement standards and codes of practice (CoP) outlining verification procedures that are traceable to a standard reference value. Standard CoP valid for simpler treatment modalities are not independently sufficient for the verification of advanced conformal radiation therapy.

The quantum conditions created in advanced conformal radiation therapy do not adhere to the conditions required for the appropriate use of standard CoP.

Standard dosimetry CoP describe a set of measurement implementation parameters which influence physical quantities for which the standard CoP defined detector correction factors are valid, these measurement parameters are known as the reference conditions. These reference conditions are characterized by a broad field, usually $10\,\mathrm{x}\,10\,\mathrm{cm}^2$, where the physics and subsequent measurement are simplified to reduce dose uncertainty. Radiation fields created by advanced conformal radiation therapy are not represented by standard CoP reference conditions and are referred to as small and nonstandard fields.

The point dose found using standard CoP detector corrections are valid only at the point specified by the reference conditions. To obtain dose at points or field sizes outside the reference conditions, the standard CoP determined reference point dose must be extrapolated. The extrapolation method generally uses measurements of ionization chamber output ratios to transfer the standard CoP measured dose. The limitations of these extrapolation methods will be discussed in Section 2.5 and are the fundamental quandary in this investigation. This work aims to quantify the limitations based on the traceability of the standard absorbed dose to water detector calibration coefficient from the standards laboratory to small and nonstandard fields used in advanced conformal radiation therapy. This approach enables a complete dosimetric profile of the physical relations relevant to ionization chamber based dosimetry for absorbed dose determination without intermediate steps.

1.2 Description of upcoming chapters

Chapter 2 describes the influence of technological advancements in external radiation therapy on the need for improved dosimetric verification. The current CoP for broad beam reference dosimetry are elaborated on in detail and their ionization chamber

correction factors are derived from first principles. The proposed protocol for small and nonstandard field reference dosimetry is then introduced as a possible solution for current dosimetric shortcomings. An overview is given for the dosimeter systems used in this work.

Chapter 3 describes the characterization of the TLD system used in this work for absorbed dose to water measurements. The system is characterized in detail with studies relating to the relevant TLD correction factors. The results of the energy correction factor experiments are compared against literature and available TLD service values.

Chapter 4 outlines the dosimetric issues facing small field and nonstandard field dosimetry compared to broad field reference dosimetry. The nomenclature for the measurements performed in this work are explained. Measurement methods and results are given to document the transfer of ionization calibration coefficients for the absorbed dose to water from the standard laboratories measurement conditions to the small and nonstandard field reference conditions with associated uncertainty explained. A solid phantom with which the proposed formalism can be performed is designed. Experimental determination of ionization correction factor values for various ionization chambers are found using TLD and alanine for static and composite fields in water and solid phantoms.

Chapter 5 focuses on the Monte Carlo component of small field dosimetry. A model of a 6 MV photon linear particle accelerator (linac) and a ^{60}Co teletherapy unit are created using the BEAMnrc user code and phase space files are created for various field sizes. Ionization chamber models are created using EGS_chamber for the Exradin A1SL, Exradin A16, Exradin A19 and PTW PinPoint 3100. Benchmark of the BEAMnrc-generated linac and ^{60}Co teletherapy spectra and egs_chamber

ionization chamber models by comparing simulated and measured beam quality data (e.g. percentage depth dose, profiles, overall chamber response) is discussed. The design and implementation of a Monte Carlo data base at the UWMRRC is explained. The chapter is concluded with future applications of the models and a database for small and nonstandard beams.

Chapter 2

Background and Theory

2.1 Advancements in external beam radiation therapy

Radiation has been used in the medical setting for approximately 100 years and many technological advancements have improved the degree to which the high-dose region is able to conform to the to the target volume (dose conformity).[35] Improved dose conformity has been achieved through multiple major advancements including the development of treatment planning, imaging, and delivery technologies. Improved dose conformity creates the opportunity for margin reduction and greater normal tissue sparing. However, dose conformity is achieved through the use of small and nonstandard fields which represent a dosimetric challenge. The dosimetry of these fields must be addressed before patients can fully utilize the benefits of current precision treatment methods. This section will discuss treatment methods that are impacted by the dosimetric issues addressed in this work.

Intensity modulated radiation therapy (IMRT) is currently the most common radiation therapy treatment technique in the United States. IMRT delivers precise radiation doses to the target volume by modulating the intensity of the radiation in multiple small beams (beamlets). In conjunction with advanced imaging and

positioning techniques, IMRT is able to target tissues with millimeter precision. Traditional IMRT treatments are performed using linear accelerators equipped with a multileaf collimator (MLC). Treatments are generally performed using modulated photon beams delivered at discrete gantry angles with the MLCs defining multiple discrete beamlets or dynamic MLC leaf positions to define multiple beamlets. The precise delivery of IMRT allow for the possibility of planned tumor volume (PTV) margin reduction in treatment plans. This precise dose conformality has the potential to improve the therapeutic ratio and reduce normal toxicity leading to improved cancer outcomes using dose-escalation and/or altered fractionation schemes. There are many types of specialized IMRT techniques that expand on traditional IMRT practices. These specialized techniques can be used alone or in combination to increase the delivery precision and accuracy required for a given treatments histology.[21]

Image guided radiation therapy (IGRT) is a broad term used to describe any imaging used to directly guide the treatment delivery accuracy and/or other inputs. IGRT uses imaging modalities to visualize the treatment site and other biological factors to optimize the IMRT delivery based on improved positioning, inter and intra-fractional motion management, dose verification, and the biological radiosensitivity of the histologies. The most common IGRT techniques are integrated on-board cone beam (CBCT) or Megavoltage Computed Tomography (MVCT) to account for inter- and intra-fractional motion due to reductions in the size of the tumor and changes in the local anatomy. Another example of IGRT is dose painting in which functional images such as PET scan and genetic-molecular imaging are fused with existing anatomical imaging such as MRI and CT scan allowing treatment plans to account for cellular expression and radio-sensitivities/reactivities.[13]

Stereotactic radiosurgery (SRS), stereotactic radiotherapy (SRT), and stereotactic body radiation therapy (SBRT) are high-precision forms of IMRT with margins

on the order of millimeters for SRS/SRT/SBRT compared to traditional IMRT with margins typically on the order of centimeters.[94] SRS and SRT were originally designed for the high-dose treatment of small cranial lesions using a single fraction SRS or low number of fractions. These treatments were designed based on biologically optimized hypo-fractionated dose schedules (Section 2.1.1). Dose-escalation is enabled in SRS/SRT through the integration of precise immobilization techniques, often involving a full face mask and/or implanted localization screws in the patients skull. SBRT expands SRT's hypo-fractionated dose scheme to larger tumor volumes in multiple treatment sites in the body using 3 to 5 fractions instead of the 30 to 40 fractions over 5-8 weeks used in conventional radiotherapy.[94] Multiple manufacturers make machines capable of SRS/SRT and SBRT. The addition of micro-multileaf collimators enable conventional linear accelerators to perform SRS and SBRT; examples include Axesse™ from Elekta and Novalis TX™ from Varian. CyberKnife is an image-guided robotic linac system that delivers automated high-precision doses in 1 to 3 sessions. Gamma Knife® is a dedicated SRS unit for the treatment of small to medium size intracranial lesions using 192 or 201 beams of highly collimated and focused ^{60}Co sources.

Rotational IMRT treats dynamically with up to 360 degrees of rotation around the patient. Rotational IMRT is subdivided into two subcategories: Helical IMRT and Intensity Modulated arc therapy (IMAT). TomoTherapy (Accuray, Inc.) defined Helical IMRT in which radiation is administered in a helical fashion designed around a CT scanner. TomoTherapy employs tens of thousands of tiny beamlets focused on the target from all angles. In addition to using small fields, the flattening filter is removed from tomotherapy units creating a gaussian distributed beam profile. TomoTherapy's integrated CT imaging provides high-precision IGRT capabilities. IMAT is the linac-based response to helical tomotherapy, where conventional linear

accelerators with MLCs or microMLCs treat using dynamic tiny beamlets created through the continuous and simultaneous manipulation of the gantry position and speed, MLC leaves, dose rate and collimator angle. Existing IMAT Systems include RapidArc® by Varian and VMAT by Elekta which both use on-board CBCT and or MVCBCT for IGRT capabilities.

The precise delivery of IMRT and its specialization allows for the possibility of planned tumor volume (PTV) margin reduction in treatment plans. This precise dose conformality has the potential to improve the therapeutic ratio and reduce normal toxicity leading to improved cancer outcomes using dose-escalation and/or altered fractionation schemes. The potential for reduced PTV margins and higher dose per fraction schemes necessitates lower tolerances, strict quality control and accurate dose verification. This precise dosimetric requisite of the small beamlets used in IMRT modalities is the focus of this work and is explored in detail in the following sections and chapters.

2.1.1 Biological optimization

The biological optimization method know as hypo-fractionation has led to an increased need for precise dosimetry and quality assurance (QA) due to the potential for increased consequences in dose and delivery errors associated with the use of high doses in very small fields with lower margins.[13] Treatment fractionation is a biologically-based treatment optimization method that allows for a restorative period between temporally spaced fractions, during which healthy tissue is allowed to repair a quotient of the damage induced by transversing radiation; damaged cancerous tissue lacks control points to stop proliferation resulting in inevitable cell death due to DNA damage. Treatment fractionation allows for increased dose delivery to the intended

treatment tissues by allowing dose-limiting healthy and sensitive tissues to repair between fractions. However, aggressive cancers can use the time period between fractions to repopulate from surviving cancerous-cell populations. Advanced delivery techniques which allow for greater dose conformity in the target volume have enabled larger doses to be delivered to the treatment volume per fraction while maintaining an acceptable therapeutic ratio. The ability to increase the dose per fraction allows for an accelerated treatment time schedule in a technique known as hypo-fractionation. Stereotactic radiosurgery (SRS) and stereotactic body radiation therapy (SBRT) techniques using hypo-fractionation schedules have been shown to improve outcomes in localized carcinomas and reduced acute and late organ at risk (OAR) toxicity. Hypo-fractionated radiotherapy is believed to improve patient outcome by reducing the impact of tumor cell repopulation.

2.2 Quality assurance in external beam radiation therapy

QA is a crucial function in all radiation treatment facilities. Many external and internal factors contribute to a clinic's overall treatment quality and an overarching standardized QA program positively impacts the quality of treatment administered to all patients. Western countries have more than 30-years history of QA activities. The development and establishment of a good QA program is a major challenge and primary responsibility of a radiation therapy facility. A QA program must demonstrate that the theoretical dose distributions calculated by the TPS are accurate and represent the treatments de facto physical behavior. This objective is achieved through reference calibrations with a detector traceable to a primary national or international standard.

Metrological traceability is a fundamental concept in radiation metrology. Metrological traceability refers to a measurement that is a product of a national or international standard measurement or value through an unbroken chain of comparisons, all having stated uncertainties.[43] The level of traceability establishes the level of comparability of the measurement. These primary standards are coordinated by national metrological institutes such as the National Institute of Standards and Technology (NIST) in the United States, National Physical Laboratory (NPL) in the UK, National Research Council (NRC) in Canada, and Physikalisch-Technische Bundesanstalt (PTB) in Germany. All national standards are compared individually to the international reference value held at the Bureau International des Poids et Mesures (BIPM) standard.[91] Traceability, accuracy, precision, systematic bias, evaluation of measurement uncertainty analysis are critical parts of a QA program and must be accounted for in all standard and future CoP for reference dosimetry.

Metrological traceability is obtained for absorbed dose to water dosimeters through a calibration that references the dosimeter to a primary standard measurement using calorimetric methods. The development and maintenance of standards of absorbed dose to water are the responsibility of Primary Standard Dosimetry Laboratories (PSDLs).[6,61] To meet the demand for calibrations, secondary standard dosimetry laboratories transfer the calibration factors from a PSDL to hospital users. In North America, the secondary standard dosimetry laboratories are accredited by the American Association of Physicists in Medicine (AAPM) and known as accredited dosimetry calibration laboratories (ADCL's). All absorbed dose to water calibration coefficient and relevant reference exposures for this work are obtained from the University of Wisconsin ADCL using standard ^{60}Co irradiations with NIST-traceable reference ionization chambers. A goal of this work is to provide directly traceable results that include substantive associated uncertainties.

2.3 Standard codes of practice for high energy broad beam photon and electron beam reference dosimetry

2.3.1 AAPM's Task Group-21 (TG-21)

Despite being clinically superseded, the AAPM's Task Group 21 (TG-21)[1] for the reference dosimetry of high energy photon and electron beams provides an understanding of current CoP beam quality specification and an appropriate foundation for resolving the issues facing small and nonstandard field dosimetry. The equations and derivations from TG-21 will be used as a tool to outline the underlying dosimetric concepts and issues in small and nonstandard field dosimetry.

The TG-21 was published in 1983 and was the standard CoP in the United States until it was succeeded in 1999 by the current CoP, AAPM's Task Group-51 report (TG-51).[3] TG-21 and TG-51 are ionization chamber based dosimetry protocols for the determination of absorbed dose to water at the point of the ionization chamber's effective point of measurement. The theoretical basis for TG-21 calculations of absorbed dose to water are transparent and explicitly based on cavity theory and other ab initio radiation physics approaches. Current CoP simplify the calculations of absorbed dose to water by introducing the concept of beam quality specification where measurements in well defined reference conditions determine a beam quality correction factor to account for various correction factors. The physical concepts behind the beam quality correction factor are not explicitly defined in the current CoP content.

TG-21 uses calibration coefficients based on exposure in $[^{R}/_{C}]$, $N_{X}^{Co^{60}}$, and dose to the gas in the collecting volume of the ionization chamber in $[^{Gy}/_{C}]$, $N_{gas}^{Co^{60}}$ (dose-to-gas), instead of absorbed dose to water calibration coefficients used in current CoP.

TG-21 calculates absorbed dose to water using exposure and dose-to-gas calibration coefficients through the use of cavity theory based conversions. The basic cavity theory equation is given by the Bragg-Gray relation:

$$\mathrm{D_{wall}} = \frac{\overline{W}}{e}\left(\frac{\overline{L}}{\rho}\right)_{gas}^{wall}\left(\frac{Q}{m}\right) \tag{2.1}$$

where $\frac{\overline{W}}{e}$ is the energy associated with the creation of an ion pair in air and is is used to convert the charge per unit mass of gas, $\left(\frac{Q}{m}\right)$, to energy per unit mass in [Gy] (dose-to-gas). The Spencer–Attix stopping-power ratios between water and air, $\left(\frac{\overline{L}}{\rho}\right)_{gas}^{wall}$ then converts dose-to-gas to dose in the wall at a point located at the ionization chambers effective point of measurement (dose-to-wall). Equation (2.1) assumes that the following conditions are met: 1) the detector is in a state of charged particle equilibrium (CPE) in the equilibrium spectra , $\Phi_T^{e,\delta}$, (Section 2.5.1) 2) Bremstrauhlung production is absent. If the conditions are not met, cavity theory can still be applied but the incident charged particle spectrum must be known $\Phi_T^{e,\delta}$ and $\left(\frac{S}{\rho}\right)_a^t$ evaluated over the spectrum energies. All realistic applications of cavity theory based dosimeters perturb the equilibrium spectra to some extent. These perturbations are characterized and the appropriate correction factors are applied to the dosimeter reading to account for the spectral variations in Φ_T^{δ} compared to the CPE spectrum $\Phi_T^{e,\delta}$.

TG-21 provides cavity theory based equations and approximate correction factor calculations to convert the ionization chamber response in the user's beam quality Q to absorbed dose to water, D_w^Q, from exposure and dose-to-gas based calibration coefficients determined in the standards lab ^{60}Co reference beam.[9,23] The entire ionization calibration transfer from the the standards lab to the user's beam quality and how conversions are accomplished, i.e. exposure reading $\rightarrow$ absorbed dose in the chambers gas volume $\rightarrow$ absorbed dose to water at the effective measurement

point is outlined in TG-21. This transfer chain is shown in derivation 2.1, 2.2, and 2.3 adapted from the TG-21 protocol.[1]

The exposure X[R] for the standard ^{60}Co beam quality is shown in derivation 2.1 and the variables and coefficients for the derivation are given as follows: the specific charge in the gas (air) of the standard ionization chamber J_{gas} in (C/kg), the Spencer-Attix mass collisional stopping power ratio or mean restricted collision mass stopping power ratio $\frac{\overline{L}}{\rho}$, the mean mass energy-absorption coefficient $\frac{\mu_{en}}{\rho}$, the charge-exposure constant for air k, the buildup in the wall β_{wall}, and the sum of TG-21 defined "minor" corrections $\prod_i K_i$. The standard ionization chamber J_{gas} is found in the standard ^{60}Co beam quality by taking the raw charge reading from the electrometer over the ionization chamber volume (equation (2.2)).

$$J_{\text{gas}} = M_{\text{raw}}/V \tag{2.2}$$

Note that the detection system, an electrometer in this case, must be calibrated for any non-linearity in its response (P_{elec}). k has a value of 2.58x10^{-4} $\left[\frac{\text{C}}{kg\,R}\right]$. $\prod_i K_i$ represents additional factors including corrections for humidity, ion recombination efficiency, and stem scatter. The users ionization chambers are calibrated against A NIST-traceable ionization chamber in the standard ^{60}Co beam quality to obtain an exposure calibration coefficient, $N_{\text{X}}^{\text{Co}^{60}}[R/\text{C}]$, uncorrected for ion recombination (P_{ion}). The users ionization chamber exposure calibration coefficient $N_{\text{X}}^{\text{Co}^{60}}$ can then be used to measure exposure in the users beam quality (Q).

$N_{\text{gas}}^{\text{Co}^{60}}$ is the ionization chamber cavity-gas calibration coefficient in [Gy/C]. Dose-to-gas D_{gas} can be calculated in the standard ^{60}Co beam quality as a function of air kerma for the detector volume and can be derived directly from the measurement of J_{gas} [C/kg] multiplied by $\frac{\overline{W}}{e}[eV/\text{i.p.}]$. However, the air kerma calculation is chamber

Derivation 2.1 Exposure (X) based calibration: from the ADCL standard ^{60}Co to the user's beam quality

		standard beam quality(^{60}Co)
$X_{^{60}\mathrm{Co}}$ [R]		$X_{^{60}\mathrm{Co}} =$ $^{1}/_{k}\left[\frac{\mathrm{C}}{kg\,R}\right] J_{\mathrm{gas}}^{^{60}\mathrm{Co}}\,[^{C}/_{kg}]\,\frac{\overline{L}}{\rho}\left[\frac{\mathrm{MeV\,cm^2}}{\mathrm{g}}\right]\left(\frac{\mu_{en}}{\rho}\right)_{wall}^{air}(\beta_{wall})_{wall}^{air}\prod_i K_i$
$\downarrow$	$N_{\mathrm{X}}^{\mathrm{Co}^{60}}$ $[^{R}/_{\mathrm{C}}]$	**calibration coefficient** $N_{\mathrm{X}}^{\mathrm{Co}^{60}}\,[^{R}/_{\mathrm{C}}] = (X\,[\mathrm{R}]\,/M\,[\mathrm{C}])\,_{^{60}\mathrm{Co}}$
X_Q [R]		**user beam quality** (Q) $X_Q = N_{\mathrm{X}}^{\mathrm{Co}^{60}}\,[^{R}/_{\mathrm{C}}]\,M_Q\,[\mathrm{C}]\,P_{\mathrm{ion}}$

dependent and subsequent direct calculations of the cavity-gas calibration coefficient $\left(N_{\mathrm{gas}}^{\mathrm{Co}^{60}}\right)$ would only be valid for the standard ionization chamber. In order to provide a cavity-gas calibration coefficient $N_{\mathrm{gas}}^{\mathrm{Co}^{60}}$ for the users ionization chamber, derivation 2.2 from TG-21, is provided based on the users exposure X calibration coefficient $N_{\mathrm{X}}^{\mathrm{Co}^{60}}\,[^{R}/_{\mathrm{C}}]$. $N_{\mathrm{X}}^{\mathrm{Co}^{60}}\,[^{R}/_{\mathrm{C}}]$ is converted to the cavity-gas calibration coefficient $N_{\mathrm{gas}}^{\mathrm{Co}^{60}}$ for the user's ionization chamber by correcting for the standard ionization chamber's exposure $X[\mathrm{R}]$ measurement used to obtain the users ionization chamber's $N_{\mathrm{X}}^{\mathrm{Co}^{60}}\,[^{R}/_{\mathrm{C}}]$ value. The standard ionization chambers values accounted for are: $k\left[\frac{\mathrm{C}}{kg\,R}\right]$, $\frac{\overline{W}}{e}[^{eV}/_{\mathrm{i.p.}}]$, $\left(\frac{\overline{L}}{\rho}\right)_{wall}^{gas}$, $\left(\frac{\mu_{en}}{\rho}\,(\beta_{wall})_{wall}^{water}\right)$, and P_{wall}. The factor $A_{wall}^{\mathrm{Co}^{60}}$ corrects for the attenuation and scatter in the wall and build up region of the standard ionization chamber. This derivation assumes the ionization chambers wall and surrounding media are matched and a constant temperature and pressure are assumed.

D_{med} is the dose to the medium at the ionization chamber's effective point of measurement. The derivation of D_{med} is shown in derivation 2.3. $\mathrm{D_{med}}$ is found from the D_{gas} derivation of the cavity-gas calibration coefficient, $N_{\mathrm{gas}}^{\mathrm{Co}^{60}}$, by applying cavity theory equations, related stopping power ratios $\left(\frac{\overline{L}}{\rho}\right)$ and mass attenuation coefficients

Derivation 2.2 Dose to gas (D_{gas}) based calibration: from the ADCL standard ^{60}Co to the user's beam quality

$D^{^{60}\text{Co}}_{gas}$ [Gy]

standard beam quality(^{60}Co)

$D^{^{60}\text{Co}}_{gas}[\text{Gy}] = J^{^{60}\text{Co}}_{\text{gas}}[C/\text{kg}]\frac{\overline{W}}{e}[eV/\text{i.p.}]$

standard ionization chamber calibration coefficient

$N^{\text{Co}^{60}}_{\text{gas}}[\text{Gy}/\text{C}] = D_{\text{gas}}[\text{Gy}]A^{\text{Co}^{60}}_{\text{ion}}M^{-1}\,[\text{C}]$

standard beam quality(^{60}Co)

$X_{^{60}\text{Co}}[\text{R}] = 1/k\left[\frac{\text{C}}{kg\,R}\right]J^{^{60}\text{Co}}_{\text{gas}}[C/\text{kg}]\frac{\overline{L}}{\rho}\left[\frac{\text{MeV cm}^2}{\text{g}}\right]\left(\frac{\mu_{en}}{\rho}\right)^{air}_{wall}(\beta_{wall})^{air}_{wall}\prod_i K_i$

user ionization chamber X calibration coefficient

$+\ N^{\text{Co}^{60}}_{\text{X}}\,[R/\text{C}] = (X/M\,[\text{C}])_{^{60}\text{Co}}$

---

user ionization chamber calibration coefficient

$N^{\text{Co}^{60}}_{\text{gas}}[\text{Gy}/\text{C}] =$

D^{Q}_{gas} [Gy]

$N^{\text{Co}^{60}}_{\text{X}}\,[R/\text{C}]\,k\left[\frac{\text{C}}{kg\,R}\right]\frac{\overline{W}}{e}[eV/\text{i.p.}]\left(\frac{\overline{L}}{\rho}\right)^{gas}_{wall}\left(\frac{\mu_{en}}{\rho}\right)^{air}_{wall}(\beta_{wall})^{air}_{wall}P_{\text{wall}}A^{\text{Co}^{60}}_{wall}$

user beam quality (Q)

$D^{Q}_{\text{gas}} = N^{\text{Co}^{60}}_{\text{gas}}M_Q P_{\text{ion}}$

$\left(\frac{\mu_{en}}{\rho}\right)$. P_{repl} corrects for the addition of the detector into the beam and is discussed in detail in Section 2.3.3.

2.3.2 AAPM's Task Group- 51 (TG-51) and IAEA's TRS-398

The TG-51 and IAEA's TRS-398 are the current standard CoP for clinical reference dosimetry of high energy photon and electron beams. These current CoP are based on ionization chamber dosimetry and theory. TG-51 is the primary CoP in the United States and is intended for calibrating photon beams with energies between 1.25 MV (^{60}Co) and 50 MV, and electron beams of nominal energies between 4 and 50 MeV. TRS-398 is the primary CoP in Europe and is written for a wide range of beam qualities and energies. TG-51 and TRS-398 ionization chamber calibration

Derivation 2.3 Dose to medium (D_{med}) based calibration: from the ADCL standard ^{60}Co to the user's beam quality

$D^{^{60}\text{Co}}_{\text{med}}$ [Gy]

standard beam quality "cavity theory" (^{60}Co)

$$D^{^{60}\text{Co}}_{\text{med}}[\text{Gy}] = J_{\text{gas},^{60}\text{Co}}[{}^{C}/_{\text{kg}}]\frac{\overline{W}}{e}[{}^{eV}/_{\text{i.p.}}]\left(\frac{\overline{L}}{\rho}\right)^{wall}_{gas}$$

$\downarrow$ $N_{\text{D}}[{}^{\text{Gy}}/_{\text{C}}]$

calibration coefficient

$$N_{\text{D}}[{}^{\text{Gy}}/_{\text{C}}] = N^{\text{Co}^{60}}_{\text{gas}}[{}^{\text{Gy}}/_{\text{C}}]\left(\frac{\overline{L}}{\rho}\right)^{wall}_{gas}\left(\frac{\mu_{en}}{\rho}\right)^{water}_{wall}P_{\text{ion}}P_{\text{repl}}$$

D^{Q}_{med} [Gy]

user beam quality (Q)

$$D^{Q}_{\text{med}} = N_{\text{D}}[{}^{\text{Gy}}/_{\text{C}}]M_Q\,[\text{C}]\,P_{\text{ion}}$$

coefficients, $N^{^{60}Co}_{D,w}$, are based on absorbed dose to water measurement standards determined by PSDL-traceable ionization chambers.

Beam quality specification

The determination of absorbed dose to water in clinical radiotherapy beams from first principles involves the application of several coefficients and correction factors to transfer the calibration coefficient from the standards beam quality to the clinic's beam quality. This transfer process requires intensive measurements and theoretical calculations, providing for possible error and large uncertainty when performed in the encumbered clinical environment. In order to simplify these procedures and reduce the possibility of errors in the determination of absorbed dose, current CoP (TG-51 and TRS-398) are performed in well-defined reference conditions. The current CoP procedures are simplified by introducing the concept of beam quality specification where measurements in the well defined reference conditions correlate to a beam quality correction factor which accounts for corrections such as ionization chamber replacement corrections and stopping power ratios. The beam quality specification methodology allows CoP to provide ionization chamber make/model-specific beam

quality correction factor, decreasing the measurement and computational workload. The reference conditions are described by a set of measurement implementation parameters which influence physical quantities for which the beam quality correction factor is valid without further correction factors; therefore, the dose determined with the CoP is only valid at the reference point of measurement. To get dose at points or field sizes outside the reference conditions the CoP determined reference point dose must be extrapolated. The extrapolation method generally uses measurements of ionization chamber output ratios. The limitations of these extrapolation methods will be discussed in Section 2.5 and are the fundamental quandary in this investigation.

Absorbed dose to water methodology

The current absorbed dose CoPs (TG-51 and TRS-398) calibrate photon and electron beams with ionization chamber measurements using reference conditions with a constant source-to-surface distance (SSD) or source-to-axis distance (SAD)(Figure 2.1).[3,7] The SSD reference conditions in TG-51 are a depth of 10 cm in water, a field size of $(10\,\mathrm{x}\,10)$ cm^2 on the surface of the water phantom (volume $\geq (30\,\mathrm{x}\,30\,\mathrm{x}\,30)$ cm^3), and a constant SSD of 100 cm. The SAD reference conditions in TG-51 use a depth of 10 cm in water, a field size of $(10\,\mathrm{x}\,10)$ cm^2 at the isocenter on a plane perpendicular to the beam, and a constant source-to-chamber distance (SCD) of 100 cm. TRS-398 calibrates photon beams with the ionization chamber measurements in the reference conditions of a depth of z_{ref} (expressed in g cm^{-2}), source-to-chamber distance of 100 cm, and a field size of $(10\,\mathrm{x}\,10)$ cm^2 at the isocenter.

Absorbed dose to water (D_w^Q or $D_{w,Q}$) from a beam of quality Q correlating to the beam type and energy of the clinic beam is determined using an ionization chamber under TG-51 reference condition using equation (2.4) and under TRS-398

reference conditions using equation (2.5).

$$M \textbf{ or } M_{Q=} M_{\text{raw}} P_{\text{ion}} P_{\text{TP}} P_{\text{elec}} P_{\text{pol}} \tag{2.3}$$

$$D_w^Q = M k_Q N_{D,w}^{^{60}\text{Co}} (\text{TG} - 51) \tag{2.4}$$

$$D_{w,Q} = M_Q k_{Q,Q_0} N_{D,w,Q_0} \, (\text{TRS} - 398) \tag{2.5}$$

In equation (2.3), the quantities M and M_Q are the ionization chamber readings corrected for ion recombination (P_{ion}), temperature and pressure variations (P_{TP}), polarity (P_{pol}), and electrometer calibration (P_{elec}) in the reference conditions. $N_{D,w}^{^{60}\text{Co}}$ and N_{D,w,Q_0} are the absorbed dose to water calibration coefficient obtained from the national standards lab or an ADCL for the standard beam quality (Q_0), which is generally a ^{60}Co and (10×10) cm^2 field. k_Q and k_{Q,Q_0} are the beam quality correction factors, which correct for differences between ionization chamber response in the calibration standard beam quality (Q_0) and the beam quality used in the clinic's reference conditions (Q). The beam quality specification measurement conditions and method for determining beam quality correction factors is dependent on the CoP and its reference conditions (Figure 2.1).

Beam quality specification reference conditions

TG-51 uses the percentage of maximum dose measured at 10 cm depth (%dd(10)$_{\text{x}}$), corrected for electron contamination, to determine the beam quality specification using the general equation (2.6). If the measured %dd(10) falls outside of the general equations tolerances listed in equation (2.6), %dd(10) must be found using a lead scattering foil to add a constant electron contamination (%dd(10)$_{\text{PB}}$) and (%dd(10)$_{\text{x}}$) is then found using equation 13 or 14 in the TG-51 protocol.[3] For photon beams,

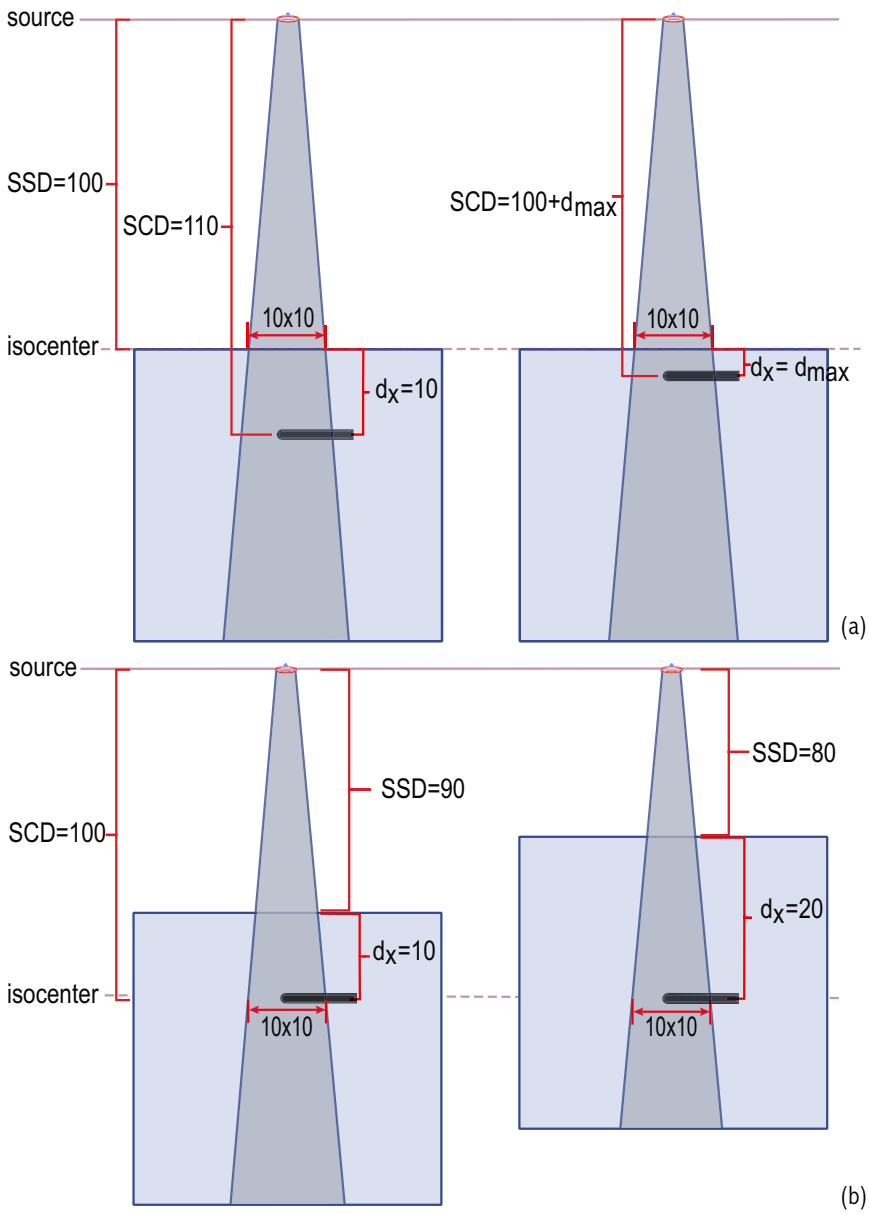

Figure 2.1: TG-51 and TRS-398 beam quality specification conditions for determination of beam quality correction factor. (a) TG-51 uses the percentage of maximum dose measured at 10 cm depth ($\%\mathrm{dd}(10)_x$) corrected for electron contamination ($\%\mathrm{dd}(10)_x$) to determine the beam quality specification. (b) The beam quality specification in TRS-398 is ascertained by the tissue-phantom ratio of ionization chamber response at depths of 10 cm and 20 cm with a constant SAD setup ($\mathrm{TPR}_{20,10}$). From the beam quality specification the beam quality correction factor k_Q in TG-51 and the beam quality correction factor k_{Q,Q_0} in TRS-398 can be found in published tables.

a shift to the effective point of measurement of the ionization chamber is applied ($0.6\mathrm{r_{cav}}$) when determining the beam quality specification.

$$\%\mathrm{dd}(10)_{\mathrm{x}} = 1.267\%\mathrm{dd}(10) - 20 \ (\mathrm{for} 75 < \%\mathrm{dd}(10) < 89) \tag{2.6}$$

The beam quality specification in TRS-398 is ascertained by the tissue-phantom ratio of ionization chamber response at depths of 10 cm and 20 cm with a constant SAD setup ($\mathrm{TPR_{20,10}}$).[7,3]

From the beam quality specification, the beam quality correction factor k_Q in TG-51 and the beam quality correction factor k_{Q,Q_0} in TRS-398 can be found in published tables. The beam quality correction factor for photons in TG-51 range from 1.0 to 0.937 for k_Q and in TRS-398 range from 1.0 to 0.966 for k_{Q,Q_0}. Ionization chamber beam quality correction factors used in standard CoPs are determined computationally using Monte Carlo methods.[5,77] Computational and experimental k_Q determination is described in Section 2.3.4.

TG-51 calibration of electron beams involve reference conditions with the ionization chamber placed at the reference depth d_{ref} using equation (2.7).

$$d_{\mathrm{ref}} = 0.6\, R_{50} - 0.1\,\mathrm{cm} \tag{2.7}$$

The electron beam quality specification reference conditions include a field size of $(10\,\mathrm{x}\,10)\ \mathrm{cm}^2$ defined on the surface of the phantom and a nominal SSD between 90 and 110 cm. The TG- 51 equation for determining absorbed dose to water from high energy electrons is given in equation (2.8).

$$D_{w,Q} = P_{\mathrm{ion}}\, P_{\mathrm{TP}}\, P_{\mathrm{elec}}\, P_{\mathrm{pol}}\, M_{\mathrm{raw}}\, P_{gr}^{Q}\, k'_{R_{50}}\, k_{\mathrm{ecal}} \tag{2.8}$$

The electron beam quality Q is specified by the coefficient R_{50}. R_{50} is determined at the depth in the water phantom where the ionization reading falls to 50% (I_{50}) of the maximum ionization reading ($I_{\max}$). A shift of $0.5r_{\text{cav}}$ is applied to the ionization chamber to place it at the effective point of measurement for electron beams. All electron parameters are the same as for photons, except for the beam quality correction factor k_Q which is replaced by beam quality correction factor P_{gr}^{Q}, $k'_{R_{50}}$, and k_{ecal}. The gradient correction $\left(P_{gr}^{Q}\right)$ is dependent on the ionization gradient at the point of measurement. The electron quality conversion factor $\left(k'_{R_{50}}\right)$ is fixed for a given chamber model and converts the absorbed dose to water calibration coefficient $\left(N_{D,w}^{^{60}Co}\right)$ for the gamma emitting ^{60}Co calibration source to the absorbed dose to water calibration factor $\left(N_{D,w}^{Q_{\text{ecal}}}\right)$ for an electron beam of arbitrary quality Q_{ecal}. The photon-electron conversion factor (k_{ecal}) converts $N_{D,w}^{Q_{\text{ecal}}}$ to an absorbed dose to water calibration factor $\left(N_{D_w}^{Q}\right)$ for a beam of quality Q. TG-51 reference conditions are used in this work due to it being the accepted standard CoP in the United States where this work was performed.

Uncertainty

Equation (2.6) for determining the TG-51 beam quality specification $\%\text{dd}(10)_{\text{x}}$ is a global fit to data. Using this general equation may cause errors in assigning $\%\text{dd}(10)_{\text{x}}$ of up to 2% in extreme cases, which would lead to an error in k_Q resulting in an uncertainty of 0.4% in absorbed dose calculations.[3]

2.3.3 Derivation of beam quality correction factor from AAPM's Task Group- 21 (TG-21)

From TG-21, it is simple to derive the dependencies of conventional CoPs beam quality specification and beam quality correction factor as shown in derivation 2.4. A comparison of the nomenclature is given in Table 2.1. From this we see that the beam quality correction factor in current CoP accounts for corrections such as stopping power ratios and perturbation factors explicitly corrected for in TG-21.

P_{fl}, P_{gr}, P_{stem}, P_{cel}, and P_{wall} are the chamber specific corrections outlined in TG-21. P_{repl} used in the derivations in Section 2.3.1 is a summation of these correction factors and represents the replacement of the phantom material by the ionization chamber. These correction factors account for source perturbation of the beam causing spectrum differences from those required for the application of cavity theory based calculations. P_{repl} is dependent on the beam quality and are conveniently folded into the beam quality correction factor used in standard CoP. These corrections are in addition to P_{ion}, the correction for ion recombination applicable to the calibration of the users beam, P_{TP}, the correction for temperature and pressure variations, P_{elec}, the correction for electrometer calibration and P_{pol}, the correction for polarity.

2.3.4 Determination of TG-51 beam quality correction factors (k_Q) for ionization chambers

Ionization chamber beam quality correction factors used in current CoPs are calculated using Monte Carlo determined stopping power ratios from International Commission on Radiological Units and Measurements Report 37 (ICRU-37). Experimentally determined ionization chamber beam quality correction factors using calorimetry have shown agreement within 1% with the Monte Carlo calculated factors. Absorbed

Derivation 2.4 TG-51 parameters and solving for k_Q

calorimetry-determined absorbed dose to water (^{60}Co)

$D_w^{^{60}\mathrm{Co}}[\mathrm{Gy}]$ $\quad D_w^{^{60}\mathrm{Co}}[\mathrm{Gy}] = \frac{1}{2} \cdot (\triangle R/R)\,[\Omega] \cdot \mid S^{-1} \mid \left[\frac{^\circ K}{\Omega}\right] \cdot c \left[\frac{Gy}{^\circ K}\right]$

$\downarrow \quad N_{D,w}^{^{60}Co}$ $\quad$ **calibration coefficient** $\left(N_{D,w}^{^{60}\mathrm{Co}}\right)$

$[\mathrm{Gy}/\mathrm{C}]$ $\quad N_{D,w}^{^{60}\mathrm{Co}}[\mathrm{Gy}/\mathrm{C}] = D_w^{^{60}\mathrm{Co}}/M_{^{60}\mathrm{Co}}$

$D_w^Q[\mathrm{Gy}]$ $\quad$ **user beam quality** (Q)

$D_w^Q[\mathrm{Gy}] = N_{D,w}^{^{60}Co} M_Q k_Q$

solving for k_Q with TG-21

$$k_Q = (M_{^{60}\mathrm{Co}}/M_Q)\left(D_w^Q/D_w^{^{60}\mathrm{Co}}\right)$$

from TG-21:

$$D_w^Q = N_{\mathrm{gas}}^{\mathrm{Co}^{60}} M_Q \left(\frac{\overline{L}}{\rho}\right)_{gas}^{wall}$$

$$k_Q = \frac{M_{^{60}\mathrm{Co}}}{M_Q} \cdot \frac{\left[\left[\frac{\overline{L}}{\rho}\right]_a^w P_{\mathrm{fl}} P_{\mathrm{stem}} P_{\mathrm{cel}} P_{\mathrm{wall}}\right]_Q}{\left[\left[\frac{\overline{L}}{\rho}\right]_a^w P_{\mathrm{fl}} P_{\mathrm{stem}} P_{\mathrm{cel}} P_{\mathrm{wall}}\right]_{^{60}\mathrm{Co}}}$$

dose calibration coefficients and experimental k_Q factors are based on the primary standard of absorbed dose to water. The National Research Council (NRC) (Ottawa,Canada) is the primary source for calculated and experimental beam quality correction factors (k_Q) used in the TG-51 standard CoP.[78] The NRC states an estimated 0.35% relative standard uncertainty in absorbed dose to water measurements using their water calorimeter and a standard uncertainty for calorimetric measurements of k_Q is estimated to be 0.27% due to correlation in the uncertainties.[59,58]

2.4 Current broad beam CoP extrapolation methods for small and nonstandard high energy photon dosimetry

The introduction of IMRT has improved treatments of small and irregular lesions using techniques employing small and modulated beams. These small modulated beams

<table>
<tr><th></th><th>TG-21</th><th>TG-51</th><th>TRS-398</th></tr>
<tr><td>corrected raw reading (M)</td><td colspan="3">$M = M_{\text{raw}} P_{\text{ion}} P_{\text{TP}} P_{\text{elec}} P_{\text{pol}}$</td></tr>
<tr><td>^{60}Co calibration coefficient</td><td>$N_{\text{gas}}^{\text{Co}^{60}}$ [Gy/C]$_{\text{gas}}$</td><td>$N_{D,w}^{Q_0}$ [Gy/C]$_{\text{water}}$</td><td>N_{D,w,Q_0} [Gy/C]$_{\text{water}}$</td></tr>
<tr><td>beam quality specification</td><td rowspan="2">$\left[\left[\frac{\bar{L}}{\rho}\right]_a^w P_{\text{fl}} P_{\text{stem}} P_{\text{cel}} P_{\text{wall}}\right]$</td><td>$k_Q$</td><td>$k_{Q,Q_0}$</td></tr>
<tr><td>beam quality correction factor(s)</td><td>$\%\text{dd}(10)_{\text{x}}$</td><td>$\text{TPR}_{20,10}$</td></tr>
<tr><td>dose to medium</td><td>any</td><td colspan="2">water</td></tr>
<tr><td>reference conditions</td><td>flexible</td><td colspan="2">strict</td></tr>
</table>

Table 2.1: Comparison of current CoP and TG-21 formalism. The expression of beam quality correction factor for each formalism derived in derivation 2.1-TG-51 parameters and solving for k_Q are summarized along with the appropriate calibration coefficients and reference conditions.

provide precise conformal dose distributions and dose delivery. Current standards of practice require verification of IMRT treatment plans before implementation in the clinic, but there is not a clear consensus in the Medical Physics community as to what the verification process should entail.[33] Standard CoP provide the methodology to perform dosimetry in a reference field, usually (10 x 10) cm^2, where the CoP provided beam quality correction factor are available and valid.

It is common practice to extrapolate calculations of dose [Gy] per monitor unit [MU] from standard CoP (10 x 10) cm^2 broad beam reference conditions down to small and nonstandard field sizes ($D_{w,Q_{\text{small fields}}}^{f_{\text{small fields}}}$) using ratios of total scatter factors ($\text{s}_{\text{c,p}}$) for the nonstandard field over the (10 x 10) cm^2 broad beam reference condition, equation (2.9).

$$D_{w,Q_{\text{small fields}}}^{f_{\text{small fields}}} = D_{w,Q_{ref}}^{f_{\text{ref}}} \text{s}_{\text{c,p}} \tag{2.9}$$

Minimally corrected detector output factors determined by film, diodes, or a small volume ionization chambers are often considered equivalent to $s_{c,p}$. Using these detectors output factors in small and nonstandard fields with currently available standard CoP provided beam quality correction factor could result in incorrect estimations of $s_{c,p}$ and dose due to the spectral variations and amplified detector beam quality dependencies associated with measurements in the field-edge regions and spread out penumbra occupying a significant portions of the total field size. These issues effect both the phantom (s_p) and collimator scatter (s_c) components of the total scatter factor dose determination leading to a complicated dosimetric issues which are discussed in detail in Section 2.5.

$$s_{c,p} = s_c s_p \tag{2.10}$$

Obtaining absorbed dose accuracy within $\pm 3\%$ and overall dosimetric accuracy reference levels of $\pm 5\%$ is difficult to achieve using current $s_{c,p}$ measurement methods in small and nonstandard fields.[33] In addition, the RPC has shown in inter-institutional comparisons significant IMRT dosimetry differences among institutions.[23,93] These uncertainties indicate a widespread dosimetric issue and a need for a revised dosimetry protocol for small and nonstandard beams.

2.4.1 Total scatter factors and output factors

Total scatter factors ($s_{c,p}$) are used to extrapolate calculations of dose [Gy] per monitor unit [MU] from standard CoP (10×10) cm^2 broad beam reference conditions down to small and nonstandard field sizes (Section 2.4). $s_{c,p}$ is the ratio of dose rate in the small and nonstandard field over the standard CoP (10×10) cm^2 broad beam. In practice, the minimally corrected ratio of the detectors raw charge reading in a nonstandard field over the standard CoP reference condition (OF) is consider equivalent to $s_{c,p}$.

Derivation 2.5 Derivation of relationship between total scatter factors ($s_{c,p}$) and output factors (OF)

$$s_{c,p}(r) = \frac{D_{w,Q_r}^{f_r}}{D_{w,Q_{ref}}^{f_{ref}}} \quad (2.11) \qquad , OF = \frac{M_{Q_r}^{f_r}}{M_{Q_{ref}}^{f_{ref}}} \quad (2.12)$$

$\downarrow$ *Standard* CoP *nomenclature (Equation):*
$D_w^Q = M k_Q N_{D,w}^{Q_0}$

$$s_{c,p}(r) = OF \cdot \frac{k_{Q_r,Q_0}^{f_{fr},f_{Q_0}}}{k_{Q_{ref},Q_0}^{f_{fref},f_{Q_0}} \, (\text{standard CoP } k_Q)} \quad (2.13)$$

Methods for $k_{Q_r,Q_0}^{f_{fr},f_{Q_0}}$ determination

$\downarrow$ *Experimental Method* (2.14)
(Chapter 4)
$$k_{Q_r,Q_0}^{f_{fr},f_{Q_0}} = \left[\frac{M}{D_w^Q}\right]_{Q_0}^{Q_r}$$

$\downarrow$ *Computational Method* (2.15)
(Chapter 5)
(Derivation 2.4)
$$k_{Q_r,Q_0}^{f_{fr},f_{Q_0}} = \left[\left[\frac{\overline{L}}{\rho}\right]_a^w P_{fl} P_{stem} P_{cel} P_{wall}\right]_{Q_0}^{Q_r}$$

The OF is only equivalent to $s_{c,p}$ when the measured dose rates are from the same beam quality and the standard CoP provided beam quality correction factor used to determine absorbed dose still apply. The relationship between $s_{c,p}$ and OF is derived from the standard CoP nomenclature and beam quality correction factor definitions in Derivation 2.5. The $s_{c,p}$ and OF are shown to be related by the ratio of beam quality correction factor in the small or nonstandard field (Q_r) over the standard CoP beam quality correction factor (Q_{ref}).

Beam quality changes very little from the standard CoP reference conditions if charged particle equilibrium (CPE, Section 2.5.1) is maintained and the additional dose uncertainty from the assumption that OF are equivalent to $s_{c,p}$ can generally be ignored. However, small fields often lack lateral CPE resulting in large differences between OF and $s_{c,p}$. Figure 2.2 shows output factor measurements for various de-

tectors compared to Monte Carlo calculated total scatter factors, with the differences between detector output measurements and Monte Carlo calculated $s_{c,p}$ range of 0 to 14%. These OF discrepancies are due to variations in the charged particle spectrum at small field sizes which results in a different beam quality for the small field than the broad beam CoP reference conditions.[82,24] Derivation 2.4 demonstrated that ionization chamber determined dose is a function of cavity-theory-dependent Spencer-Attix stopping power ratios and detector perturbation corrections which are both a function of the dependence on the charged particle spectrum. Assuming output factors are equivalent to $s_{c,p}$ for small and nonstandard fields dose extrapolation from standard CoP dose measurements without additional beam quality corrections results in increased dose uncertainty and the possibility of harmful over-exposures.

Alternate beam quality correction factors are needed for measurements of fields lacking CPE to reduce their associated uncertainty. Derivation 2.5 demonstrates the computational method for beam quality correction factor determination based on first principle cavity theory calculations. To directly apply cavity theory in small fields lacking CPE the charged particle spectra must be known explicitly and mass stopping power ratios found by integrating over the incident charged particle spectrum. This value can then be used in place of the single Spencer-Attix stopping power ratio used in cavity theory calculations of dose under CPE conditions.

In small fields lacking lateral CPE, the charged particle spectrum is hard to quantify because it is influenced by multiple variables including field size, detector size and composition, and photon energy. These variables are not independent and determining the charged particle spectrum is complicated by the variables' complex correlation (discussed in section 2.5). The field size and energy affect both the phantom (s_p) and collimator scatter (s_c) components of the total scatter factor dose determination, leading to complicated dosimetric issues. The issue is further

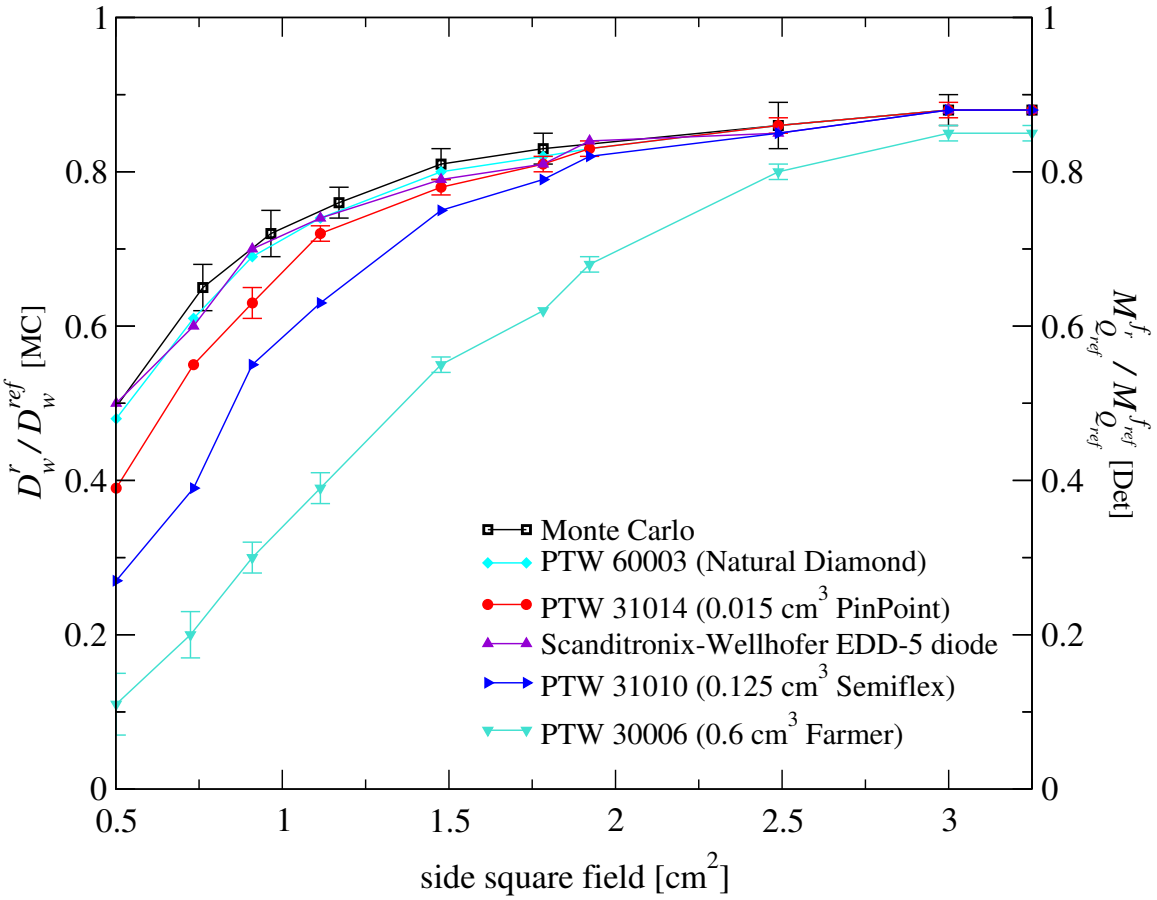

Figure 2.2: Total scatter factors determined by Monte Carlo (black) and measured output factors for various detectors (colored lines) as a function of field size.[82,24]

complicated by the addition of the detector since the detector response is a function of the charged particle spectrum, but concurrently the detector's presence perturbs the charged particle spectrum. Determining the charged particle spectrum implicitly is also difficult as there is no practical method to measure MV spectra nor would it be feasible to perform spectrometry in a clinical setting. Our research group's Dr. Bartol has made the first steps to measuring MV spectra using Compton spectrometry,[11] but currently the technique is in the research phase and is not portable.

Derivation 2.5 also demonstrates the experimental method for determining beam quality correction factor for ionization chambers from absorbed dose measured using a transfer dosimeter with a minimal beam quality dependency for the field under investigation. The experimental method for determining ionization chamber beam quality correction factors requires a transfer dosimetry system that lacks or minimizes the beam quality and dosimetric issues. Possible dosimeters for the measurement of absorbed dose to water for the determination of ionization chamber beam quality correction factor are discussed in Section 2.7.

These issues are prominent with measurements in the field-edge regions, spread out penumbra occupying a significant portions of the total field size and, to a lesser extent, non-flattened fields. The following Section 2.5 details many of the physical issues and variables involved in small field dosimetry.

2.5 Beam quality dependencies for small and nonstandard photon field dosimetry

2.5.1 Loss of lateral charge particle equilibrium

Dose calculations based on cavity theory are a function of the ratio of mass collisional stopping powers for tissue to air, which is defined by the charged particle fluence incident on the detector volume. Cavity theory is simplified under CPE conditions to allow for dose determinations without the implicit knowledge of the charged particle fluence. CPE is obtained when the point-of-measurement is located in a volume of homogeneous radiant energy, where each particle of a given energy leaving the volume is replaced by an identical particle with the same energy entering the volume (Figure 2.3 a).[9] CPE allow the doses for the different media to be related by their Spencer-Attix stopping power ratios which approximate the primary and secondary charged particle (δ-rays) energy deposition in the detector volume. Section 2.3 discussed in detail the use of cavity theory in ionization-chamber-based dosimetry and the importance of CPE in standard broad beam CoP ionization chamber reference dosimetry. Standard CoP broad beam reference conditions establish local CPE at the point of measurement allowing the doses for the different media to be related by their Spencer-Attix stopping power ratios and minimal perturbation corrections discussed in Section 2.5.7.

A small field is defined by the proposed formalism as a field in which CPE does not exist and cavity theory can not be easily applied. Field sizes of less than (3×3) cm^2 for 6 MV external beam photon therapy are generally where studies into small fields begin.[23] At these field sizes, the lateral range of the secondary charged particles in the phantom medium is often greater than the lateral dimension of the

field, which leads to the loss of lateral CPE and variations in the charged particle spectra along the lateral dimension of the cavity. In addition, other sources of spectral variation include the attenuation of the primary beam through the flattening filter with its variable thickness in the lateral and longitudinal directions, source occlusion (section 2.5.3), and changes in head and phantom scatter contributions. Figure 2.3 illustrates the different linac components effecting beam quality and their complex correlated relationship.

2.5.2 Beam energy

The degree that the charge particle spectrum incident on the detector deviates from a CPE spectrum (degree of disequilibrium) increases with photon energy at a given field size. This is due to the range of secondary electrons increasing as a function of increasing energy; lateral CPE is therefore lost at larger field sizes as the energy of the photons increase.[55,9] As a result, using lower energies for IMRT treatments is preferred over high-energy beams because smaller fields are able to be measured under CPE conditions and ionization chamber dose uncertainty due to spectral variations is less.

It is also advantageous to use lower energies to achieve the steep dose gradients desired for IMRT to obtain precise dose conformation around the target volume. Beam modulation in IMRT treatments is achieved by the lateral fall-off in intensity from compensator walls or through the use of closed MLC leaves. This leads to a less defined dose gradients with increased energy, as the lateral range of electrons increases as a function of energy.[4,81,55]

Additionally, using lower energies for IMRT treatments has been found to be advantageous due to the use of more field directions and the corresponding focusing

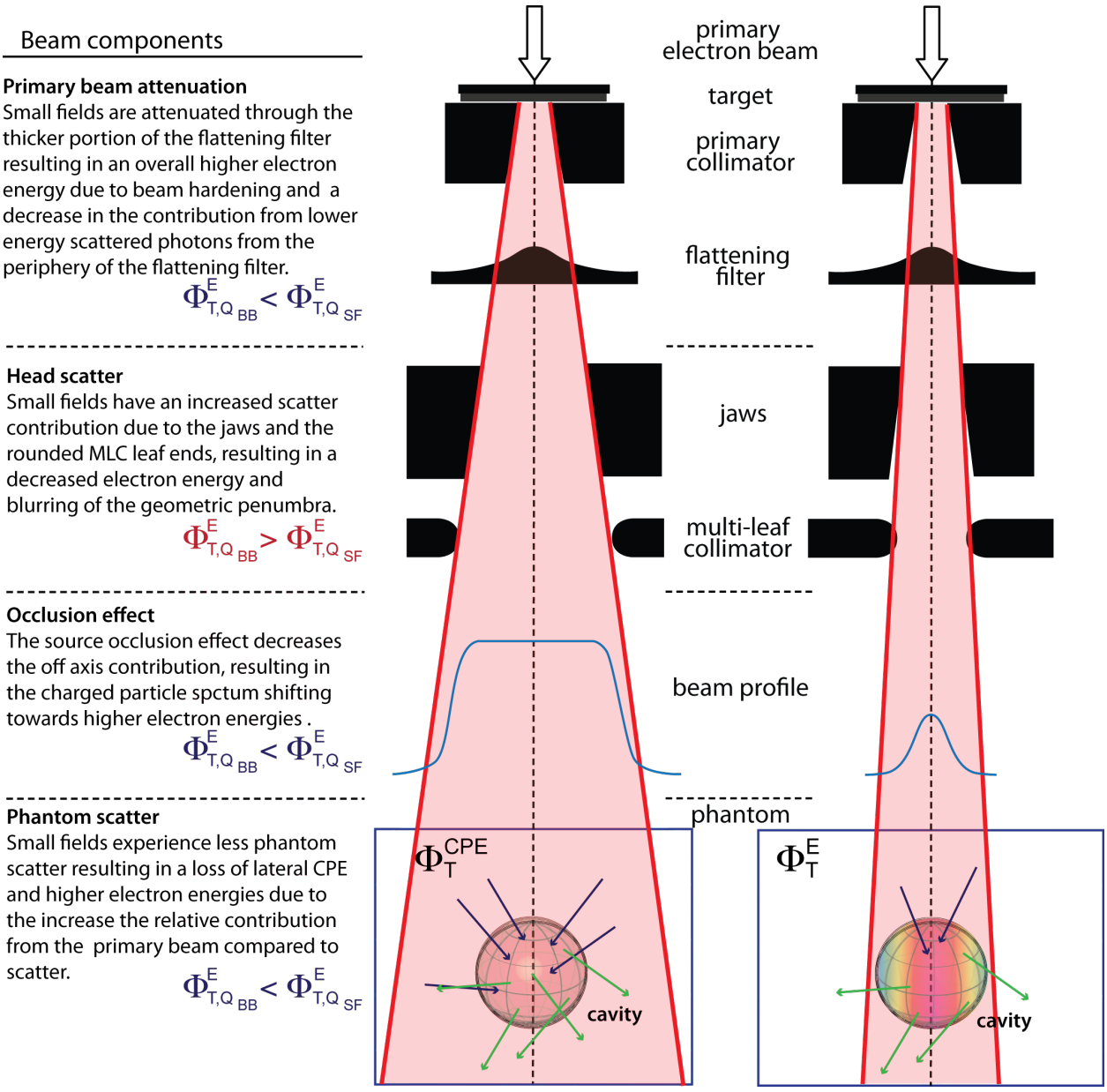

Figure 2.3: Sources of charge particle spectral variation affecting the amount of lateral charged particle disequlibrium in small and nonstandard fields, including a)primary beam attenuation, b)linac head scatter, c)source occlusion, and d)phantom scatter. Loss of lateral CPE at small field sizes due to charged particle out-scatter (green) outweighing charged particle in-scatter (blue) in the lateral dimension of the field. A field lacking CPE results in an in-homogenous charged particle spectra across the detector collecting volume.

effects leads to decreased integral and skin doses. In addition, neutron contamination is observed starting at nominal energies greater than 10 MV. Neutron contamination necessitates additional room shielding and delivers additional unwanted dose to the patient.[60,19] Due to all of these reasons, the energy investigated in this work is limited to 6 MV.

2.5.3 Source occlusion effect

Uncertainty associated with current extrapolation methods in small field dosimetry is complicated by the use of output factors measured in a field with a partially occluded source (Figure 2.4). With highly collimated fields, the source can be partially shielded by the collimators leading to a substantial decrease in the beam output and loss of the fields' point source characteristics. Partial occlusion of the source results in the penumbra region of the beam profile becoming wider and more blurred, as photons from the periphery of the source are blocked and the geometric penumbra is extended over the entire field size.[103] In addition, partial occlusion of the source produces a charged particle energy spectrum with an increased scatter dose component and decreased primary dose component compared to non-occluded fields. As a result, the beam quality and subsequent dose calculations for small fields with source occlusion are more sensitive to small variations in dose influencers such as source size, scatter contributors and detector type.

2.5.4 Volume-averaged detector response

Small and nonstandard fields do not provide flat dose profiles which results in a charged particle fluence gradient across the detector.[16] The energy deposited in an ionization chamber located on a dose gradient is averaged over the detector volume

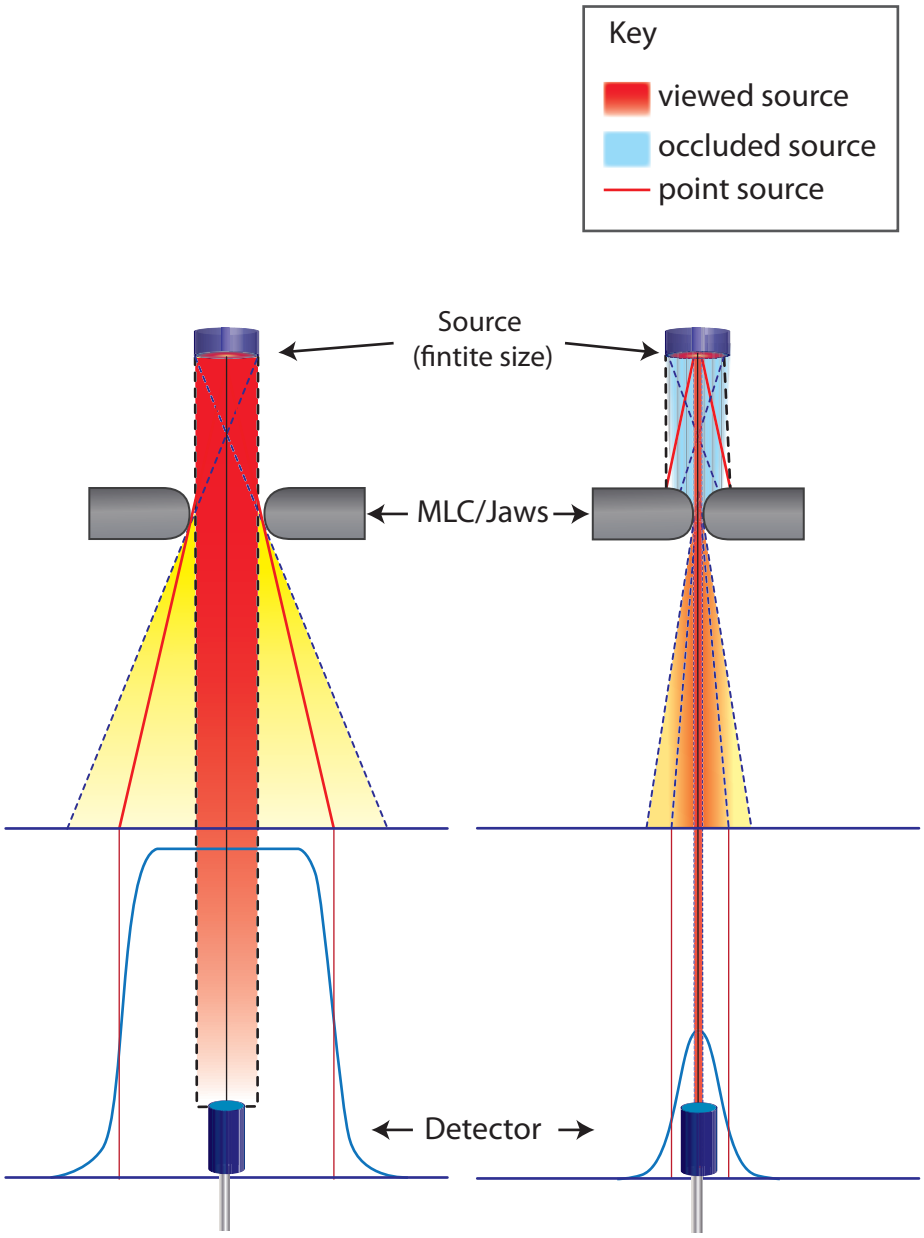

Figure 2.4: Source occlusion effect. The source can be partially shielded in highly collimated fields, leading to a substantial decrease in the beam output and loss of the fields' point source characteristics.

and is used as the point dose assumption which results in a systematic underestimation of dose. As the level of disequilibrium or dose-gradient across the detector increases, the volume averaging and dose underestimation effect increases. In the case of very small fields, significant errors can occur if the size of the field approaches that of the active volume of the detector. Using inappropriately large volume detectors can and has lead to overdosing and severe misadministration.[15,14] Dosimeters for small and nonstandard fields must provide increased spatial resolution for accurate dose measurements by minimizing volume averaging effects. However, ionization chambers size reduction is limited as very small ionization chambers have been shown to have signal to noise and stability issues.[65]

2.5.5 Field size determination

Current practice uses the penumbra regions and full width at half maximum (FWHM) of larger fields with broad beam characteristics to extrapolate down to small field sizes. However, as the range of the secondary charged particles approaches the size of the treatment field, using broad beam-determined penumbra regions and the FWHM field size determination method to extrapolate to small field sizes will result in an inaccurate field size and dose determinations.[98] FWHM methods will result in estimated field sizes are larger than the geometric field sizes and the calculated maximum doses is less than the actual maximum doses (Figure 2.5).[23,55] The clinical consequence of this is systematic exposure of larger volumes of healthy tissue in the region of the targeted tumor and systematic under-dosing the targeted tumor. It also leads to miscalculation of dose volume histograms (DVH) as well as tumor control and normal tissue complication probabilities (TCP and NTCP respectively).[94,34]

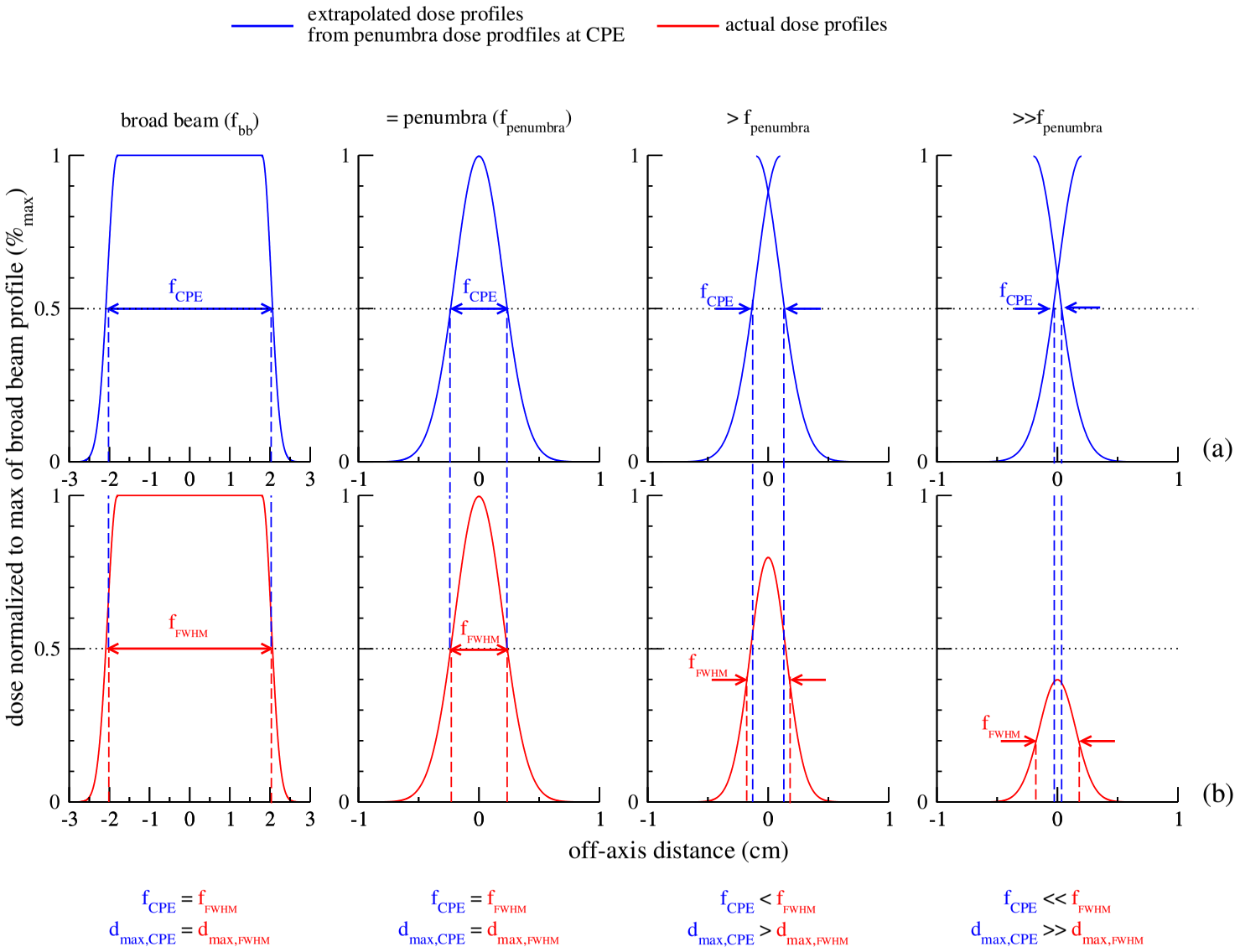

Figure 2.5: FWHM field size determination method

2.5.6 Modulation factor

Complex beam modulation in advanced conformal radiation therapy is achieved through the incorporation of multi-leaf collimator (MLC) and advanced CT based treatment planning systems. The IMRT beamlets are defined by the lateral fall off from the MLC leaves. The beamlets are either dynamically or statically modulated by the MLC leaves movement through the primary beam. By modulating the fluence across multiple beams and beam angles, IMRT is capable of producing intricate isodose distributions while sparing sensitive tissue around the target area.[79] Ionization chamber measurements present dosimetric challenges for IMRT and related stereotactic modalities. The variable charged particle energy distributions incident on the detector and resultant beam quality detector response function are difficult to measure and simulate. These methods will require additional specialized dosimetric verification methods and in addition to the standard 2-D and 3-D conformational therapy quality assurance tests.

2.5.7 Detector perturbation

Another complication beyond the loss of lateral CPE when dealing with small fields is the addition of a detector into the field. This results in perturbation of the spectrum and further complicates this problem. The effects of perturbation are hard to quantify because the detector medium is often different than the surrounding medium in density and composition. Additionally, as the field size decreases, determining the energy spectrum becomes more difficult. Perturbation effects can be minimized by detectors with water equivalent composition. These effects in ionization chambers are discussed further in Chapter (5).

2.6 Proposed code of practice for small and non standard high energy photon reference dosimetry

In a joint effort between the IAEA and the AAPM, a working group was formed to develop a CoP for reference dosimetry in small and nonstandard fields. The working group has published a new formalism, which will be referred to as the "proposed formalism" in this work.[2] The IAEA and AAPM's proposed formalism for small and nonstandard fields is an extension of the IAEA (TRS-398) CoP and expands on its current procedure and nomenclature. The international proposed formalism aims to create new and expanded beam quality specification definitions for small and nonstandard fields that provide ionization chamber based reference calibrations at the same level of accuracy as present standard CoP (approximately $\pm 2\%$). The proposed formalism suggests new beam quality correction factors for the new and expanded beam quality specification definitions to be determined with Monte Carlo simulations or a dosimeter traceable to a primary standard of absorbed dose to water. The proposed formalism introduces two calibration methods for performing reference dosimetry of small and nonstandard fields. The first method involves small, static-field reference geometries, while the second involves composite-field reference geometries.

The small static-field dosimetry method introduces the machine-specific-reference field (f_{msr}) and its related beam quality correction factor ($k_{Q_{\mathrm{msr}},Q_{ref}}^{f_{\mathrm{msr}},f_{ref}}$). The f_{msr} is defined by a static beam at the user's facility. The f_{msr} was created for the calibration needs of stereotactic radio surgery systems (e.g, TomoTherapy, Gamma Knife, CyberKnife) which are unable to establish the standard CoPs reference conditions. Figure 2.6 shows the progression from the standard CoPs' reference broad beam conditions, f_{ref}, to the protocol's static small field condition, f_{msr}. The absorbed dose

to water ($D_{w,Q_{\mathrm{msr}}}^{f_{\mathrm{msr}}}$) in the proposed formalism's static field (f_{msr}) calibration reference conditions is determined at the reference depth in water in a beam of quality Q_{msr} is given by equation (2.16).[2]

$$D_{w,Q_{\mathrm{msr}}}^{f_{\mathrm{msr}}} = M_{Q_{\mathrm{msr}}}^{f_{\mathrm{msr}}} N_{D,w}^{Q_0} k_{Q,Q_0} k_{Q_{\mathrm{msr}},Q_{ref}}^{f_{\mathrm{msr}},f_{ref}} \tag{2.16}$$

$M_{Q_{\mathrm{msr}}}^{f_{\mathrm{msr}}}$, $N_{D,w}^{Q_0}$, and k_{Q,Q_0} are related to M_Q, N_{D,w,Q_0}, and k_{Q,Q_0} respectively, used in equation (2.5). $k_{Q_{\mathrm{msr}},Q_{ref}}^{f_{\mathrm{msr}},f_{ref}}$ corrects for the difference in ionization chamber response to the beam quality of the conventional CoPs reference field (f_{ref}) and the machine-specific reference field (f_{msr}). For modalities such as CyberKnife, Gamma Knife, and TomoTherapy where the standard CoPs f_{ref} is unobtainable, a hypothetical $(10\,\mathrm{x}\,10)\,\mathrm{cm}^2$ reference condition is established to enable determination of intermediate beam quality correction factor k_{Q,Q_0}. Factors that affect the beam quality include field size, geometry, and phantom material. This factor, $k_{Q_{\mathrm{msr}},Q_{ref}}^{f_{\mathrm{msr}},f_{ref}}$, is defined as the ratio of dose (D_w) per unit reading ($M_{\mathrm{raw}}P_{\mathrm{ion}}P_{\mathrm{TP}}P_{\mathrm{elec}}P_{\mathrm{pol}}$) for f_{msr} and f_{ref}, as shown in equation (2.17).

$$k_{Q_{\mathrm{msr}},Q_{ref}}^{f_{\mathrm{msr}},f_{ref}} = \frac{\left(D_{w,Q_{\mathrm{msr}}}^{f_{\mathrm{msr}}} / M_{Q_{\mathrm{msr}}}^{f_{\mathrm{msr}}}\right)}{\left(D_{w,Q_{ref}}^{f_{\mathrm{ref}}} / k_{Q_{\mathrm{ref}},Q_0}^{f_{\mathrm{f_{ref}}},f_{Q_0}}\right)} \tag{2.17}$$

The composite-field reference geometry method introduces the plan-class-specific reference field (f_{pcsr}) and its related $\left(k_{Q_{\mathrm{pcsr}},Q_{ref}}^{f_{\mathrm{pcsr}},f_{\mathrm{ref}}}\right)$. The calibration coefficient progression to the composite field reference conditions is shown in Figure 2.7. The f_{pcsr} is a composite field composed of clinically relevant beams, which are similar to a treatment plan used for a patient.[76] The f_{pcsr} is a reference field can be either a 3-D irradiated volume or 4-D delivery sequence represents real clinical plans. One requirement is that the f_{pcsr} provides a uniform dose over the detector volume in order to theoretically alleviate some of the small and nonstandard field dosimetric issues.

$$D_w^{Q_{msr}} = M \cdot N_{D_w}^{^{60}Co} \cdot k_Q \cdot k_{Q_{msr},Q}^{f_{msr},f_{ref}}$$

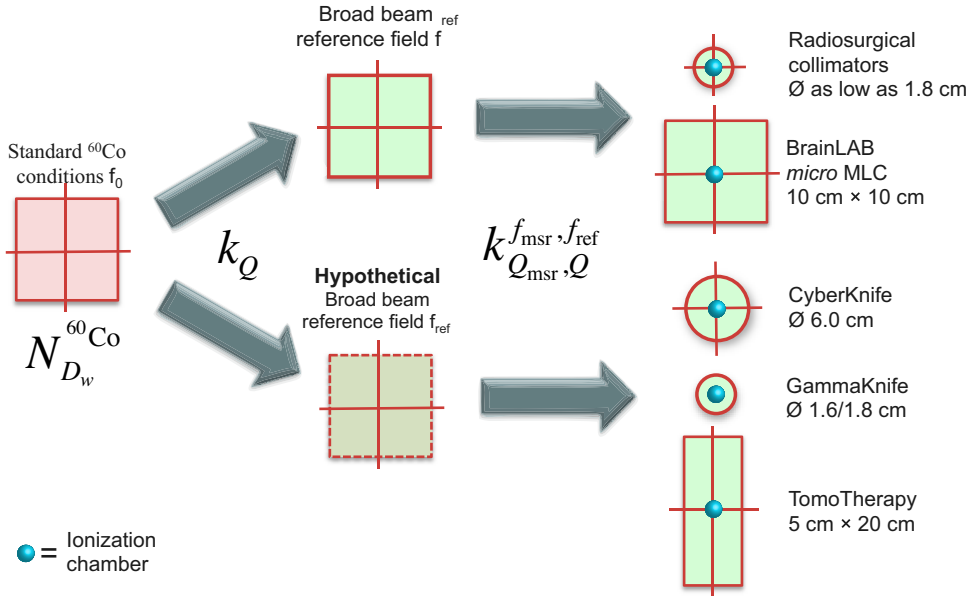

Figure 2.6: proposed formalism dosimetry of static fields using the new machine-specific reference field. The figure is adapted from Alfonso *et al.*[2]

$$D_w^{Q_{msr}} = M \cdot N_{D_w}^{^{60}Co} \cdot k_Q \cdot k_{Q_{msr},Q}^{f_{msr},f_{ref}}$$

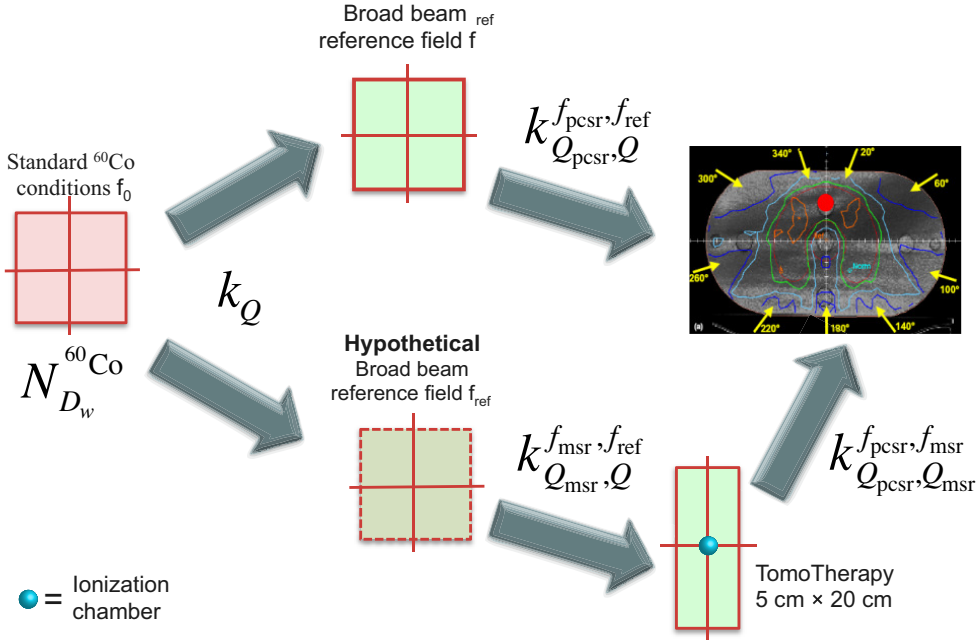

Figure 2.7: proposed formalism dosimetry of composite fields using the plan class-specific reference field (f_{pcsr}). [2]

For the composite field calibration, the f_{msr} is replaced with the f_{pcsr} and $Q_{\text{msr}}$is replaced with Q_{pcsr}. Equations (2.16) and (2.17) become equations (2.18) and (2.19), respectively.

$$D_{w,Q_{\text{msr}}}^{f_{\text{pcsr}}} = M_{Q_{\text{pcsr}}}^{f_{\text{pcsr}}} N_{D,w}^{Q_0} k_{Q,Q_0} k_{Q_{\text{pcsr}},Q_{ref}}^{f_{\text{pcsr}},f_{\text{ref}}} \tag{2.18}$$

$$k_{Q_{\text{pcsr}},Q_{ref}}^{f_{\text{pcsr}},f_{ref}} = \frac{\left(D_{w,Q_{\text{msr}}}^{f_{\text{pcsr}}} / M_{Q_{\text{pcsr}}}^{f_{\text{pcsr}}}\right)}{\left(D_{w,Q_{ref}}^{f_{\text{ref}}} / k_{Q_{\text{ref}},Q_0}^{f_{\text{f}_{\text{ref}}},f_{Q_0}}\right)} \tag{2.19}$$

2.6.1 Small and nonstandard field reference dosimetry traceability

The proposed formalism is in its preliminary phase, and the traceability to a calibration standard from a national or secondary standards lab is still under development. It has been proposed that the standards lab could provide a linac-based calibration coefficient for an ionization chamber in the proposed formalism's reference conditions: $N_{D,w}^{Q_{\text{msr}}}$ for f_{msr} or $N_{D,w}^{Q_{\text{pcsr}}}$ for f_{pcsr}[2]. Traditionally, standards laboratories base their calibrations on ^{60}Co, but as calorimetry technology develops, linac-based calibrations will become more prevalent. The National Physical Laboratory (NPL) has a program in place which provides linac-based calibration coefficients for use in standard CoPs by measuring absorbed dose using a graphite calorimeter for photon beams ranging from ^{60}Co to 19 MV.[32,31]

Alternatively, the traditional ^{60}Co-based calibration coefficients, $N_{D,w}^{Q_0}$, could be used and the factors $k_{Q_{\text{msr}},Q_{ref}}^{f_{\text{msr}},f_{ref}}$ and $k_{Q_{\text{pcsr}},Q_{ref}}^{f_{\text{pcsr}},f_{\text{ref}}}$ in equations (2.16) and (2.18) could be determined for each type of ionization chamber using a primary standard or an appropriate absorbed dose to water dosimeter whose calibration is traceable to a primary standard. Dosimeters which have been considered to measure $k_{Q_{\text{msr}},Q_{ref}}^{f_{\text{msr}},f_{ref}}$ and $k_{Q_{\text{pcsr}},Q_{ref}}^{f_{\text{pcsr}},f_{\text{ref}}}$ include alanine, radiochromic film, TLD, and ferrous sulphate.[55,2]

A phantom will be used in the proposed formalism and it is expected that the phantom used for composite fields will not be the standard CoPs rectangular water tank. The suitability of the standard calibration coefficient measured in water will need to be determined for use in a phantom of an alternate material. The optimal phantom geometry and material will also need to be determined for use as a standard phantom in the proposed formalism.

The standards laboratories' reference conditions for determination of the calibration coefficient are under investigation and variables in the standard reference condition include beam quality Q_0=linac or ^{60}Co, medium (i.e., water or acrylic) and static or composite field delivery (f_{msr} or f_{pcsr}). One option is for the calibration coefficients to be determined in phantom, instead of in water, using the ^{60}Co standard and eliminating the material component of the beam quality correction factor (i.e., providing the user with $N_{D,w}^{Q_{0,\text{in phantom}}}$).

2.7 Dosimeters for absorbed dose to water relative dosimetry

This work utilizes several types of dosimeter systems for measurements of absorbed dose to water. The systems selected for this investigation are designed to allow for precise traceability to a primary standard reference beam. As discussed in Section 2.3.4, the absolute method for the measurement of absorbed dose to water is achieved through water calorimetry. Absolute dosimeters directly measure energy imparted to the detector medium. Relative dosimeters are calibrated against an absolute measurement provided by a national metrological institute standard and subsequently absorbed dose is determined through the relative dosimeters corrected relative response. Transfer dosimeters are relative dosimeters with adequate accuracy and precision for the transfer of standard values from a primary standard laboratory

to a secondary standard laboratory. Dosimeter systems for secondary standard and clinical applications are referenced to water calorimetry absolute measurement provided by a national metrological institute standard.

For this work, solid state dosimeter systems based on the thermoluminescent response of lithium fluoride and the electroparamagnetic resonance of L-α-alanine are used as dosimeters for the determination of relative absorbed dose to water. Measurements of relative absorbed dose to water utilizing these solid state dosimeter systems document the transfer and traceability of ^{60}Co determined ionization chamber calibration coefficients, $N_{D,w}^{^{60}Co}$, to the end-users clinical beam quality Q. These observations allow for an analysis of the effect of beam quality on ionization chamber beam quality correction factors and enables quantification of the applicability of standard CoP beam quality specification and beam quality correction factor in nonstandard beams. Table 2.2 gives a summary of the detectors used and referenced in this work.

2.7.1 Ionization chamber dosimetry

Ionization chambers are the recommended transfer dosimeter for clinical external beam reference dosimetry. The standard CoPs and the proposed formalism (Section 2.4) calibration methods utilize ionization chambers as their standard dosimeter. Other active dosimeters are available but ionization chambers will be the primary clinical dosimeter of choice for the foreseeable future due to their stability, availability, and extensive characterization.

Ionization chamber dosimetry is based on the theoretical complete collection of all ion pairs created in a volume of gas by interacting charged particles. An electric field is applied across the gas volume to enable charged particle collection and convert

Dosimeter	Dosimetry type	Measured quanta	Method of readout	Typical absorbed dose range (Gy) [$< 1\%$ (1σ)]
water calorimetry	absolute	$\triangle$T $(^{\circ}K)$	thermocouple resistance [$\triangle\Omega$]	$10^1 - 10^4$
alanine (organic crystal)	relative (transfer)	$\mathrm{N}_{\mathrm{radical\,species}}$	EPR spectrometry [signal (a.u.)]	$5 - 10^5$
TLD (LiF:Mg,Ti) (inorganic crystal)	relative	$KE_{\lambda_{light}}$ (eV)	light detection $\left[\int \mathrm{nC}\right]$	$10^{-3} - 10^1$
ionization chamber	relative (transfer*)	$J_{\mathrm{gas}}[^{C}/_{\mathrm{kg}}]$	electrometry [A or C]	$0 - 10^4$

Table 2.2: Summary of dosimeters used and characterized in this work.[37,87,62,72,83] The measured quanta is the expression of the dosimeters physical mechanism due to the absorption ionization energy and the method of readout is the detector system data acquisition processes.

*Certain ionization chamber makes that have been verified as stable and precise enough for transfer calibrations.

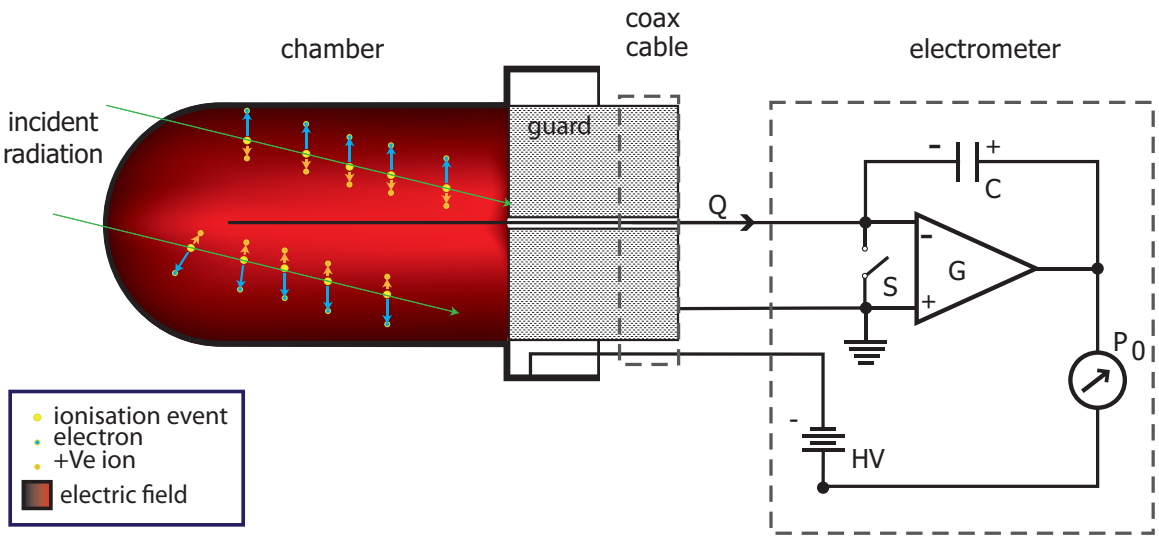

Figure 2.8: Illustration of ionization chamber operation and operational-amplifier electrometer circuit displayed with capacitor for charge collection.

the ion pairs to an electrical signal to be read out with the appropriate electronics (Figure 2.8). Incident charge particles interact with the gas molecules in the ionization chamber cavity volume, instigating ionization events that release a ion pair consisting of a free electron and positively charged gas molecule (+Ve ion). An electric field applied to the chamber volume accelerates the charged particles to the anode and cathode for collection and read out by an electrometer. The electrometer measures electrical current using a ammeter and total charge collection with a coulommeter.

Equation (2.20) demonstrates how an ideal ionization chamber, with perfect collection efficiency, determines dose to the gas (equation (2.20)) by measuring the charge per unit mass of gas $\left(\frac{Q}{m}\right)$ multiplied by the quotient of energy expended by the charged particles required to create the sum of ion pairs $(\frac{\overline{W}}{e})$ equivalent to charge reading Q .

$$\mathrm{D_{gas}} = \left(\frac{Q}{m}\right)\frac{\overline{W}}{e} \tag{2.20}$$

Ion pairs are created when a charged particle directly or indirectly ionizes a

molecule creating a positive ion and negative free electron. The number of ion pairs formed is a function of the gas' $\frac{\overline{W}}{e}$ in [$^{eV}/_{\text{i.p.}}$]. The average $\frac{\overline{W}}{e}$ for a source with a distribution of energies is found using the equation (2.21),

$$\frac{\overline{W}}{e} = \frac{n\overline{\mathrm{T}_0}(1-g)}{Q} \tag{2.21}$$

where $\overline{\mathrm{T}_0}$ is the average charged particle starting energy and Q is the charge created by the number of interacting charged particles, n. g is the radiation yield or portion of the charged particles energy escaping the system as Bremsstrahlung photons. The $\frac{\overline{W}}{e}$ in air is 33.97 [$^{eV}/_{\text{i.p.}}$] and is considered practically constant for fast electrons defined as those with energies above 10 keV. This is the energy where the electrons velocity is more than 10 times the velocity of an electron in the first Bohr orbit of the gas molecules. Energies above 1 keV and below 10 keV are found to have less than a 2% variation in the value of $\frac{\overline{W}}{e}$. $\frac{\overline{W}}{e}$ is dependent on the particles linear energy transfer (LET), with alpha particles having a 3-5% greater $\frac{\overline{W}}{e}$ than lower LET electrons.[59,57] While $\frac{\overline{W}}{e}$ is energy dependent and it has been shown to vary in megavoltage energies, the nominal value of 33.97 is sufficient for the required significant figures and precision in clinical and transfer calibration dosimetry used in this work.

To calculate the clinically relevant quantity of dose to tissue from the dose to gas calculation in Equation (2.20), conversions and corrections must be applied to transfer the dose to air to dose to tissue. An ideal ionization chamber is only a function of $\frac{\overline{W}}{e}$ and is energy independent, but in realistic conditions ionization chamber response as a function of dose to tissue is dependent on beam quality. There are many factors and corrections that must be applied to be able to directly use ionization chambers in radiation dosimetry and there has been substantial research regarding the characterization ionization chambers and their beam quality dependencies.[59,57]

These dependencies are corrected for using beam quality correction factor and are determined for standard broad beam CoP using either calorimetry to experimentally determine or Monte Carlo techniques to computationally determine absolute dose for a given beam quality correlated to an ionization chambers response. The dependencies of ionization chambers are discussed in more detail in Section 2.5.

2.7.2 Lithium Fluoride thermoluminescent dosimetry

Thermoluminescent dosimeters (TLDs) are solid state detectors that have been in use for radiation dosimetry purposes since the 1970s.[54] For many years, the primary use of TLDs was personnel dose monitoring, but their use has also become quite common in the field of radiation therapy. The low atomic number of LiF approximates that of air and soft human tissue[22] resulting in minimal perturbation of the beam and making it a viable cavity theory based detector. TLDs have found applications in both research and clinical work, because they can be adapted to accurately measure dose in a wide variety of conditions. The most common radiation therapy dosimetric applications for TLDs are the following: brachytherapy source characterization for AAPM's Task Group 43 protocol (TG-43), calibration auditing/verification, in-phantom treatment plan verification, various forms of in-vivo dosimetry, and clinical trial assessment.

There are many forms of TL materials on the market, but the most commonly used in radiation therapy is LiF:Mg,Ti, which can be purchased under the trade name of TLD-100 (Thermo Scientific, Franklin, MA). Thermoluminescent dosimeters consist of scintillating crystals containing trace amounts of impurities that provide two types of activation centers: traps and luminescence centers (Figure 2.9). These activation sites allow the crystal to store ionizing radiation induced excitation energy in the form of electron-hole pairs. These traps are stable enough to prevent prompt

recombination and allow the energy to be stored for relatively long periods of time. When a radiation beam interacts with the dosimeter, a quotient of the energy expended by the beam is deposited in the crystal causing a fraction of the atoms to become ionized and allowing the separated charge to migrate to the conduction and valence bands resulting in stable charge storage by the hole-pairs. Figure 2.10 shows an illustration of the TL mechanism for a typical thermoluminescent material.

Figure 2.10 illustrates an example where the electron trap is shallower than the hole trap, but this is not always the case; the hole trap may be the closest to the conduction band. An ionizing event causes an electron to pass into the conduction band and then to be trapped as shown in side A of Figure 2.10. These traps are metastable states that can decay through the emission of light photons as shown in side B of Figure 2.10. The recombination of the electron-hole pair can be induced by heating the material causing crystal lattice vibrations (phonons) that disturb the potential barrier of the traps and allow the recombination to take place which releases energy in the form of visible light. The addition of impurities decreases the amount of heat energy required for recombination of the electron-hole pairs by creating more of these shallower transitional energy states in the crystalline structure. The different energy levels of the crystalline structure can be observed in the readout of the TLD known as a glow curve. The glow curve is a plot of light intensity measured by a photomultiplier tube as a function of applied heat per time. The different energy states reveal themselves in the deconvolution of the glow curve as glow peaks (Figure 2.11). The TL glow peaks correspond to the release of an electron or hole from a particular trapping level (Figure 2.9 and Figure 2.10). In general, higher-temperature glow peaks correspond to traps lying deeper within the band gap and electrons requiring more thermal energy for release. The discrete energy levels correspond to a defect in the TLD lattice. Generally peaks 4 and 5 are optimized when designing a TLD

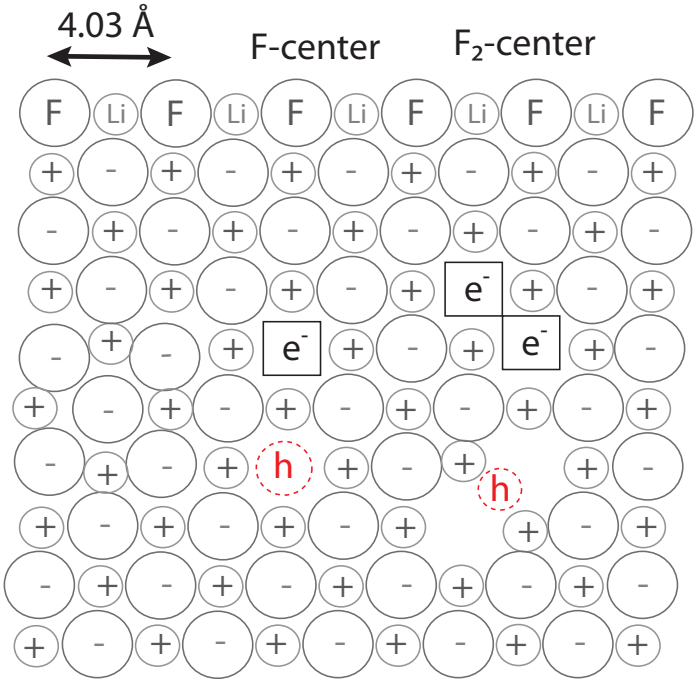

Figure 2.9: TLD luminescent and hole center structures.[10]

dosimetry system.[20,41,53]Thermoluminescent materials are classified by this delayed light energy emission with the application of heat energy.

Thermoluminescent detectors are commonly used as part of the radiation treatment delivery quality assurance program. TLDs can be utilized to compare the actual delivered dose to the predicted dose by the treatment planning system. Generally, TLD-100 micro-cubes ($1 \times 1 \times 1\,\mathrm{mm}^3$) and chips ($3\,\mathrm{mm} \times 1\,\mathrm{mm} \times 1\,\mathrm{mm}$) are used to avoid the complexities that can be associated with dose gradients. The smaller size allows the dose to a smaller voxel to be calculated which is more clinically relevant than an average over a larger volume. Traditionally, high gradient regions are avoided since small uncertainties or errors in positioning can have a large impact on the data collected. TLDs can be used on the skin, in vivo, or in a specially designed phantom. The major drawback of using TLDs is the time required to process and read out the charge that is collected as a result of the radiation.

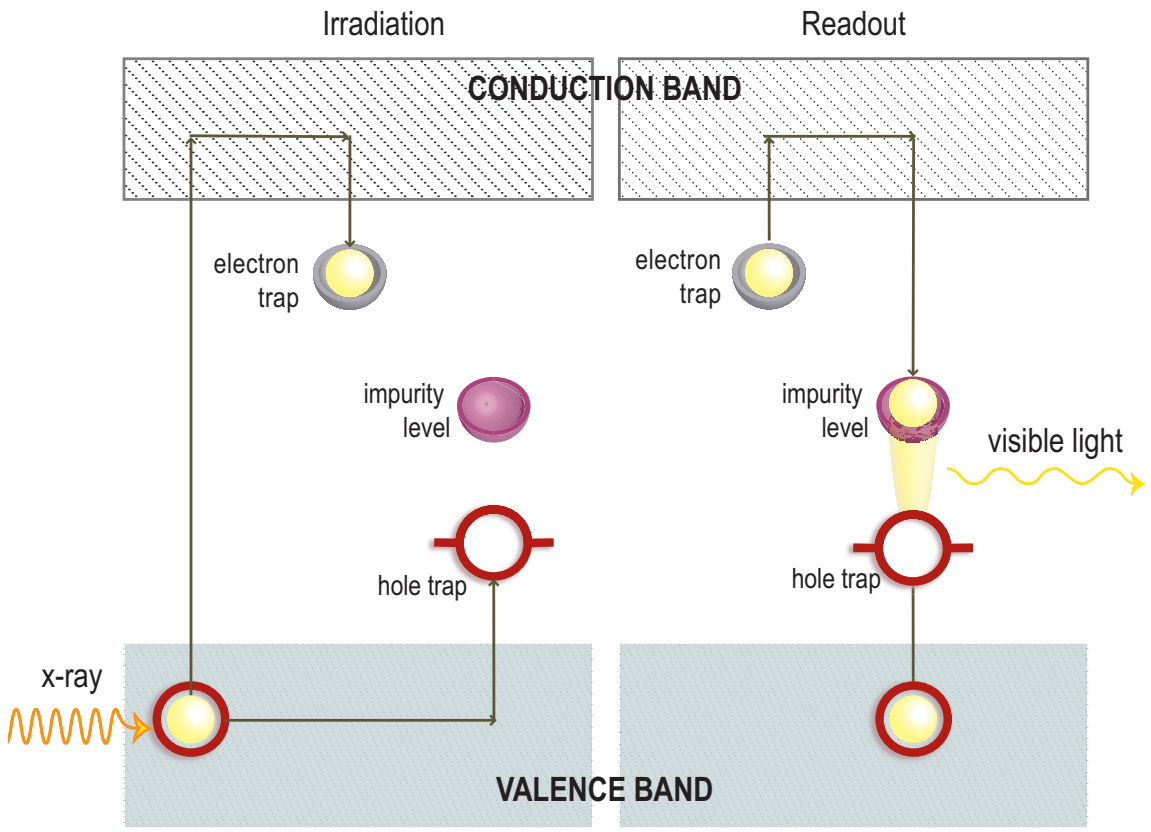

Figure 2.10: Charged particle interactions in the TLD lattice structure deposit a quotient of particles deposited energy which then cause the ionization events in which the separated charges migrate to the conduction and valence valence band resulting in stable charge storage by the hole-pairs.

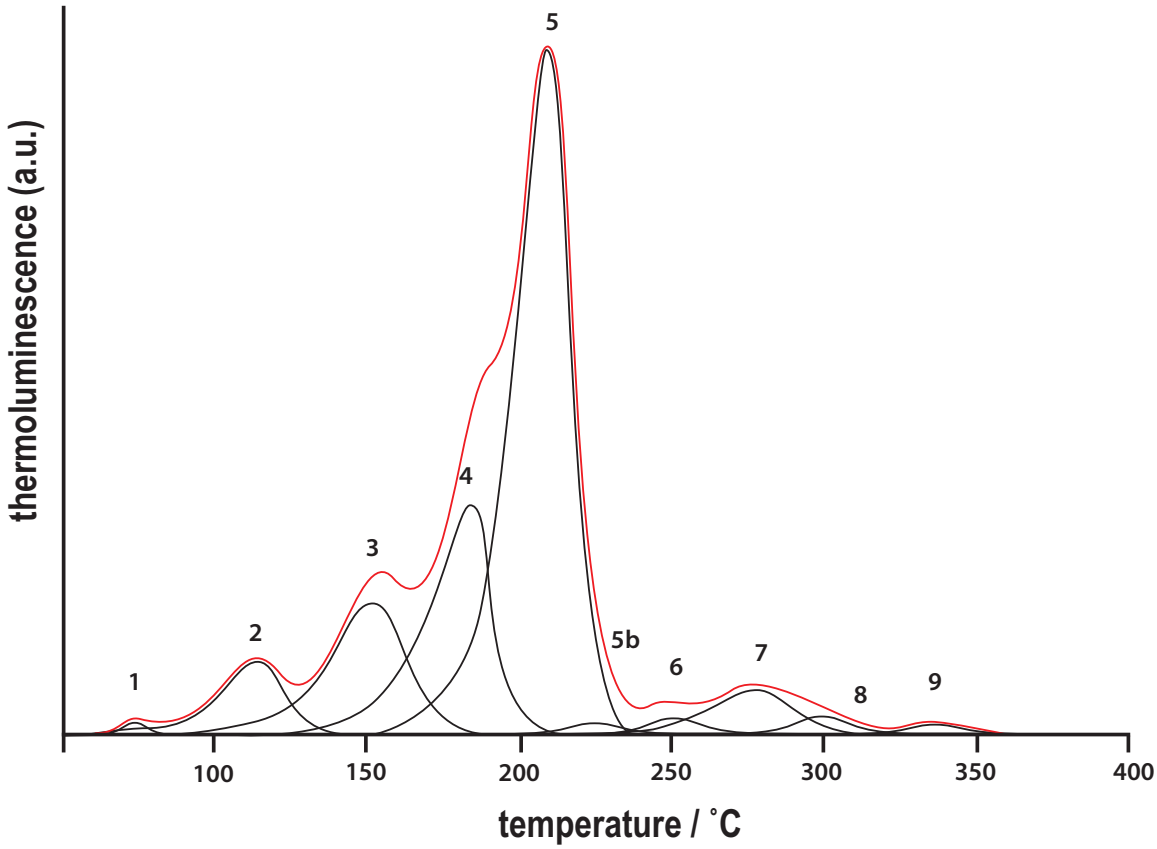

Figure 2.11: Characteristic LiF:Mg,Ti glow curve obtained by measuring the light output as a function of temperature and time. The black lines show the deconvolved glow curve with each peak corresponding to a discrete energy level within the TLD lattice.

Phantoms provide a method for treatment delivery verification using TLDs by providing the appropriate build up and scatter conditions. A phantom can be designed to be tissue equivalent using liquid water or plastics and replicate almost any body region. By designing the phantom to hold TLDs in places of interest where the dose gradient is not extreme, optimal measurements can be made. Although phantoms are difficult to design to be used for patient specific QA, they can be used to test the accuracy of the treatment delivery modality for situations very similar to actual patients. These can be designed to give very accurate results. Using a commercial spherical PMMA phantom to test dosimetry for head and neck cases, it has been shown that the TLD dosimetry is within 2% at isocenter.[73]

Advantages of TLDs include their small size, tissue equivalence, lack of directional dependence, and a well-established characterization and use as a radiation dosimeter. Some disadvantages of TLDs are that they exhibit a non-linear dose response and have an energy dependence.[39,44,62,40] Both dose response and energy dependence can be corrected for when processing the thermoluminescent signal and has been the subject of much research.[25,70,44,62] In this work, an energy correction factor, based on experimental measurements, was applied to correct for the difference in TLD response in a linac-produced MV beam versus the ^{60}Co beam in which the TLDs are calibrated.[44] TLDs require rigorous handling procedures and annealing protocols to obtain acceptable precision. With correct and careful handling the standard deviation have been approximated from 1% to 3%.[9,50,44,54]

2.7.3 L-α-Alanine electron paramagnetic resonance dosimetry

Electron Paramagnetic Resonance (EPR) dosimetry with L-α-Alanine is a standard dosimetry method in most major national metrology institutes for both reference and

transfer dosimetry, including as a secondary standard for dose to water in megavoltage photon irradiations.[52] These include the National Institute of Standards and Technology (NIST, US), the National Physical Laboratory (NPL, UK), the Japanese Atomic Energy Research Institute (JAERI, Japan), the National Institute of Metrology (NIM, China), the Laboratoire de Mesure des Rayonnemants Ionisants (LMRI, France), the International Atomic Energy Agency (IAEA), the European Organization for Nuclear Research (CERN), and many others. The useful dose range for these applications has often been taken to be from 5 to 100 Gy.[37] The use of alanine dosimetry in the clinical setting is currently limited to remote verification systems offered by a few of the national labs.

Molecular alanine is a nonessential amino acid in human physiology that is a constituent of many proteins controlling functions such as the transport ammonia from muscle to liver via bloodstream. Alanine for radiation dosimetric applications is classified as a solid state organic crystalline dosimeter. The alanine crystal structures can be found in nature or synthesized in a laboratory. Naturally occurring alanine bio-dosimeters include tooth enamel, bone, and quartz; these materials are used for retrospective environmental health physics applications such as accidents and epidemiological dose reconstructions. Therapeutic radiation dosimetric applications use commercially grown alanine with a refined crystalline lattice structure to improve precision and reproducibility (Figure 2.12). While TLD and alanine are both solid state crystalline dosimeters, they employ different solid state mechanisms to retain the energy deposition in the detector due to charged particle interactions and dosimeter mechanism-specific readout methods to release and record the energy deposition. Electron paramagnetic resonance (EPR) dosimetry with L-α-alanine has been in development since the 1980s for therapeutic radiation dosimetry.[74,75]

The basic concept of mass charge is well understood in radiation physics as

Figure 2.12: Laboratory grown L-α-Alanine crystal

Figure 2.13: L-α-alanine radiation dosimeters

an intrinsic property of an electron. A less common intrinsic property of electrons in radiation physics is its magnetic moment.[26] The magnetic moment of an electron is dependent upon the molecular structure. The magnetic moment of a molecule is defined by the electrons occupying either of two spin states (ms=+1/2 or -1/2). The quantum-mechanical spin state of an electron, or any elementary particle, is an intrinsic form of angular momentum. Alkali atoms express a characteristic spectra in a strong magnetic field that is indicative of their molecular structures orbital electrons expressing a magnetic moment that is linked to electron spin (Figure 2.14).

Radiation interactions with alkali materials produce dose-dependent paramagnetic centers or unpaired electrons in the form of stable radical alanine species. Irradiation of the polycrystalline L-α-alanine creates unpaired electrons and the resultant stable alanine deamination radical, the hydrogen abstraction radical, and the (COOHCCH3)NH2+ radical (Figure 2.15).[45] EPR/alanine dosimetry systems detect the the formation of radiation induced free radicals based on their characteristic magnetic moment. The deamination radical is the primary stable radical and produced via a reductive pathway involving the protonated anion.[45,68] The primary stable alanine radical is shown to exhibit structure 1 and is formed by deamination from a protonated alanine radical anion. EPR measurements of the stable alanine radical

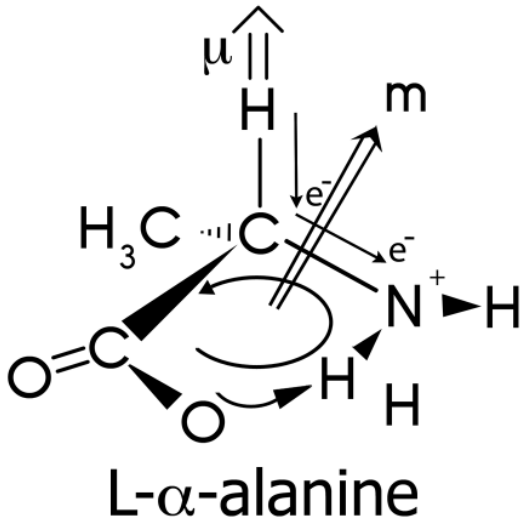

Figure 2.14: Magnetic moment of the paramagnetic species L-α-Alanine. L-α-Alanine oscillating molecular structure and subsequent electronic current results in a magnetic dipole moment, m, and electric dipole moment, μ.[97]

is mainly due to interactions of the unpaired electron with the proton bonded to C_2 and with the three equally coupled (rotationally averaged) methyl protons. At least two other radicals are present in radiation dosimetry applications including the hydrogen abstraction radical and the $-NH^2$ radical, shown in equilibrium in Figure 2.15, and are taken into account in high precision dosimetry applications.[80] The magnetic moment linked to these radicals differ from the initial alanine molecule and from each other. The radical molecules are detected by reading their characteristic energy distribution using EPR spectroscopy. The concentration of the radicals is proportional to the absorbed dose.[30]

EPR is a spectroscopic technique which detects species that have unpaired electrons. It is also often called ESR, Electron Spin Resonance. EPR detects the resonant absorption of microwave energy, set to a fixed frequency, in paramagnetic species by transition of the spin of an unpaired electron from one energy level to the next in the presence of a strong magnetic field (Figure 2.16). Microwaves of

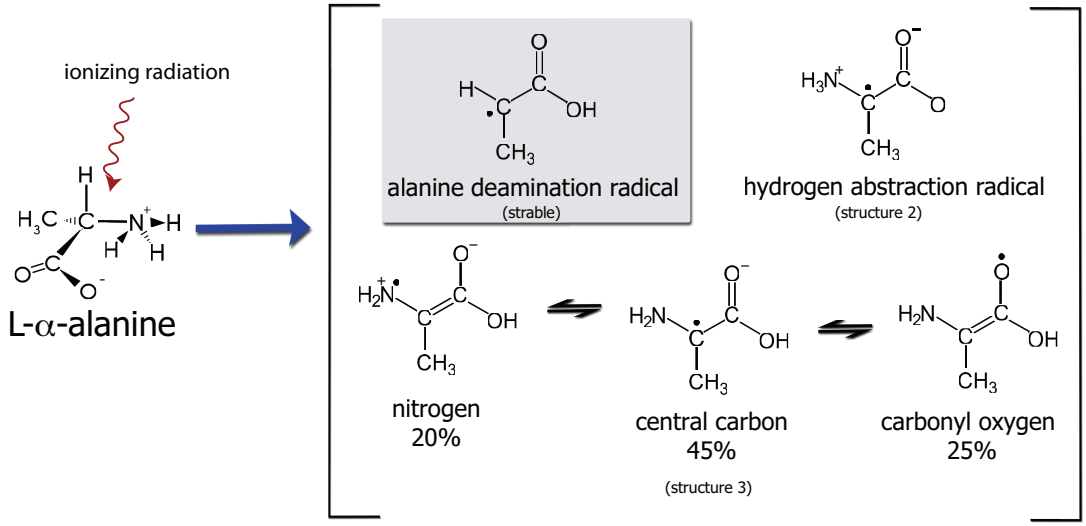

Figure 2.15: Illustration of L-α-alanine radical formation due to interactions with ionizing radiation.

a constant frequency are incident upon the L-α-alanine sample and the reflected waves are measured. A strong magnetic field is applied to the sample and at the frequency correlating electron spin states energy differential. The introduction of a strong magnetic field increases the gap between the two electron spin states. When the electromagnetic induced frequency between electron spin states corresponds to the microwave frequency, one of the two electron spin states becomes more statistically favored and the electrons in the bound ionized L-α-alanine radical transition between energy state in what is know as a spin-flip transition(Figure 2.17).[42] A single electron in free space has a fundamental property associated with it called spin, arising from the spinning of an asymmetrical charge distribution about its own axis. The electron spinning about its axis has associated with its motion a well defined angular momentum. Each electron has the possibilities of a +1/2 or -1/2 spin-spin state. In addition the angular momentum magnetic quantum number of the electron Azimuthal/Orbital angular momentum interact with the spin-spin states to create

additional energy levels. There are (2l +1) values of ml for each l value.

These transitions allow for the absorption of the microwave energy and thus the detection of the energy transitions. The magnitude of the applied magnetic field will will reveal the difference between the energy states and thus the corresponding ionization species. The intensity of the transition is proportional to the number of unpaired spins in the material and thus the absorbed dose.[89,87,80] The result is a characteristic absorption resonance spectra. A derivative is taken over a define section of the absorption curve as a function of applied magnetic field revealing the samples identifying spectra characteristics such as shape, width, intensity, and spectroscopic splitting factor (g-factor). An alternative is to take the amplitude of the most intense central line of the EPR signal, under the assumption that the shape of the EPR signal is invariant to the absorbed dose.[71] EPR resonance wavelength is at approximately $0.3\,\mathrm{cm}^{-1}$ for detection of the deamination radical. For calibration a peak to peak amplitude of a subset of the spectrum lines corresponding to the radiation induced radicals of interests spin-flips energy level is taken and the signal is normalized to the ^{60}Co spectrums corresponding amplitudes.

Advantages of the alanine/EPR system are its near water equivalence, directional independence, and minimal energy dependence.[75,85] The method is suitable for measuring gamma and x-rays, electrons, protons, and high-LET radiation of doses in the 1 Gy to 100 kGy range. The detectors are just about sensitive enough for measurements in small therapy-level fields and are close to water-equivalent (density, atomic no.), enabling reduction of the perturbation of the beam through the detector volume. The energy dependence of alanine has been thoroughly studied for high-energy photons and was generally found to be less than 1%.[8,102] In addition, the decay rate is minimal at approximately 0.5% to 1.5% per year following ^{60}Co and Linac-produced x-ray or electron exposures.[36] The radicals in alanine are unusually

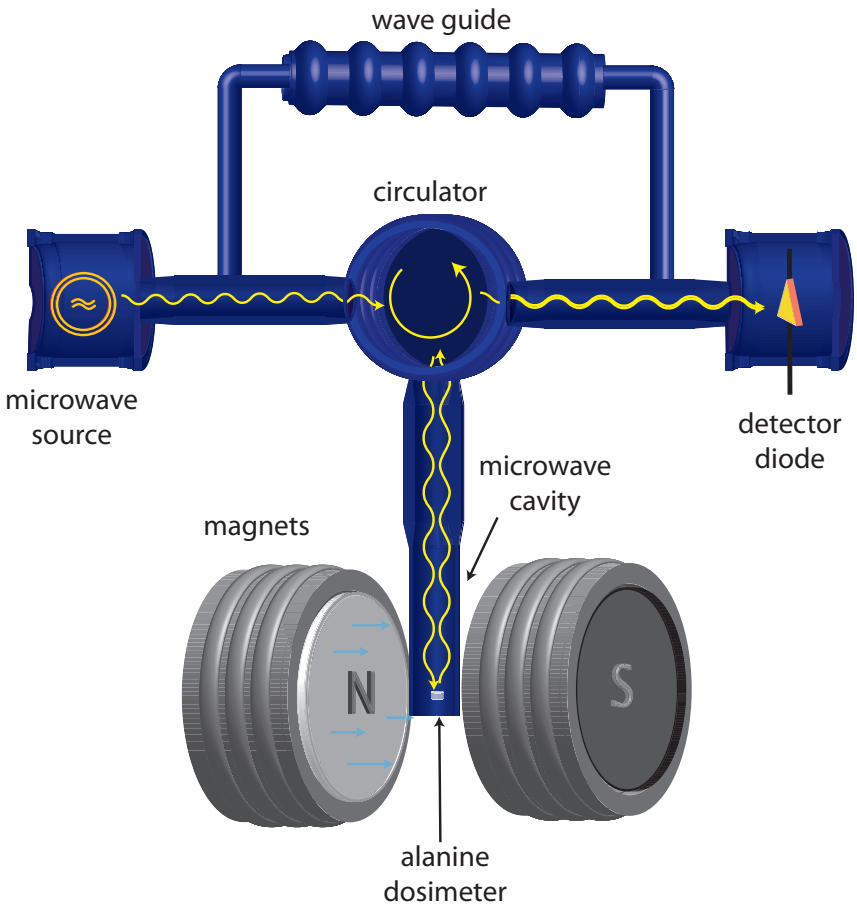

Figure 2.16: Electron paramagnetic resonance spectrometer for the readout of irradiated L-α-alanine dosimeters.

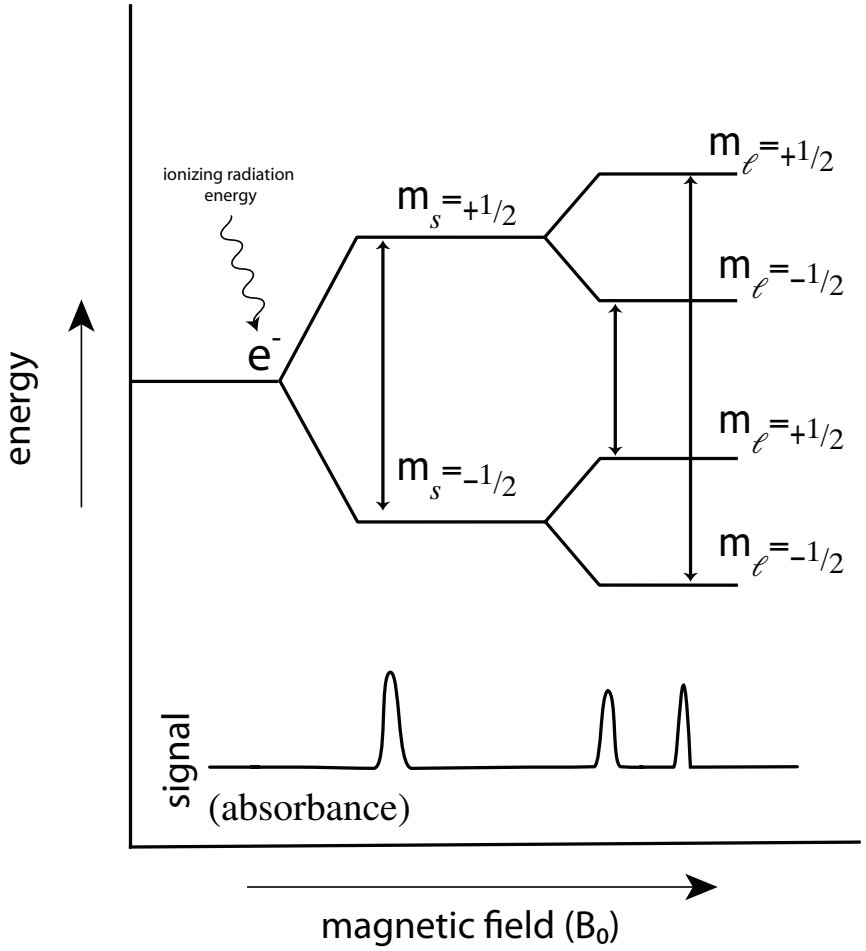

Figure 2.17: Discrete energy states of a paramagnetic species unpaired electrons induced by ionizing radiation. ms identifies the orientation of the spin of one electron relative to those of other electrons in the system.

stable because of the crystalline form, and in pure dry crystals the signal loss is only about 4% during the first year after irradiation.[8,12,18,37,42]

Some disadvantages of alanine dosimetry include its temperature dependence and dose sensitivity. Alanine dosimeters are sensitive to the temperature in which they are irradiated and demonstrate a complex dose-temperature-dependent behavior. It is important that the temperature in which the irradiation occurs is carefully monitored so that corrections can be applied.[88] The dose-sensitivity of alanine is also an important issue, with it increasing as a function of dose. Historically, doses for alanine have ranged from 40 Gy to 100 kGy. Recently, alanine radiotherapy applications that require lower doses have become available for exposures from 5 to 10 Gy. In addition, alanine sensitivity depends on the dosimeters physical size (mass) to obtain a relevant SNR. Currently they are available in cylinders with Ø5 mm (diameter) × 1 mm (length) nominal dimensions and investigations are underway for micro Ø1 mm × 1 mm rods. These limitations have made alanine less suitable for clinical use, but are well apt for precise research applications and secondary standard laboratories calibration transfers.

2.8 Project motivation and goals

Advancements in radiation therapy treatment techniques have lead to the utilization of small and nonstandard fields to achieve precise dose-conformality and enabled the possibility for margin reduction. Biological optimization through hypo-fractionated treatment schedules has increased the dose per fraction for SRS and SBRT treatments. The use of decreased margins and escalated dose per fraction increases the magnitude of negative repercussions due to miscalibration and necessitates strict QA protocols

and improved dosimetry for the small and nonstandard fields used in these advanced treatment modalities.

Current absorbed dose to water extrapolation methods from standard CoPs broad beam reference conditions to clinical small fields involve output factor measurements using ionization chambers, diodes, or gafchromic film. These methods have been shown repeatably to have beam quality dependencies that lead to increased uncertainty in the ascertained absorbed dose. There has been a need for a revised protocol for the dosimetry of small and nonstandard fields that addresses these issues. Currently the IAEA and AAPM are working towards a new standardized formalism, which will be used as the starting point for this dissertation.

The primary objective of this dissertation is to design and demonstrate a viable methodology for transferring ionization chamber calibration coefficients from a primary or secondary standard laboratory to hypothetical clinical small and nonstandard reference fields in accordance with emerging dosimetry formalisms. This is accomplished through the characterization of two possible dosimetry systems for the transfer of absorbed dose to water standards to the end user beam, using a detailed calibration coefficient transfer pathway designed to maintain metrological traceability. The last step of this work set up a computational model based on the experimental findings for calculations of ionization chamber beam quality correction factor designed for eventual use with future small and nonstandard field protocols.

Chapter 3

TLD system characterization for absorbed dose to water determination in high energy photon and electron beams

3.1 Introduction

Thermoluminescent dosimeters (TLDs) can be used as a quality assurance technique to measure absorbed dose to water by calibrating them to a known dose from ^{60}Co beam traceable to a primary standard. TLDs have an inherent uncertainty due to statistical variations in their solid state response mechanisms which results in a minimum response uncertainty of approximately 1.5% at one sigma (Section 3.6). Traditional use of TLDs for radiation safety applications and patient specific dose estimates can have associated uncertainties on the order of 10%-30% due to beam quality dependent TLD response factors and the lack or inability to properly characterize the incident beam quality in these applications. This uncertainty can be reduced though precise TLD response characterization and handling methods. Advanced TLD characterization methods can measure absorbed dose to water with an associated uncertainty approaching the TLDs inherent uncertainty level which enables TLDs to

be utilized in sensitive applications such as research dose measurements of standard quantities and clinical calibration dosimetry.

Conversion from absorbed dose from a standard ^{60}Co beam quality to absorbed dose from a linac beam quality (Q) requires an energy correction factor to account for the difference in the solid state response of the thermoluminescent material in different radiation qualities. The energy correction factor allows for a therapy-grade level of precision in absorbed dose to water determination and enables TLDs to be utilized as a method for primary standard calibration coefficient transfer and secondary verification of linac output calibration referenced to a NIST traceable standard. Secondary external verification is an essential part of a radiation clinic's quality assurance program. This research characterizes a TLD dosimetric system for therapy-grade dose measurements and provides measurements of the energy correction factor of LiF:Mg,Ti, also know as TLD-100, (Thermo Scientific, Franklin, MA) chips for high energy electron and photon beams, relative to ^{60}Co.

3.2 Absorbed dose nomenclature

There are three sets of measurements required to calculate the absorbed dose: the measured TLD response, system calibration factor, and "batch characteristics" (i.e. energy correction, non-linearity correction, and fading correction).[70] Absorbed dose (D_w^Q) determined by TLD-100 was calculated using the standard equation[62] (equation (3.1)), which fully corrects for the TLD energy dependence and dose dependence compared to ^{60}Co.

$$D_w^Q = \mathrm{TL} \cdot S \cdot K_L \cdot K_e \cdot K_f - \mathrm{bk} \tag{3.1}$$

Equation (3.1) was used to determine absorbed dose (D_w^Q) to water using equation (3.1), where TL is the mean thermoluminescent response per scalar response

$[^{TL}/_{\text{scalar}}]$, and S is the system calibration coefficient determined from an exposure traceable to a primary standard value. K_L is the dose-response linearity correction as a function of intrinsic and extrinsic dose-response factors (Section 3.4). K_e is the energy correction factor to convert the absorbed dose system calibration factor from the standard beam quality to the user beam quality Q (Section 3.5). K_f is the fading correction to account for signal reduction as a function of time. To account for baseline TL response (bk), 10 to 20 TLDs were not irradiated and used as background controls.

The system calibration factor (S), also referred to as the sensitivity factor, is the only factor that must be determined for each readout session. S is the system calibration coefficient is the absorbed dose per unit TL response and is given in units of Gray per TL per scalar, $[^{Gy}/_{\frac{\text{TL}}{\text{scalar}}}]$. The ^{60}Co standard source is used in this work to determine the sensitivity and calibrate the TLD set. S is defined by the dose delivered by ^{60}Co to the standard TLD set divided by the thermoluminescence response corrected for fading and dose response nonlinearity. S is given in absorbed dose per unit TL $[^{\text{Gy}}/_{\text{C}}]$ and is defined in equation (3.2). TL is the mean thermoluminescent response of the ^{60}Co irradiated TLDs [nC]. The subscript "0" indicates the terms that were determined for the ^{60}Co standard source.

$$S = \frac{D_0}{TL_0 K_{f_0} K_{L_0}} \tag{3.2}$$

The factor K_f corrects for fading of the TL signal as a function of time, as a TLD's thermoluminescent response will decrease as a quotient of the traps are spontaneously released at lower temperatures. For this work, all TLD's are read out at approximately the same time and the time span between exposure and readout is relatively short resulting in a negligible fading correction (K_f= 1). An experiment was also performed

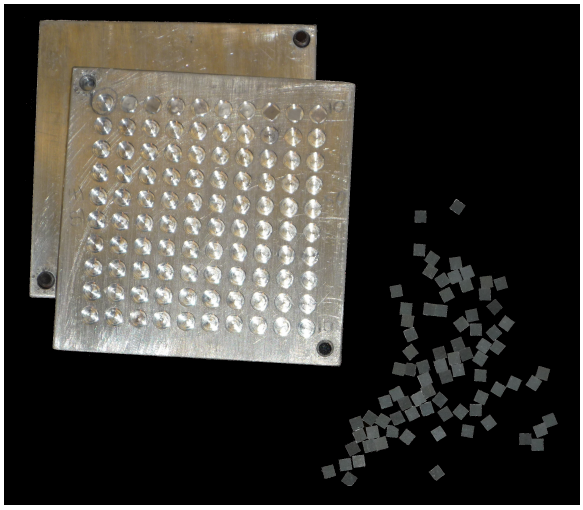

Figure 3.1: TLD-100 (LiF:Mg,Ti) thermoluminescent dosimeters with oxidized aluminum annealing tray.

to test what the extent of fading would be over the time period of a month and the fading factor was found to be inconsequential. Based on these studies, this work assumed that fading was not an issue at the energies and doses used and is not discussed further.

3.3 General methods

TLD-100 (LiF:Mg,Ti) were used to measure absorbed dose to water in this work (Figure 3.1). The nominal dimensions of the TLDs were $(3.2 \times 3.2 \times 0.89)$ mm^3.

3.3.1 Initial sorting criteria

A set of 380 TLD chips was selected from an initial batch of 800 TLDs using a standard sorting process used at the University of Wisconsin Medical Radiation Research Center (UWMRRC). The initial TLDs were chosen based on sensitivity

(within 2% of the mean reading) and reproducibility (within 1%) from the initial batch of 800 TLDs. The 800 TLDs were measured 5 times for the initial sorting.

3.3.2 Annealing protocol and TLD readout data acquisition

TLD chips were annealed prior to each use, to prevent residual signal from uncleared traps. The annealing procedure consisted of a 400 °C anneal for 60 minutes, 15 minute cooling to room temperature on an aluminum plate, and an 80°C anneal for 24 hours. TLDs were annealed in oxidized aluminum (Al^2O^3) trays with individual holes to hold the TLDs in place. In order to oxidize the aluminum trays and create a nonreactive surface, the trays were heated to 400°C for at least 6 hours prior to use with TLDs. TLDs were irradiated at least 12 hours after annealing.

The TLD chips were read using a Harshaw 5500 (Thermo Scientific, Franklin, MA) hot nitrogen gas reader at least 24 hours after exposure (Figure 3.2). The time-temperature profile for the reader included a 50°C preheat, followed by a data collection region that used a $10°Cs^{-1}$ heating rate and a maximum temperature of 350°C. The photomultiplier tube (PMT) charge collection is integrated over the temperature ramp-up and plateau regions of the heating profile to obtain the final TLD readout in nanoCoulombs (Figure 3.3). TLDs were marked on one side to ensure consistent orientation toward the PMT for all reads. The post-irradiation 24 hour read-out delay and 80°C anneal were used to reduce signal from the lower energy traps with low half lives.

3.3.3 Relative response coefficients (n_{cc})

The mean thermoluminescent response per scalar response [$^{TL}/_{\text{scalar}}$] was obtained using the individual chips relative response coefficients (n_{cc}, Eq. 3.3). The n_{cc} scales

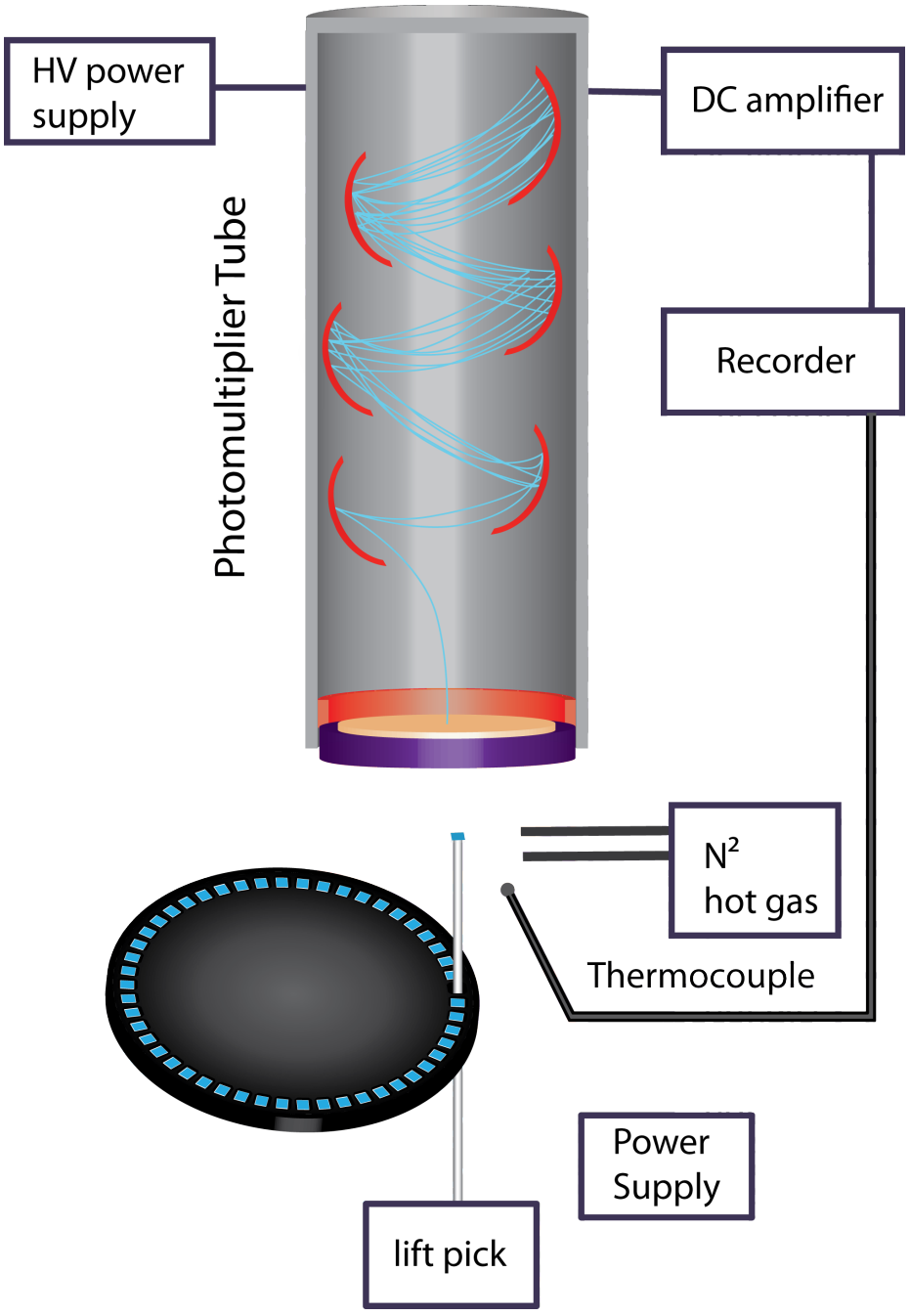

Figure 3.2: Generic TLD hot gas reader schematic. TLDs are heated with hot nitrogen gas and the light output is collected by a photo-multiplier tube. The signal is amplified and recorded as a function of time and temperature from an integrated thermocouple.

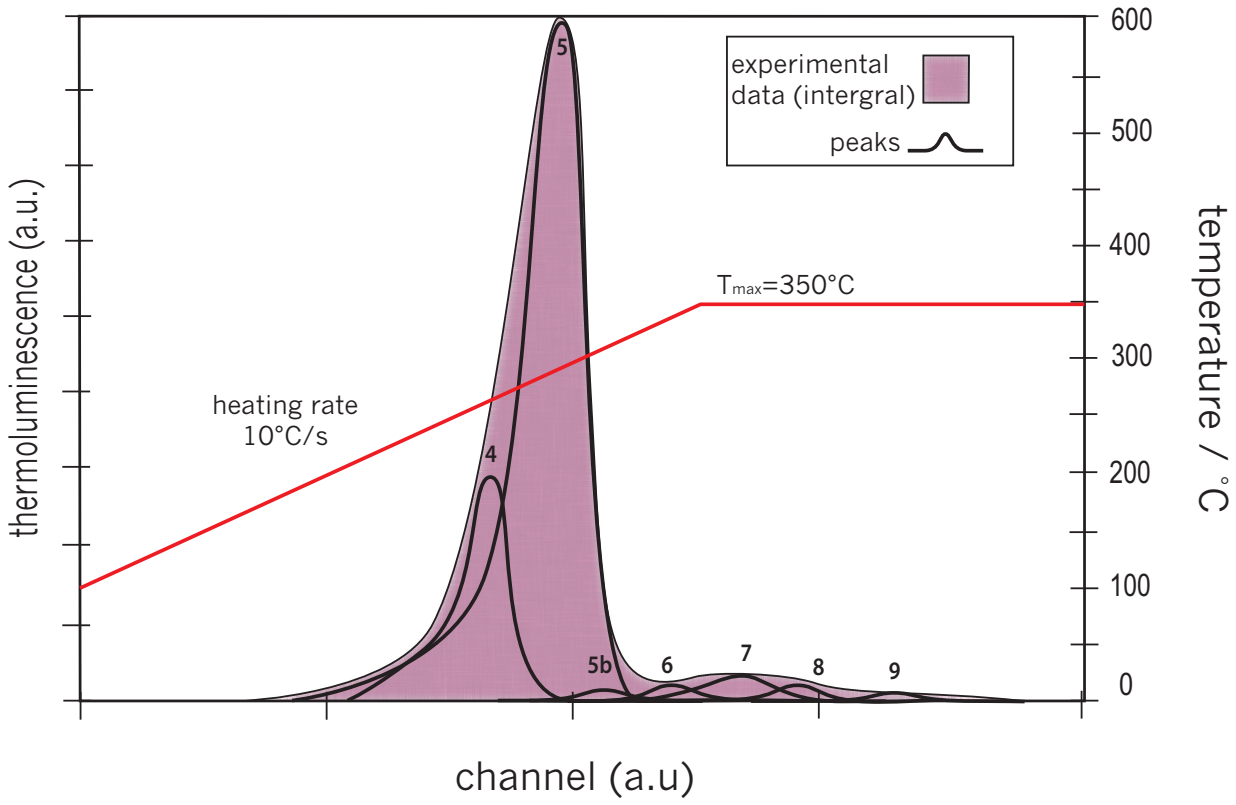

Figure 3.3: Example experimental TLD data acquisition of a characteristic TLD-100 glow curve. Annealing treatments before irradiation alter the optical absorption spectrum favoring the energy band absorption corresponding to peak 5 (Figure 2.9 and Figure 2.11). An integral of the signal over the data acquisition period is used for the final raw TL signal.

the raw TLD light output measurements (TL_{raw}) [nC] of an individual TLD to the median response of the TLD set .

$$TL = (TL_{raw} \cdot n_{cc}) \tag{3.3}$$

Relative response coefficients (n_{cc}) were determined using ^{60}Co exposures in the University of Wisconsin-ADCL Theratronics El-Dorado 78 ^{60}Co irradiator. TLDs were irradiated in a polymethylmethacrylate (PMMA) positioning jig that held 100 TLDs in a $(10\,\mathrm{x}\,10)\,\mathrm{cm}^2$ square plane perpendicular to the central axis of the ^{60}Co beam (Figure 3.4). The positioning jig was comprised of two square PMMA pieces. The front face was 5.2 mm thick and a back face was 8.8 mm thick. The 5.2 mm of PMMA front face was sufficient to provide charged particle equilibrium in the ^{60}Co beam. Equally spaced cylindrical wells of approximately 6 mm diameter and 1.1 mm depth were drilled into the back-face to accommodate 100 TLDs. The wells created an approximate 0.2 mm air gap around the TLDs. Monte Carlo simulations demonstrated a negligible effect on dose uniformity across the TLD plane due to the presence of this air gap. The $(10\,\mathrm{x}\,10)\,\mathrm{cm}^2$ jig was irradiated in a $(20 \times 20)\,\mathrm{cm}^2$ field size with a 100 cm source-to-detector-surface distance providing uniform exposures to the TLD set.

Irradiation times for relative response coefficient exposures were performed for equivalent doses to water of approximately 2 Gy equivalent. Doses to water was determined using air kerma measurements on a reference date using a NIST-calibrated ionization chamber, corrected for source decay, and converted to dose to water using Monte Carlo methods. Relative response coefficients were calculated by taking the individual TLD responses (TL_x) relative to the median of the set of 380 chips (TL_{median}), as

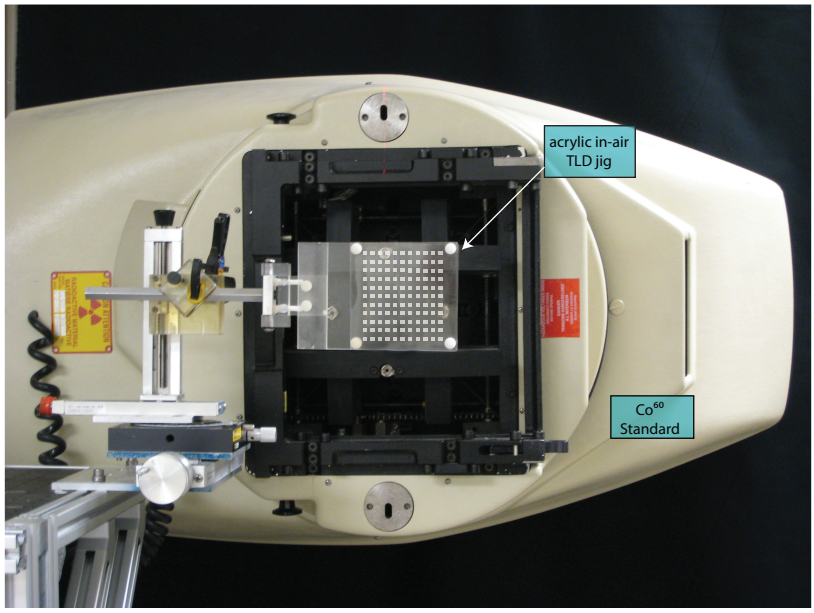

Figure 3.4: Experimental set up to determine in air relative response coefficients (n_{cc}) with PMMA TLD holder.

demonstrated in equation (3.4).

$$n_{cc} = \frac{\mathrm{TL}_x}{\mathrm{TL}_{\mathrm{median}}} \tag{3.4}$$

n_{cc}were determined for each of the 380 TLDs before and after an experimental investigation. The average of the relative response coefficients from before and after was applied to experimental TLD data. By carefully tracking the relative response factors, it was possible to maintain a high level of precision in the experiments. Relative response coefficients were tracked for the individual TLDs (n=380) through a time period of 6 years. The TLD set response reproducibility is discussed in the investigation described in Section 3.6.

3.4 Dose response linearity correction (K_L)

The factor K_L in Equation (3.1) corrects for the nonlinear dose response of the TLD. Studies have shown the dose response to be nearly linear from 100 - 500 cGy, with typically less than a 2% correction for doses from 200 to 400 cGy.[56,41,51,64] This level of uncertainty is acceptable for personnel dose monitoring, but correcting for this non-linearity was essential in this work where the measured correction factors were often less than 2%.

TLD dose response non-linearity was corrected using an experimentally determined correction program at the UWMRRC. TLD dose response is a function of both intrinsic ($K_{L_{\text{int}}}$) and readout system ($K_{L_{\text{sys}}}$) factors (Equation (3.5)).

$$K_L = K_{L_{\text{int}}} \cdot K_{L_{\text{sys}}} \tag{3.5}$$

$K_{L_{\text{int}}}$ corrects for the intrinsic response of the TLD due to the light emission from the solid state mechanics detailed in Section 2.7.2. $K_{L_{\text{int}}}$ is a function of the light emitted by the detector per unit absorbed dose due to the intrinsic characteristic of the energy levels of the electron-hole traps in the TLD crystalline structure. This quantum-physical relationship is dependent on both beam energy and type (beam quality). $K_{L_{\text{sys}}}$ refers to the response of the detector readout system as a function of dose and is influenced by the detector electronics and procedures. Ultimately, $K_{L_{\text{sys}}}$ is a function of the PMT readers luminous intensity [cd] to current [A] conversion as a function of dose.

It is not possible to delineate the $K_{L_{\text{int}}}$ from $K_{L_{\text{sys}}}$ as there is no direct method to measure the luminous intensity of the TLD process. Measurements of the PMT dose-response K_L using TLDs will inherently include both factors. To deconvolve

$K_{L_{\text{int}}}$ from K_L, $K_{L_{\text{sys}}}$ would need to be calibrated against a known light quanta. This work required corrections for both factors, so the specific elements were not deconvolved.

The PMT in the Harshaw 5500 hot gas reader used in this work displayed a nonlinear dose-response at high TL induced currents.[70] Without correcting for the PMT over response, the TLD data demonstrated a nonlinear dose-response at exposures above approximately 1 Gy equivalent absorbed dose to water. The PMTs nonlinearity response as a function of dose was characterized by taking measurements at a number of dose points ranging from 0 to 10 Gy. It was found that for doses between 0 and 10 Gy the PMT over-responded from 0% to 60%. A correction algorithm from these experiments was developed for the UWMRRC TLD laboratory and was applied to all TLD measurements in this work. The PMTs nonlinearity corrections for the dose points (0 to 3 Gy) used in this work ranged from 0% to 12%. The correction values are compared with values of intrinsic TLD dose-response non-linearity from Horowitz et. al in Figure 3.5. It can be hypothesized from the work of Horowitz et. al[38] that the K_L correction algorithm is primarily due to the PMT non-linearity and not the dose response for the dose ranges used in this work. In either respect, both were corrected for with the in house dose-PMT-nonlinearity corrections. To verify dose nonlinearity was accounted for in the experimental beam qualities, TLDs were irradiated to varying absorbed dose levels of 100, 150, 200, and 300 cGy during the experiment. The dose-response curve from the experimental beam qualities was normalized to a ^{60}Co dose-response curve read in the same batch to enable temporal and beam quality dose-response comparisons, as discussed in Section 3.4.1. The PMT corrected dose-response were found to be linear using the UWMRRC correction algorithm over the beam qualities and dose points investigated in this work.

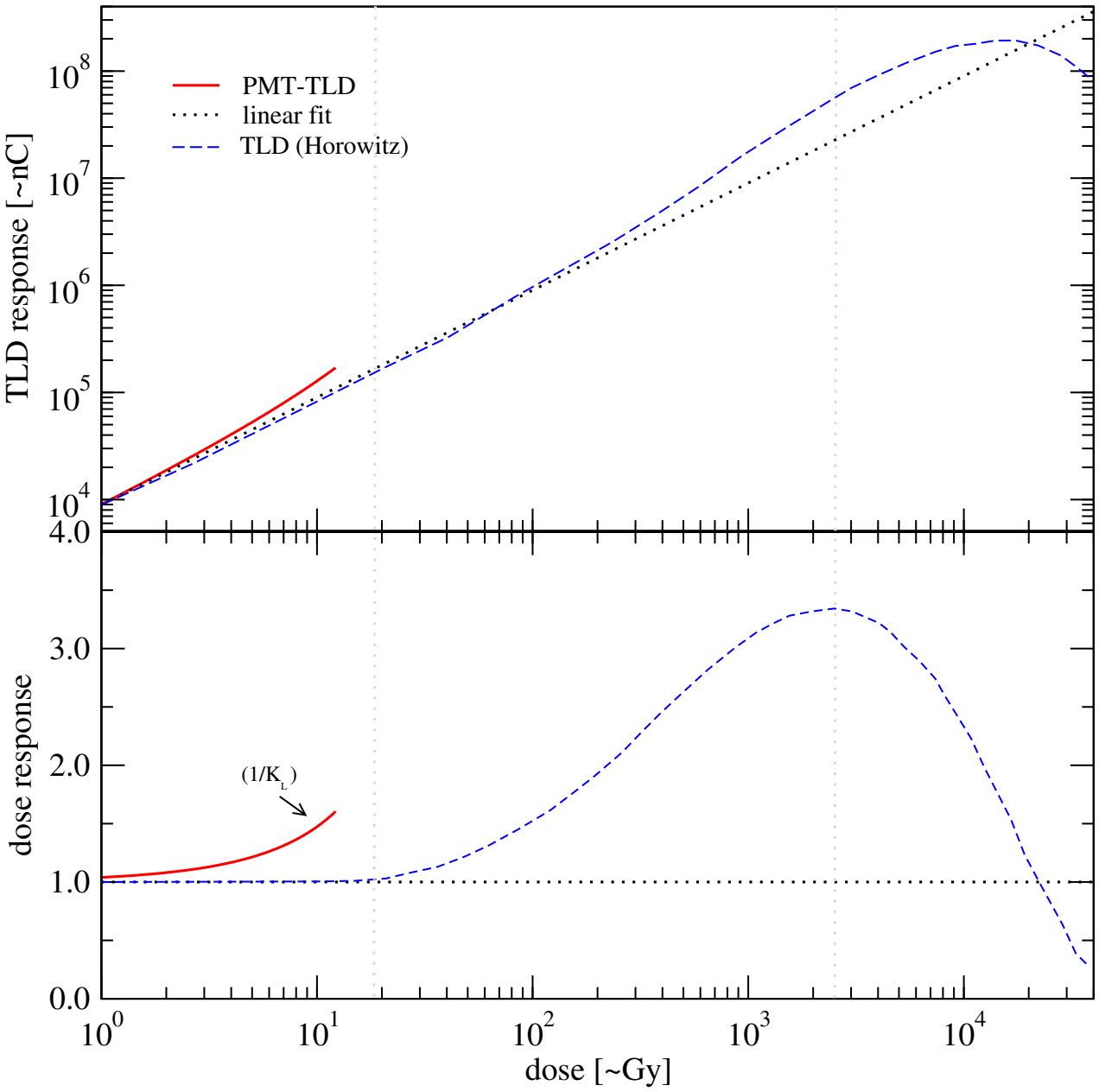

Figure 3.5: The normalized TLD response as a function of dose (top) and the dose response relative to the linear function to illustrate linearity, supralinearity, and sublinearity (bottom). The K_L correction algorithm is the inverse function of the over-response at high currents (red). $K_{L_{\text{int}}}$ values determined by Horowitz et. al[38] (blue) show that the K_L for the dose ranges used in this work are primarily due to non-linearity of the readout systems PMT dose response function.

3.4.1 Temporal considerations

An investigation was performed to characterize the stability of PMT dose-response as a function of time (response-sensitivity function). A set of 300 TLDs were irradiated to multiple dose points and then read out over the course of 15 days. The PMT was found to have high temporal variations in its response-sensitivity function, as shown in Figure 3.6, with the overall dose-response function expressing uniform positive or negative gain. The standard deviation of the PMT dose-response function over the course was found to be $\pm 5\%$ (Figure 3.6). Any fading over the course in the TLDs signal was considered null, this is supported by the positive trend in the first half of the experiments time frame. Due to the variability in the PMT response-sensitivity function, all experimental raw light output readings were normalized per PMT data acquisition session to a set of TLDs exposed to a known dose level from a well characterized standard source (control TLDs) to enable inter-comparison of the raw TLD light output between temporally variant experiments.

The large quantity of TLDs required for each experiment resulted in a single PMT data acquisition session spanning up to 8 hours. The PMT response-sensitivity function was monitored over the prolonged time interval by temporally placing control TLDs at the beginning and end of every sequence of 50 TLDs to establish control points. Generally, each control point consisted of the average of 5 sequentially analyzed TLDs exposed to an experimentally relevant dose from the ^{60}Co standard source. To account for any variability in PMT response-sensitivity across the PMT data acquisition period, each control point was analyzed against the average over all the control points. The average of all the control TLDs was used for normalization if their standard deviation was less than the inherent uncertainty of our TLD methods (1.5%), indicating a constant PMT response-sensitivity across

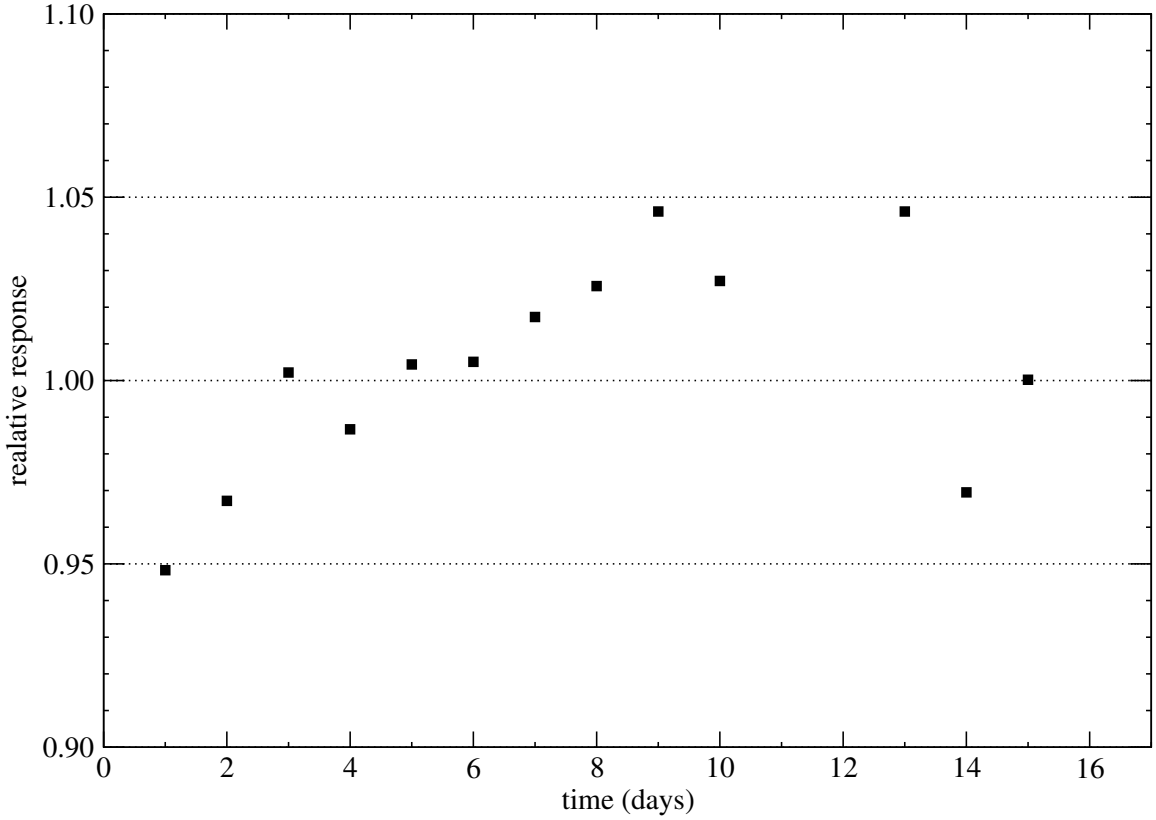

Figure 3.6: Temporally variant response of the Harshaw 5500 automatic TLD reader relative to the final reading

the data acquisition session. If the standard deviation of the control TLDs varied by more than the inherent uncertainty, an average of two adjacent control points was used to normalize the experimental TLDs located temporally between their data acquisition positions and account for the PMT response-sensitivity function. In a few rare circumstances adjacent control points displayed PMT reader variations outside of the expected inherent uncertainty that could not be accounted for and the data had to be discarded. These instances generally indicated a larger issue with the PMT and were not representative of the normal temporal stability of the PMT response-sensitivity function.

3.5 Energy correction (K_e)

TLDs posses a nonlinear energy response and have been found to over-respond at low energies[70] and under-respond at high energies relative to ^{60}Co. The energy response correction factors determined in this work accounts for the differences in TLD light output per unit dose as a function of beam quality for varying nominal photon and electron beam energy relative to the TLD response in the ^{60}Co standard source beam quality. Dose was measured using a calibrated ionization chamber in the same measurement conditions. This is an essential correction if TLDs are to be used alone in determining clinically relevant values of absolute dose to water (Section 3.5).

The aim of this investigation is to determine the relationship between measured TLD light output per unit absorbed dose to water as a function of energy for high-energy photon and electron therapy beams. This relationship is used to determine the TLD energy correction factor, represented by the variable K_e. The energy correction factor relates the TLD dose-response in a linac of beam quality, Q to the TLD dose-response in the traceable ^{60}Co calibration standard. K_e accounts for the difference in response of TLDs in nC light output per unit dose for different beam qualities relative to ^{60}Co. For this work, dose is determined using standard absorbed dose to water protocols based on ionization chamber dosimetry in the same conditions. K_e is an essential correction for determining absolute dose using TLDs without an additional reference dosimeter.

K_e was determined experimentally by taking the ratio of the response of a TLD set exposed to the beam quality of interest (Q) over the response of the set exposed to ^{60}Co, both normalized to absorbed dose determined using standard CoP ionization chamber measurements. The factor K_e is not a measure of the true "energy

dependence" of the TLD, but relative energy dependence compared to the standard TLD set exposed to ^{60}Co. This investigation examined the relative response of TLD-100 (LiF:Mg,Ti) to irradiations with high energy photon (6-23 MV) and electron (6-18 MeV) beams relative to ^{60}Co (1.250 MeV photons).

3.5.1 Experimental methods

The methodology is similar to those presented by Davis et al[25] and Nunn et al,[70] but applied to high-energy photon and electron radiotherapy beam qualities in place of the lower energies relevant to brachytherapy investigated by Davis and Nunn. Measurements were taken for photon energies of 6, 10, 15, 18 and 23 MV and for electron energies of 2, 9, 10, 15, 18 MeV on Varian and Elekta linacs. Measurements were performed at multiple locations, including the University of Wisconsin Carbone Cancer Center (UW-Madison, Madison, WI), University of Pittsburgh Cancer Institute (UPIC, Pittsburgh, PN), University of Wisconsin Cancer Center Johnson Creek (UW-Johnson Creek, WI), Turville Bay MRI & Radiation Oncology Center (TBMRC-Madison, WI), and Helen K Spears Cancer Center (HSCC-Grants Pass, OR). For each energy the TLDs were irradiated to varying absorbed dose to water levels ranging from 100- 300 cGy.

The energy correction factor (K_e) for TLD-100 was determined by taking the ratio of the thermoluminecent response (TL) per unit dose to water (D_w) for the linac beam quality Q normalized to the TLD response per dose in the standard ^{60}Co source (Equation (3.6)).

$$K_e = \frac{\left(\mathrm{TL}^{Q}/D_w^{Q}\right)}{\left(\mathrm{TL}^{^{60}\mathrm{Co}}/D_w^{^{60}\mathrm{Co}}\right)} \tag{3.6}$$

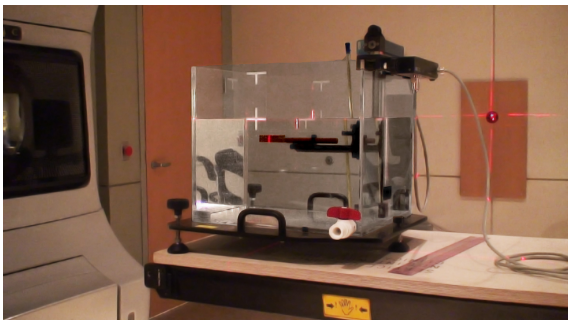

Figure 3.7: Experimental set up of linac photon beam quality Q from the Varian Trilogy located at UW Carbone Cancer Clinic (Madison, WI). TLD exposures were irradiated in TG-51 reference conditions.

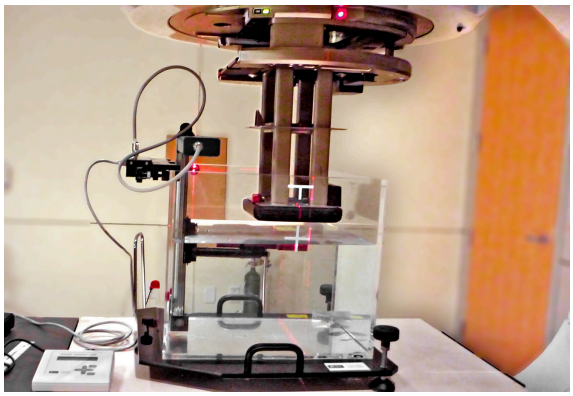

Figure 3.8: Experimental set up for 6, 9, 12, 15, and 18 MeV electron TLD irradiations referenced to ^{60}Co irradiations. TLDs irradiated by the Varian Trilogy in TG-51 reference conditions.

Absorbed dose to water was determined according to the TG-51 protocol using a calibrated Exradin A12 ionization chamber, Standard Imaging Max 4000 electrometer, and a water tank. Ionization chamber and TLD measurements were made at the TG-51 protocols reference depth of 10 cm in water for all linac produced photon measurements (Figure 3.7). All photon irradiations were performed with a SSD of 100 cm, the front surface of the TLDs placed at a depth of 10 cm in water, and a field size of $(10\,\mathrm{x}\,10)\,\mathrm{cm}^2$. The TG-51 calculated depth d_{ref} was used for all linac produced electron measurements (Figure 3.8). The ionization chamber was then replaced with TLDs housed in a custom designed holder, with the central point of the TLD array located in the same position as the effective point of measurement of the ionization chamber.

The custom TLD holder is constructed of Virtual Water™ (VW) and holds an array of five TLDs in a cross shape in a plane perpendicular to the beam axis (Figure 3.9). The TLD holders are composed of four pieces of VW material. The

bottom pieces measurements were $(6.35 \times 5.08 \times 1.0)\,\mathrm{cm}^3$. A thin 1 mm sheet of VW was modified so that when glued to the bottom piece the TLDs were held in filled out hole that fit tight to the TLDs with a minimal air gap between the TLD and the VW encasement ($<$0.1 mm). The top of the VW encasement $(5.08 \times 5.08 \times 0.5)\,\mathrm{cm}^3$ was constructed with a watertight o-ring to prevent damage to the TLDs when submerged in the water tank. The parts are held together with four nylon screws which allow for removal and insertion of the TLDs. The perturbation of the beam through the VW encasement was investigated and is described in Section 3.5.3.

The mean TL output of the TLDs divided by the absorbed dose to water the TLDs received as measured by an ionization chamber was found for the ^{60}Co standard (Figure 3.10) and the clinics linac beam qualities. ^{60}Co measurements were made at equal time intervals before and after TLDs were irradiated with the linac beam qualities. The averages of the two ^{60}Co measurements were used to normalize the linac measurements.

The ^{60}Co TLD and ionization chamber measurements were performed using a method similar to that used for linac measurements. TLDs irradiated by the University of Wisconsin Accredited Dosimetry Calibration Laboratory's (UWADCL) Theratronics El- Dorado 78 ^{60}Co irradiator in standard reference conditions. The ^{60}Co reference conditions consisted of a SAD of 100 cm, a depth of 5 cm in water, a field size of $(10 \times 10)\,\mathrm{cm}^2$ at the isocenter on a plane perpendicular to the beam, and the water phantom had the nominal dimension of $(50 \times 50 \times 50)\,\mathrm{cm}^3$.

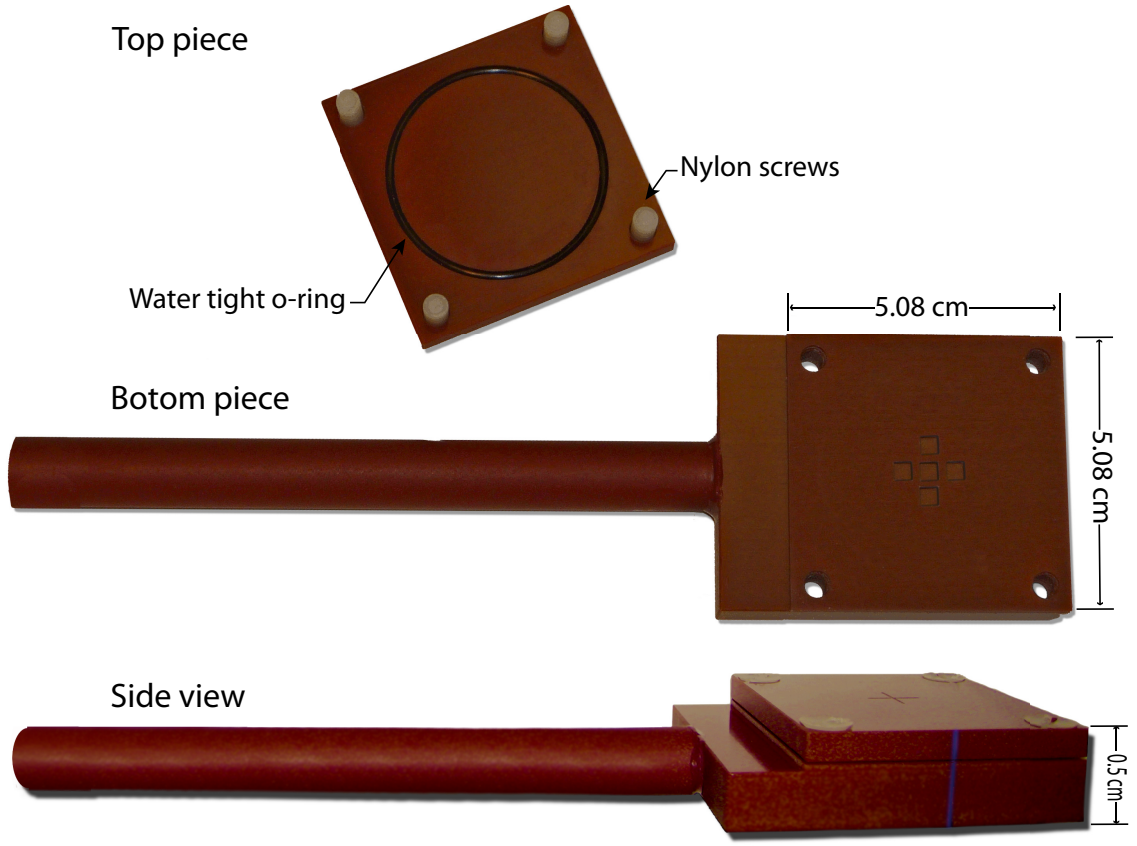

Figure 3.9: Virtual Water™ TLD holder with watertight O-ring. Five TLDs are positioned in a cross shape at the center of the VW encasement .

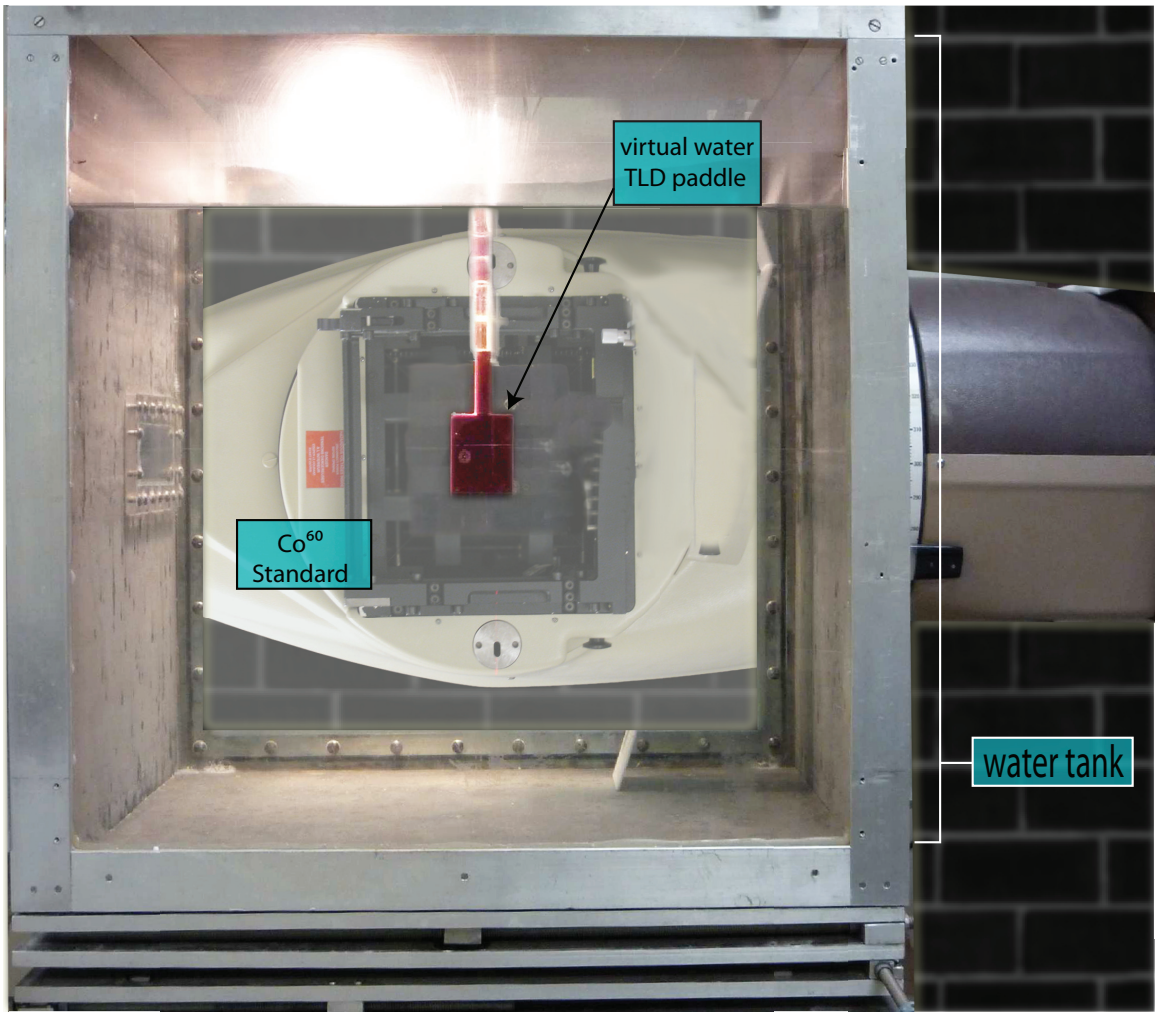

Figure 3.10: Experimental set up of ^{60}Co TLD exposures.

3.5.2 Experimental results

Photon energy correction factors

The experimental results found less than a 0.97 to 0.95 energy correction factor for TLD-100 chips relative to ^{60}Co energy for 6 MV and 23 MV photon beams (Table 3.4). The energy correction factor was found to increase as a function of energy. The reproducibility was found to be less than 2% with a standard deviation of the mean of less than 0.2% (Table 3.1, 3.2, and 3.3). No dose dependence was observed over the range 100 to 300 cGy. The machine comparison of TLD-100 energy correction factor found in Elekta and Varian machines yielded no statistical difference outside the TLDs reproducibly uncertainty(Table 3.5).

Electrons energy correction factors

The experimental results showed a 5% average energy correction factor for TLD-100 chips relative to ^{60}Co energy for the 6, 9, 12, 15, and 18 MeV electron beams created by Varian linacs (Table 3.7). The standard deviation of the mean for the energy correction factors found in each experiment ranged from 0.3% to 0.5% (Table 3.6). The standard deviation of the energy correction factor over the entire data set ranged from 2% to 5% for each energy (Figure 3.11). These results demonstrate the TLD's ability to measure electron beams precisely on a single day with increased variability when measurements are made on separate days with different data acquisition sessions. TLD processing and sensitive intrinsic TLD response mechanisms due to variations in the electron beam may account for this variability. No dose dependence was observed for the set up over the range 100 to 300 cGy.

Table 3.1: 6 MV experimental results of TLD-100 energy correction factor irradiations relative to ^{60}Co.

Exp.	Linac Make	Location	K_e	σ	n	STDEV of the mean	w_i
1	Varian	UW-Madison	0.97	0.019	25	0.0038	0.057
2	Varian	UW-Madison	0.99	0.016	50	0.0022	0.115
3	Varian	UW-Madison	0.97	0.014	75	0.0017	0.172
4	Varian	UW-Madison	0.97	0.016	35	0.0027	0.080
5	Varian	UW-Johnson Creek	0.96	0.015	40	0.0024	0.092
6	Varian	UW-Madison	0.97	0.017	40	0.0027	0.092
7	Varian	UW-Johnson Creek	0.98	0.016	40	0.0025	0.092
8	Varian	UW-Madison	0.98	0.015	40	0.0023	0.092
9	Elekta	UPIC-Pittsburgh	0.97	0.013	45	0.0020	0.103
10	Varian	TBMRC-Madison	0.97	0.034	25	0.0069	0.057
11	Varian	HSCC-Grants Pass	0.97	0.020	20	0.0045	0.046

Average	0.97
σ	0.02
n_{TLDs}	435
STDEV of the mean	0.001

Table 3.2: 10 MV experimental results of TLD-100 energy correction factor irradiations relative to ^{60}Co.

Exp.	Linac Make	Location	K_e	σ	n	STDEV of the mean	w_i
1	Varian	UW-Madison	0.95	0.017	25	0.0033	0.063
2	Varian	UW-Madison	0.96	0.013	50	0.0018	0.127
3	Varian	UW-Madison	0.96	0.015	75	0.0018	0.190
4	Varian	UW-Madison	0.95	0.014	40	0.0022	0.101
5	Varian	UW-Johnson Creek	0.95	0.016	40	0.0025	0.101
6	Varian	UW-Madison	0.97	0.018	40	0.0028	0.101
7	Varian	UW-Johnson Creek	0.96	0.014	40	0.0022	0.101
8	Varian	UW-Madison	0.96	0.018	40	0.0028	0.101
9	Elekta	UPIC-Pittsburgh	0.96	0.016	45	0.0024	0.114

Average	0.96
σ	0.02
n_{TLDs}	395
STDEV of the mean	0.001

Table 3.3: TLD energy correction factor experimental results for 15 MV and 23 MV photon beams relative to ^{60}Co.

Energy	15 MV	23 MV
Experiment	9	11
Linac Make	Elekta	Varian
Location	UPIC-Pittsburgh	HSCC-Grants Pass
K_e	0.96	0.95
σ	0.01	0.02
n_{TLDs}	50	20
STDEV of the mean	0.002	0.00

Table 3.4: Summary of results: TLD-100 energy correction factors for 6, 10, 15, and 23 MV photons relative to ^{60}Co.

Energy (MV)	K_e	σ	n_{TLDs}	STDEV of the mean	$n_{experiments}$
6	0.97	0.02	435	0.001	11
10	0.96	0.02	395	0.001	9
15	0.96	0.01	50	0.002	1
23	0.96	0.02	20	0.005	1

Table 3.5: Machine comparison of TLD energy correction factor found in 6 and 10 MV Varian and Elekta machines.

Energy	6 MV		10 MV	
Make	K_e	σ	K_e	σ
Varian	0.97	0.01	0.96	0.01
Elekta	0.97	0.01	0.96	0.02
(%) difference	0.3%		0.1%	

Table 3.6: Individual TLD-100 energy correction factor experiment results for 6, 9, 12, 15, and 18 MeV electron TLD irradiations relative to ^{60}Co irradiations.

Exp.	Energy (MeV)	K_e	σ	n	STDEV of the mean
1	6	0.93	0.02	40	0.002
	9	0.93	0.01	40	0.002
	12	0.93	0.01	40	0.002
	15	0.92	0.01	40	0.002
	18	0.93	0.01	40	0.002
2	6	0.93	0.01	35	0.002
	9	0.94	0.01	35	0.002
	12	0.95	0.02	30	0.003
	15	0.96	0.02	30	0.003
	18	0.96	0.01	35	0.002
3	6	0.92	0.02	30	0.003
	9	0.93	0.02	30	0.004
	12	0.98	0.01	30	0.003
	15	0.94	0.01	30	0.003
	18	0.93	0.02	30	0.004
4	6	0.94	0.01	30	0.002
	9	0.96	0.03	30	0.005
	12	0.99	0.01	30	0.002
	15	0.97	0.01	30	0.002
	18	0.95	0.01	19	0.003
5	6	0.97	0.01	45	0.001
	9	0.98	0.01	45	0.002
	12	0.98	0.01	45	0.002
	15	0.96	0.01	45	0.002
	18	0.99	0.04	45	0.005

Table 3.7: Summary of Results: energy correction factors for 6, 9, 12, 15, and 18 MeV electron TLD irradiations referenced to ^{60}Co irradiations.Dose to water was determined by a calibrated ionization chamber in the same TG-51 reference conditions as the TLD irradiations.

Energy (MeV)	K_e	σ	n	STDEV of the mean
6	0.94	0.03	180	0.002
9	0.95	0.04	180	0.003
12	0.97	0.03	175	0.002
15	0.95	0.03	175	0.002
18	0.95	0.05	169	0.004

Average	0.95
σ	0.01
n	879
STDEV of the mean	0.001

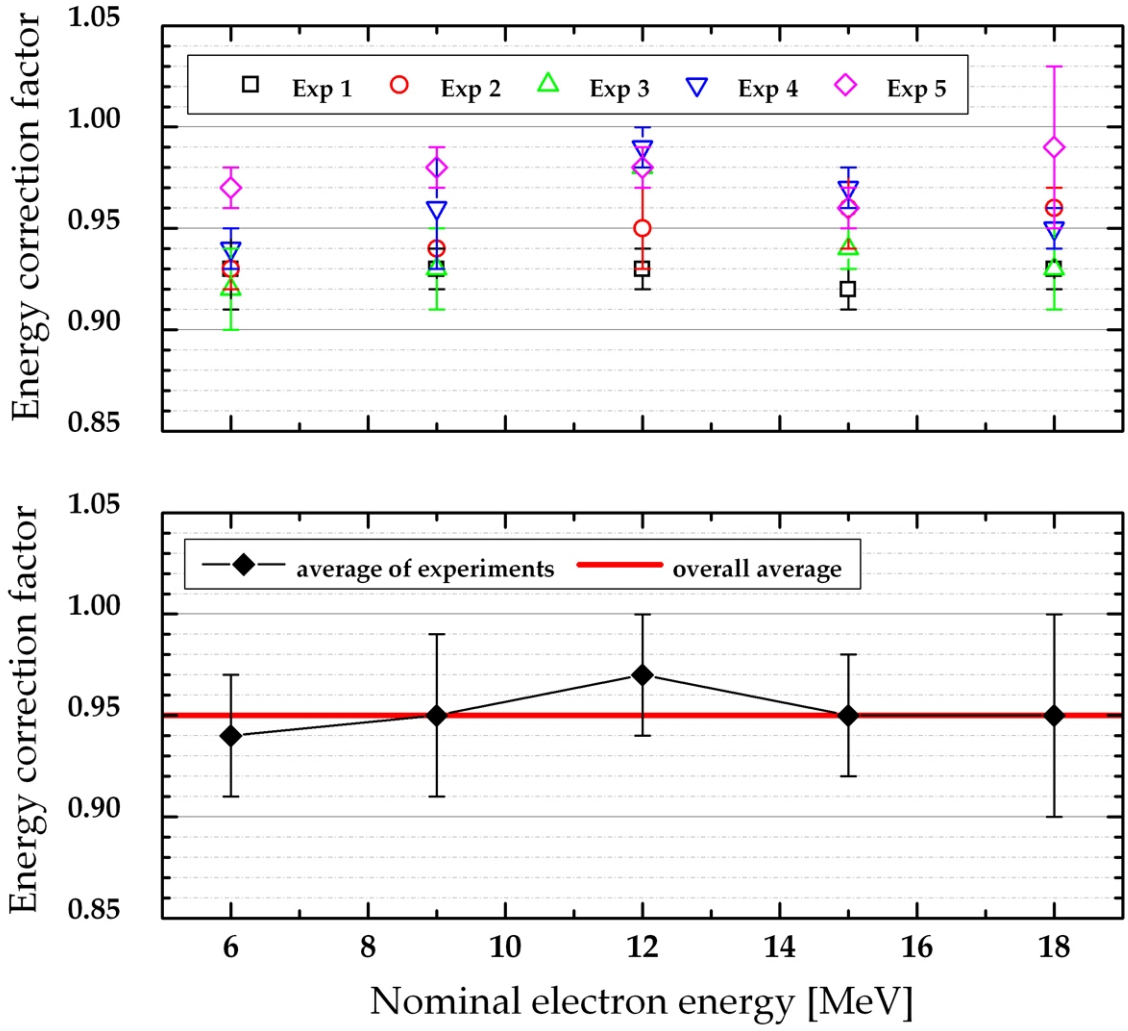

Figure 3.11: Plot of energy correction factors for 6, 9, 12, 15, and 18 MeV electron TLD irradiations referenced to ^{60}Co irradiations for experiments performed on different dates. Dose to water was determined by a calibrated ionization chamber in the same TG-51 reference conditions as the TLD irradiations.

3.5.3 Monte Carlo

A Monte Carlo investigation was performed in this work to determine the relationship between measured light output from TLD-100 (LiF:Mg,Ti) as a function of photon energy absorbed dose in the TLD detector volume. Absorbed dose to TLD can only be determined using Monte Carlo methods. In practice TLDs are referenced to another method of absorbed dose measurement such as the ionization chamber determined absorbed dose to water that was used in the experimental energy correction factor study. This work adapts the Monte Carlo methodology set by Davis et. al. and Nunn et. al. The adaptation involved using measurements of TL response normalized to absorbed dose to water standards which differ from the air kerma standards used in Davis et. al. and Nunn et. al. The ratios of dose to TLD over dose to water were simulated and normalized to the ^{60}Co simulated value. to convert the measurements of TLD response per unit absorbed dose to TLD as a function of energy (Equation (3.7)).

$$D_{\mathrm{TLD}} = D_{w,\mathrm{experimental}} \frac{(D_{\mathrm{TLD}}/D_w)_{Q,\mathrm{MC}}}{(D_{\mathrm{TLD}}/D_w)_{^{60}\mathrm{Co,MC}}} \tag{3.7}$$

The Monte Carlo simulated absorbed dose ratios were compared to the experimental TL response to determine if Monte Carlo calculations could be used reliably to calculate TLD energy response corrections or if the measured energy response is a function of micro-dosimetric aspects of the thermoluminescence or other process not accounted for in Monte Carlo models in addition to classic radiation transport mass energy-absorption coefficients and stopping power ratio dose relationships. Monte Carlo simulations were done using MCNP5 to model the experimental set up and calculate the intrinsic energy response as a function of mass attenuation though the TLD depth.

3.5.3.1 Methods

Monte Carlo models of the experimental setup were created in MCNP5 version 1.60. The mcplib04 library was used for photon and electron cross sections. The geometry included the TLDs, VW holder, and the water tank used in the experimental setup. The TLD and VW holder setup consists of five TLDs arranged in a cross shape (Figure 3.9). The chips have nominal dimension of $(3.2 \times 3.2 \times 0.89)$ mm^2 and were positioned with the larger flat surface facing perpendicular to the source beam. The material of the detector volumes were simulated with both water and TLD compositions. The TLD-100 composition and density were from Thermo Electron Corporation composition by weight of 73.28% Li, 26.70% F, 0.02% Mg, and 0.001% Ti, with a density of 2.64 g/cm^3. The Virtual Water™ composition was obtained from Med-Cal (Verona, WI).

Simulations were run using published linac photon beam spectra as the source input. Input spectra were obtained from BEAMnrc modeled Varian photon beams published by Daryoush and Rogers.[90] Mono energetic electron beams were used for the electron source definition, due to the short range of electrons. The resulting dose to TLD and water were referenced to corresponding simulations from a ^{60}Co beam modeled using the two discrete energy peaks of 1.1730 and 1.333 MeV with relative frequencies of 0.999 and 1.0 respectively .

A cavity theory study using simulations of very thin (9.00E-07 g/m^2) and very thick (1.80E-01 g/m^2) TLDs was performed to determine if electrons should be transported at energies used in this work. Electrons were transported as their range was found to be on the order of the thickness of the TLD. Without electron transport a cavity theory correction would be required (Table 3.8).

Table 3.8: Cavity theory Monte Carlo Study

Energy (MV)	Thin	Thick	Thick/Thin
Co	6.32×10^{3}	3.14×10^{-2}	2.02×10^{5}
6	6.40×10^{3}	3.21×10^{-2}	2.00×10^{5}
10	6.53×10^{3}	3.23×10^{-2}	2.02×10^{5}

The electron transport was cut off at 0.005 MeV and photon transport cut off was set to 0.001 MeV. The *F8 tally was used in this work and gives unit energy deposition in MeV per starting particle. The *F8 tally uses an energy balance method to determine the energy deposited in each cell by calculating the difference in energy entering the cell and energy exiting the cell. This difference is then normalized to the number of starting particles. Simulations were run to calculate dose to TLD and dose to water for the experimental setup with less than 1% reported uncertainty in the Monte Carlo simulation. The dose to TLD is compared to the experimental TL [nC] output. Taking the dose to TLD over dose to water in the same volume unfolded the relationship between absorbed dose and TL output as a function of beam energy.

Monte Carlo simulations were performed to determine the perturbation of the beam and resulting spectrum change due to the addition of the VW holder compared to the surrounding liquid water. This was modeled by replacing the volume occupied by VW with water and then rerunning the simulations. F4 tallies were used to observe how the VW perturbed the beam compared to regular water by determining the spectra entering and exiting the region of interest (Figure 3.12). In addition the effect of the small amount of air surrounding the TLDs in the VW holder was also modeled using 1 mm air gaps.

3.5.3.2 Results

The Monte Carlo simulated absorbed dose to water and TLD ratios were compared to the experimental values to determine if Monte Carlo calculations could be used reliably to calculate TLD corrections. Differences of up to -3.5% were seen for photons (Table 3.9) and no difference was seen for the electrons outside the measurements uncertainty(Table 3.10). The differences could be due to micro-dosimetric mechanisms not accounted for in Monte Carlo methods or inaccuracies in MCNPs radiation transport due to sub shell electron sampling.[70] Monte Carlo is purely based on the total energy deposited in a dosimeter and does not consider ionization density or other solid state mechanisms. Nunn et al[70] saw differences of up to 10% in her Monte Carlo comparison for low energy TL relative to air kerma as a function of effective energy. In addition, it was shown that Monte Carlo showed no perturbation of the beam through the VW holder when compared to an equivalent water defined region (Figure 3.12).

3.6 TLD relative response reproducibility study

Long term stability of TLD relative response factors was investigated. The TLD efficiency is thought to be a function of the individual TLDs irradiation and thermal history.[39] The high temperature (400°C) anneal used in the standard annealing process (Section 3.3.2) has been shown in previous work to be insufficient to clear residual electron-hole traps for high doses from MV beams, leading to an altered TLD sensitivity with use.[101] The data from a set of 380 TLDs used throughout this work was analyzed to observe the behavior of the individual TLD responses as a function of accumulated time, exposures, and anneals.

Table 3.9: Monte Carlo generated energy correction factors for 6, 10, 15, and 25 MV photon TLD irradiations referenced to ^{60}Co irradiations. The Monte Carlo simulations showed the ratio of absorbed dose to TLD to absorbed dose to water for the same conditions and occupied volume.

Energy (MV)	Monte Carlo K_e $\left(\frac{Dose_{TLD}}{Dose_{water}}\right)^{Q}_{\mathrm{Co}^{60}}$	σ	Measured K_e $\left(\frac{M_{TLD}}{Dose_{water}}\right)^{Q}_{\mathrm{Co}^{60}}$	σ	Difference From Measured (Δ)	Difference From Measured (%)
^{60}Co	1	0.017	1	-	-	-
6	0.997	0.018	0.973	0.02	-0.024	-2.5%
10	0.992	0.015	0.960	0.02	-0.032	-3.3%
15	0.992	0.014	0.959	0.01	-0.033	-3.4%
23/25	0.990	0.013	0.955	0.02	-0.035	-3.6%

Table 3.10: Monte Carlo generated energy correction factors for 6, 9, 12, 15, and 18 MeV electron TLD irradiations referenced to ^{60}Co irradiations. The Monte Carlo simulations showed the ratio of absorbed dose to TLD to absorbed dose to water for the same conditions and occupied volume.

Energy (MeV)	Monte Carlo K_e $\left(\frac{Dose_{TLD}}{Dose_{water}}\right)^{Q}_{\mathrm{Co}^{60}}$	σ	Measured K_e $\left(\frac{M_{TLD}}{Dose_{water}}\right)^{Q}_{\mathrm{Co}^{60}}$	σ	Difference From Measured (%)
^{60}Co	1.00	0.038	1	-	-
6	0.956	0.010	0.940	0.03	-0.016
9	0.954	0.009	0.947	0.04	-0.008
12	0.957	0.010	0.967	0.03	-0.010
15	0.959	0.010	0.951	0.03	-0.008
18	0.963	0.010	0.953	0.05	-0.010
Average	0.958	0.003	0.952	0.04	-0.006

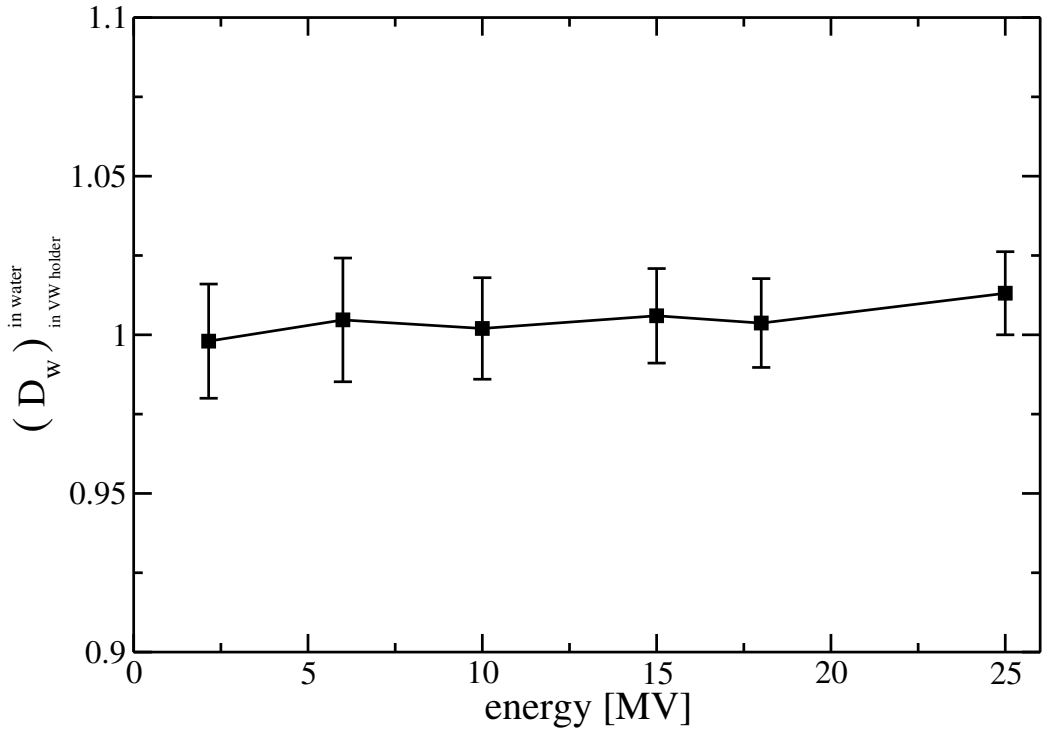

Figure 3.12: Monte Carlo VW holder comparison with in water TLDs.

3.6.1 Methods

Data from 40 TLD exposures for obtaining relative response coefficients for the set of TLDs (Section 3.3.3) was used for this analysis. Each exposure was separated by at least two full anneals, two reads, and an experimental exposure. The TLDs ended up receiving more than 80 full anneals and more than 80 exposures to various beam qualities over a time period of 6 years. The individual TLDs relative response coefficients were normalized to the mean and the distribution plotted.

3.6.2 Results

Figure 3.13 shows the histogram of the TLD relative response coefficients for each individual chip in the set of 380 TLDs, normalized to its average relative response coefficient. A total of 6840 (n=6840) separate relative response coefficients were

used. Figure 3.14a is the average standard deviation of the individual chips relative response coefficients. Figure 3.14b is the the average of the differences in relative response coefficients for sequential read out periods over the course of of all 40 reads an interim anneals and experimental exposures.

3.6.3 TLD uncertainty in Standard CoP Reference Dosimetry

Uncertainty in the TLD readings was estimated (Table 3.11). Sources of uncertainty in the TLD measurements were determined to be TLD reproducibility, TLD positioning, PMT linearity correction, reader stability, electron irradiation variation, and ^{60}Co dose variations. The TLD reproducibility differs for each electron beam as it is the average of the standard deviation of the corrected readings of the TLDs irradiated by an electron beam and the corresponding ^{60}Co readings. Positioning was estimated to be within $\pm$1 mm leading to 0.2% estimated error. Taking the quadratic sum of all estimated uncertainties lead to a estimated relative expanded uncertainty of 5.60% at k=2, which corresponds to an approximate 95% confidence interval.

3.7 Comparison to literature

The energy correction factor has been determined in previous studies and put into use in TLD monitoring services across the world. There are services in use from IAEA/World Health Organization, European Society for Therapeutic Radiology and Oncology, MD Anderson Radiological Physics Center and PTW-Freiburg. These institutions use TLDs in various forms such as powder, rods, and chips to perform dose measurements. In order to provide this service, energy correction factors would have to be calculated for their specific setup geometry and application. It is important

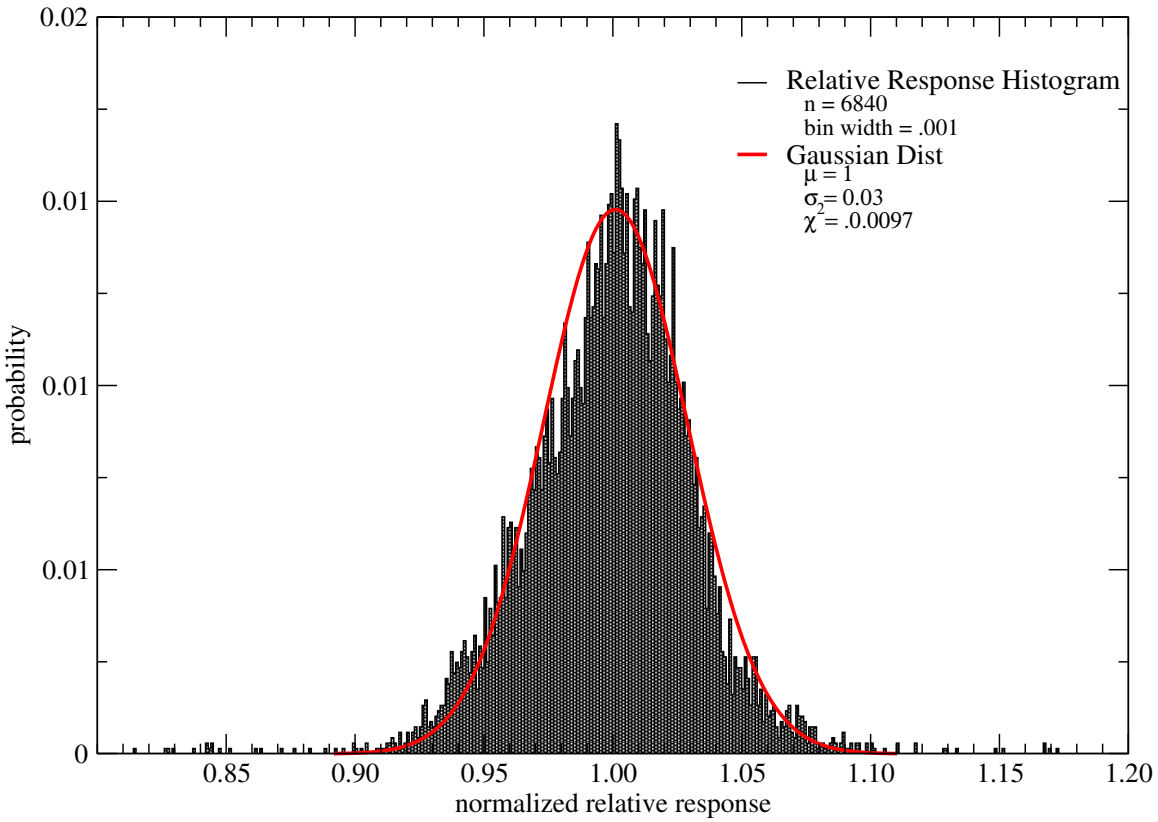

Figure 3.13: Long term relative response coefficient histogram for 380 individual TLDs irradiated more than 80 times over 6 years. Relative response coefficients for each individual chip were normalized to the average of its relative response coefficients.

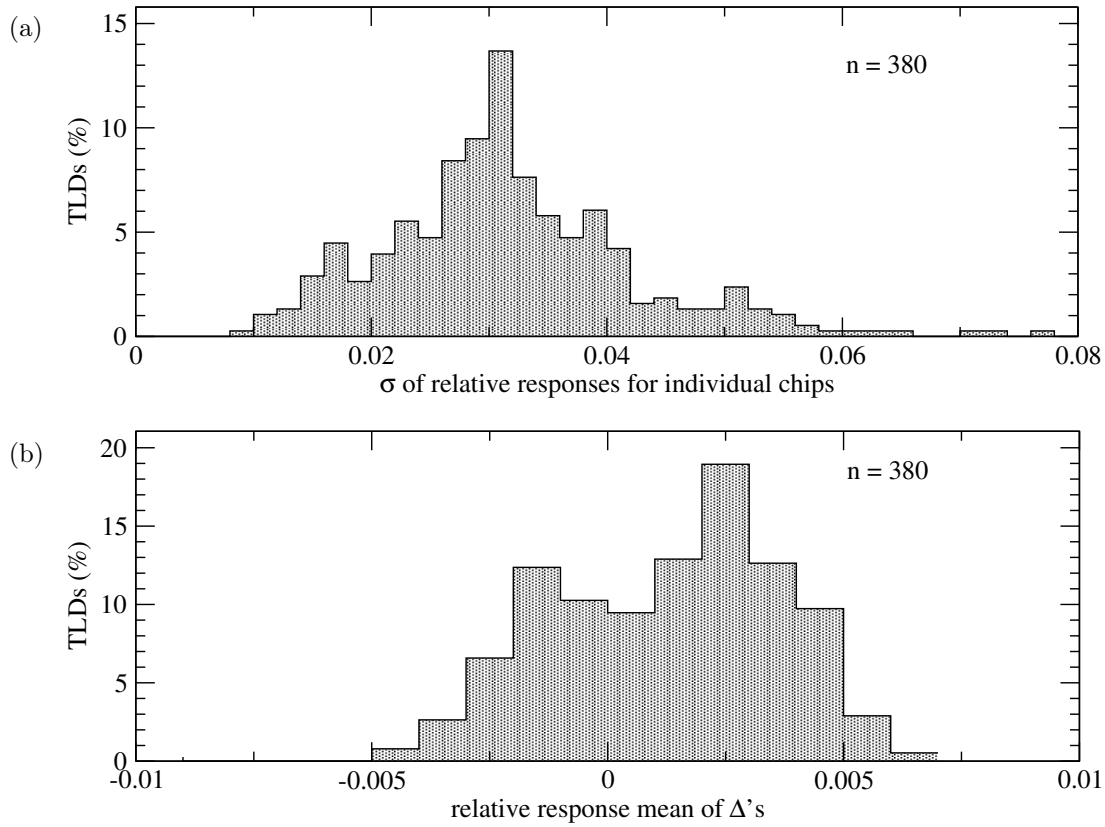

Figure 3.14: Long term relative response coefficient statistics for a set of 380 TLDs. (a) average standard deviation of the individual chips relative response coefficients for 40 read out sessions. (b) average of the differences in relative response coefficients for sequential read out periods for an individual chip

Table 3.11: Example of uncertainty analysis for measured TLD data. Values are expressed in percent.

	Type A	Type B
TLD reproducibility	1.8	
TLD positioning		0.20
PMT linearity correction		0.20
Reader stability		0.20
Electron irradiation variation		2.00
Uncertainty in ^{60}Co absorbed dose to water		0.64
Quadratic Sum	1.8	2.13
A and B Quadratic Sum	2.78	
Expanded to k=2	5.58	

to note that the values determined for these institution's programs are specific to their setup conditions and may not be directly comparable. Table 3.12 compares this work to published photon energy correction factor values. The published values range from 0.98 to 0.93 depending on photon energy.[49,84,63] The published electron energy correction factor values were found to be independent of beam energy and dependent on the readout session. Published TLD electron K_e values vary from 0.94 to 0.98 and are compared to this work in Table 3.13. The measurement methods used in this work differ from previous published work in that this work's measurement setup is identical to the current CoP reference conditions used by the AAPMs TG-51, and strived to get as close to dose in water conditions as possible.

Table 3.12: TLD photon energy correction factor literature comparison.

Condition	Junell (2009)	PTW[84] Freiburg	Mobit el al[62] (1996)	Kirby et al[49] (1986)
Medium/ Encapsulation	Water/ VW	Water/ PMMA	acrylic/water/ perspex	acrylic
TLD	LiF (3x3x1)	cylindrical chips	micro-rods and chips	LiF powder
depth	10 cm	-	5 cm	d_{max}
full scatter/ secondary CPE	yes/yes	yes/yes	-	no/yes
Energy (MV)				
6	0.97	0.97	0.98	0.96 - 0.93
10	0.96		0.97	
15	0.96	0.96		
18	0.94			
23	0.96			
25			0.97	

Table 3.13: TLD electron energy correction factor literature comparison.

Condition	Junell (2009)	PTW[84] Freiburg	Mobit el al[62] (1996)	Kirby et al[49] (1986)
depth	d_{ref}	-	d_{max}	d_{30} and d_{80}
Medium/ Encapsulation	Water/ VW	Water/ PMMA	acrylic/ perspex	acrylic
TLD	LiF (3x3x1)	cylindrical chips	micro-rods and chips	LiF powder
Energy (MeV)				
6	0.95	0.94	0.96 - 0.97	0.96 - 0.98
9				
12				
15				

3.8 Conclusions

This work has experimentally determined the energy correction factor for TLD-100 (LiF:Mg,Ti) chips. The energy correction factor relative to ^{60}Co was found to be 0.973, 0.960, 0.959, and 0.955 for 6, 10, 15, and 23 MV photon beams, respectively. The energy correction factor for electron beams was found to be 0.94, 0.95, 0.97, 0.95, and 0.95 for 6, 9, 12, 15, and 18 MeV energies, respectively. Monte Carlo simulations showed similar energy correction values to those found experimentally for electron beam qualities. Monte Carlo simulations showed no energy correction values for the different photon beam qualities, while the experimentally determined energy correction values showed the energy correction factor trending toward the value of one, with decreasing photon energy possibly displaying a difference in response due to an increase in the photoelectric effect at lower energies. The energy correction factors found in this research can be used to create a dosimetry system to determine absorbed dose to water. The TLD system can also be used as a secondary calibration method for high energy electron beams to verify standard TG-51 calibration methods.

Chapter 4

Small Field Measurements

4.1 Introduction

Codes of practice (CoP) for $(10\,\mathrm{x}\,10)\,\mathrm{cm}^2$ reference fields for photon beams are well established by the AAPM's TG-51[3] and the IAEA's TRS-398.[5] However, standard national or international guidelines have not been widely adopted by radiotherapy clinics for the calibration of small and nonstandard photon fields. In a joint effort between the IAEA and AAPM, a working group was formed and tasked with the development of a new calibration methodology and CoP for the reference dosimetry of small and nonstandard fields. The joint IAEA and AAPM working group published a proposed formalism outlining two new calibration methodologies for small and nonstandard fields (Section 2.4).[2]

Using small and nonstandard photon fields, advanced radiation therapy techniques are able to achieve highly conformal dose distributions with millimeter level precision. Treatment devices and techniques which use small and nonstandard photon fields include CyberKnife®, Gamma Knife®, TomoTherapy®, stereotactic radiosurgery (SRS), and intensity-modulated radiation therapy (IMRT). While these treatment modalities have the mechanical capabilities to deliver stunningly precise

dose distributions, they are limited by large margins due to the uncertainty in dose (accuracy) verification under current clinical calibration and quality procedures. The current tolerance criterion for IMRT and stereotactic treatment dose verification is up to 5% in clinics compared to the less than 2% uncertainty level associated with traditional broad beam radiotherapy dose calibrations. This increase in dose uncertainty is due to current extrapolation methods of dose measurements from broad beam based CoP measurements to small and nonstandard photon fields. Small and nonstandard photon fields exhibit physical behavior different than the standard CoP broad beam photon fields that are not accounted for in the dose extrapolation method (Section 2.4). The proposed formalism attempts to decrease this uncertainty for small and nonstandard photon field treatments by providing new calibration methodologies.[2]

This chapter is an investigation of the measurement components of the proposed formalism as it applies to intensity-modulated radiation therapy (IMRT) treatment fields. Multiple measurement techniques were used to derive ^{60}Co calibration coefficient beam quality correction factors for ionization chambers and provided a basis for comparison of the proposed formalism's small and nonstandard reference conditions with the secondary accredited dosimetry calibration laboratory's (ADCL) ^{60}Co standard. Ionization chambers beam quality correction factors were calculated from thermoluminescent dosimeter (TLD) and alanine absorbed dose to water measurements.

Purpose statement: The goal of this chapter is to investigate the application and traceability of the proposed formalism for small and nonstandard reference dosimetry as it applies to IMRT treatment fields by using multiple measurement techniques.

4.2 Method overview

Experimentally determined beam quality correction factors for ionization chambers in a variety of calibration conditions were the desired outcome. This work was performed in accordance with the nomenclature and methodology outlined in the proposed formalism (Section 2.6). All beam quality correction factors in the proposed formalism were combined into a single quality correction factor, $k_{Q_{\text{small fields}},Q_0}^{f_{\text{small fields}},f_0}$, directly traceable to the ^{60}Co standard beam quality (Q_0) and are related as shown in equation (4.1).

$$k_{Q_{\text{small fields}},Q_0}^{f_{\text{small fields}},f_0} = k_{Q,Q_0} \cdot k_{Q_{\text{msr}},Q}^{f_{\text{msr}},f_{\text{ref}}} \qquad \text{or} \qquad k_{Q_{\text{small fields}},Q_0}^{f_{\text{small fields}},f_0} = k_{Q,Q_0} \cdot k_{Q_{\text{pcsr}},Q}^{f_{\text{pcsr}},f_{\text{ref}}} \tag{4.1}$$

Beam quality correction factors were experimentally determined using equation (4.2);

$$k_{Q_{\text{small fields}},Q_0}^{f_{\text{small fields}},f_0} = \frac{D_{w,Q_{\text{small fields}}}^{f_{\text{small fields}}} / M_{Q_{\text{small fields}}}^{f_{\text{small fields}}}}{D_{w,Q_0}^{f_0} / M_{Q_0}^{f_0}} \tag{4.2}$$

where beam quality Q_0 was ^{60}Co and the beam quality $Q_{\text{small fields}}$ corresponds to a static or composite linac produced 6 MV photon beam. where the absorbed dose to water in the reference field ($D_{w,Q_0}^{f_0}$) and the corresponding ionization chamber reading ($M_{Q_0}^{f_0}$) are measured for the ^{60}Co standards laboratory calibration beam quality (Q_0). Similarly, the nonstandard field absorbed dose to water ($D_{w,Q_{\text{small fields}}}^{f_{\text{small fields}}}$) and corresponding ionization chamber reading ($M_{Q_{\text{small fields}}}^{f_{\text{small fields}}}$) are measured for the beam quality $Q_{\text{small fields}}$, which corresponds to multiple small field calibration conditions ($f_{\text{small fields}}$).

Because of the reasons discussed in Section 2.5.2, the linac based IMRT systems was operated at low megavoltage photon energies with a nominal energy of 6 MV.[55] Measurements were made for field sizes ranging from (1.6 x 1.6) cm^2 to

$(10\,\mathrm{x}\,10)$ cm^2 and for a f_{pcsr} representing a hypothetical head and neck case. Absorbed dose to water (D_w) was determined using both TLD and alanine. Ionization chamber readings (M) and beam quality correction factors were calculated for three different models of ionization chambers: a Farmer-type ionization chamber (Exradin A19 – 0.65 cm^3 collecting volume), a thimble ionization chamber (Exradin A1SL – 0.057 cm^3 collecting volume), and a micro-ionization chamber (Exradin A16 – 0.007 cm^3 collecting volume). All ionization chambers were manufactured by Standard Imaging, Inc. (Middleton, WI).

4.3 Absorbed dose to water experimental methods

TLDs and alanine were used to measure absorbed dose to water (D_w) in a variety of standard and small photon fields. TLD-100 chips were provided by the University of Wisconsin Medical Radiation Research Center (UWMRRC). Alanine dosimeters were provided by NPL and NIST. Section 4.4 and 4.5 describe the calibration conditions in which measurements were performed. The following section focuses on the methodology used to obtain dose to water from TLD and alanine.

4.3.1 TLD methods

TLDs were used throughout this work and a detailed description of the TLD system is given in the preceding chapter.

4.3.2 Alanine methods

Alanine dosimeters from NIST and NPL were also used to determine absorbed dose to water. A batch of eight cylindrical alanine pellets and three control pellets were

provided by NIST. A batch of 60 cylindrical alanine pellets and three control pellets were provided by NPL. Following experimental exposures, the alanine pellets were sent back to NPL and NIST and were read using EPR methods to obtain absorbed dose to water. Calibration was performed by taking a peak-to-peak amplitude of a subset of the EPR spectrum lines that corresponded to the spin-flips energy level of the radiation induced alanine radicals of interests. This signal is normalized to the ^{60}Co spectrums corresponding amplitudes to obtain a dose to water referenced to the ^{60}Co standard.[71]

4.3.2.1 NIST alanine dosimetry

The alanine pellet dosimeters provided by the NIST calibration services were fabricated at NIST. Each pellet had a diameter of 5 mm and a height of 2.4 mm. The alanine calibration was provided from a known dose rate from the NIST B036 vertical beam ^{60}Co source. This ^{60}Co source is the US national standard and is calibrated using absolute water calorimeter dose measurements.[28] The dose rate was transferred by irradiating eight alanine pellets in the calorimeter water tank. The pellets were placed in a watertight polystyrene cylinder whose axis was fixed perpendicular to the NIST vertical beam ^{60}Co source. The analysis of the alanine was done in a Bruker model ESC 106 EPR spectrometer.[28,27,26] For the experimental irradiation, a dose of approximately 40 Gy was delivered and the provided standard NIST procedure was observed. The NIST provided procedure did not require temperature monitoring during the experiment.

4.3.2.2 NPL alanine dosimetry

The NPL alanine pellets were manufactured by Harwell Dosimeters Ltd. (Oxfordshire, United Kingdom) and were comprised of 90% l-α-alanine and 10% paraffin wax with a nominal density of 1.2 g/cm^3 and melting point of 98°C.[88] Each NPL alanine pellet had a diameter of 4.9 mm and a height of 2.4 mm. The NPL alanine pellets were held at a temperature close to that of the irradiator room for at least two days before irradiation. The temperature of the phantom in which the NPL alanine pellets were housed was carefully monitored before and after each irradiation. Temperature data were reported to NPL.[86,75,85] A minimum dose of 5 Gy was delivered based on the NPLs reported achievable standard deviation of 0.05 Gy.

The alanine energy-dependence observed at the National Research Council Canada (NRCC) and NPL found the response of alanine to ^{60}Co radiation is ~0.6% larger than the response to linac beams qualities. A energy correction factor of 0.994 was applied to the alanine measurements in the 6 MV fields (Figure 4.1).[88,85] The analysis of the alanine was done in the NPL Bruker model EMX EPR spectrometer. The EPR parameters were chosen to provide the maximum signal-to-noise ratio consistent with the preservation of the major features of the alanine spectrum. An example of values used: microwave power: 6 mW, modulation amplitude: 0.6 mT, sweep width: 20 mT, scan time: 20 s (1024 points), time constant: 163 ms, number of scans: two sets of three scans each with the pellet rotated by 90 ° between the sets.[85]

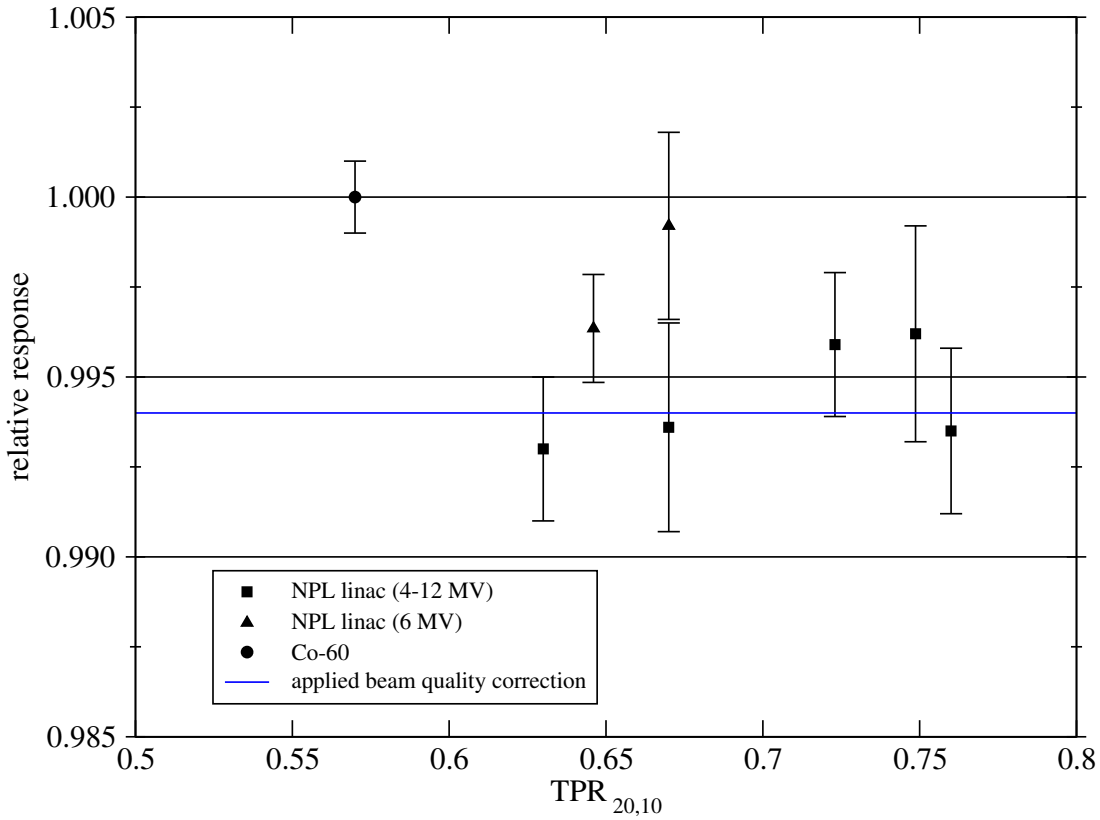

Figure 4.1: NPL alanine energy dependence for linac produced photon beams relative to ^{60}Co

4.4 In-water measurements of beam quality correction factor for static small fields

4.4.1 Methods

Absorbed dose to water measurements (refer to equation (4.2)) were performed for square static small fields ($f_{\text{small fields}}$) ranging from $(1.6\,\text{x}\,1.6)$ cm^2 to $(10\,\text{x}\,10)$ cm^2. These measurements were performed in a water phantom (volume $\geq (30\,\text{x}\,30\,\text{x}\,30)$ cm^3) at 10 cm depth with an array of five TLDs or one alanine pellet held in a VW holder (Figure 3.9). The VW holder had a watertight o-ring to prevent water from contacting the detectors. The single TLD located on the central axis of the beam was compared to the average of the five TLDs, including four located slightly off axis, to account for field uniformity. If the differences in the values were within one standard deviation of each other, all TLDs in the VW holder were used to improve statistics. Monte Carlo simulations show no difference within uncertainty between the perturbation of a 6 MV beam or a ^{60}Co beam in the VW holder versus in liquid water.

After TLD absorbed dose to water irradiations, the VW holder was replaced with each ionization chamber and exposed to a 6 MV beam at the same position on the central axis of the beam. Charge readings (M) in coulombs for each ionization chamber were recorded using a Standard Imaging MAX 4000 electrometer (Middleton, WI) with a bias of +300 V to collect negative charge. Measurements were made to determine the ratio of dose (D) per ionization chamber charge reading for the three different ionization chambers. An Elekta linac at the University of Pittsburgh Medical Center (UPMC) was used to create the different $f_{\text{small fields}}$ beam qualities. The $f_{\text{small fields}}$ measured is an intermediate reference field of arbitrary field size created to mimic the f_{msr} discussed in the proposed formalism (refer to Section 2.4 and Figure

2.6). Measurements were also made to determine the ratio of dose per ionization chamber reading for three different ionization chambers for the Q_0 beam quality from the Theratronics T1000 ^{60}Co therapy unit at the UWADCL.

Alanine-determined absorbed dose to water measurements were performed for comparison to UPMC TG-51-determined absorbed dose to water for $f_{\text{small fields}}$. Alanine pellets provided by NIST were exposed to a 6 MV photon beam in different $f_{\text{small fields}}$ to an expected TG-51-determined dose of 40 Gy. When determining the monitor units (MU) necessary to expose the alanine to 40 Gy in the $f_{\text{small fields}}$, the UPMC's existing ionization chamber-determined output factors were used to extrapolate from the $(10\,\text{x}\,10)\,\text{cm}^2$ reference conditions to the $f_{\text{small fields}}$ measurement conditions. The difference between the expected TG-51-determined 40 Gy and alanine-determined dose were compared.

4.4.2 Results

Figure 4.2 shows a plot of the ionization chamber beam quality correction factors, $k_{Q_{\text{small fields}},Q_0}^{f_{\text{small fields}},f_0}$, of the three ionization chambers for varying static field sizes. TLDs were used to determine absorbed dose to water. The Standard Imaging Exradin A19 ionization chamber exhibited loss of lateral CPE for the $(2.4\,\text{x}\,2.4)$ cm^2 field size, which resulted in the beam quality correction factors increasing as the field size was decreased. This demonstrates the challenges with using a large ionization chamber for small field dosimetry due to the detector's physical size integrating over a charged particle fluence spectra lacking CPE (Section Beam quality dependencies for small and nonstandard photon field dosimetry). Both the beam quality correction factors for the Standard Imaging Exradin A1SL and A16 ionization chambers did not display a significant dependence within one standard deviation as a function of decreasing

field size. The beam quality correction factor used in the standard TG-51 CoPs was found to be within one standard deviation for the majority of the TLD-determined values. The published TG-51 values for the ionization chambers in the 6 MV linac beam used are: 0.997 for the Standard Imaging Exradin A19,[3] 0.9946 for the Standard Imaging Exradin A1SL, and 0.9959 for the Standard Imaging Exradin A16.[59]

Table 4.1 shows the results of the NIST alanine dose measurements for varying static field sizes and the percent differences between the doses determined with alanine pellets and the UPMC determined dose of 40 Gy is given. The UPMC determined dose of 40 Gy was found using their TG-51 beam calibration. The UPMC will only take action and alter their beam dose calibration value when routine QA finds a discrepancy greater than 2%. We assumed any difference less than 2% could be attributed to this increased uncertainty. Therefore, the discrepancies at the (3.2 x 3.2) cm^2 and (4.8 x 4.8) cm^2 fields are inconsequential. However, the discrepancies of 4.9% to 3.7% observed for the (1.6 x 1.6) cm^2 field are beyond the 2% action level. These discrepancies between alanine-measured and TG-51-determined dose for the (1.6 x 1.6) cm^2 field illustrate how current practice of using ionization chambers to determine output factors for small fields is leading to miscalibration of doses at small field sizes. No formal value of uncertainty was provided in the NIST reported results.

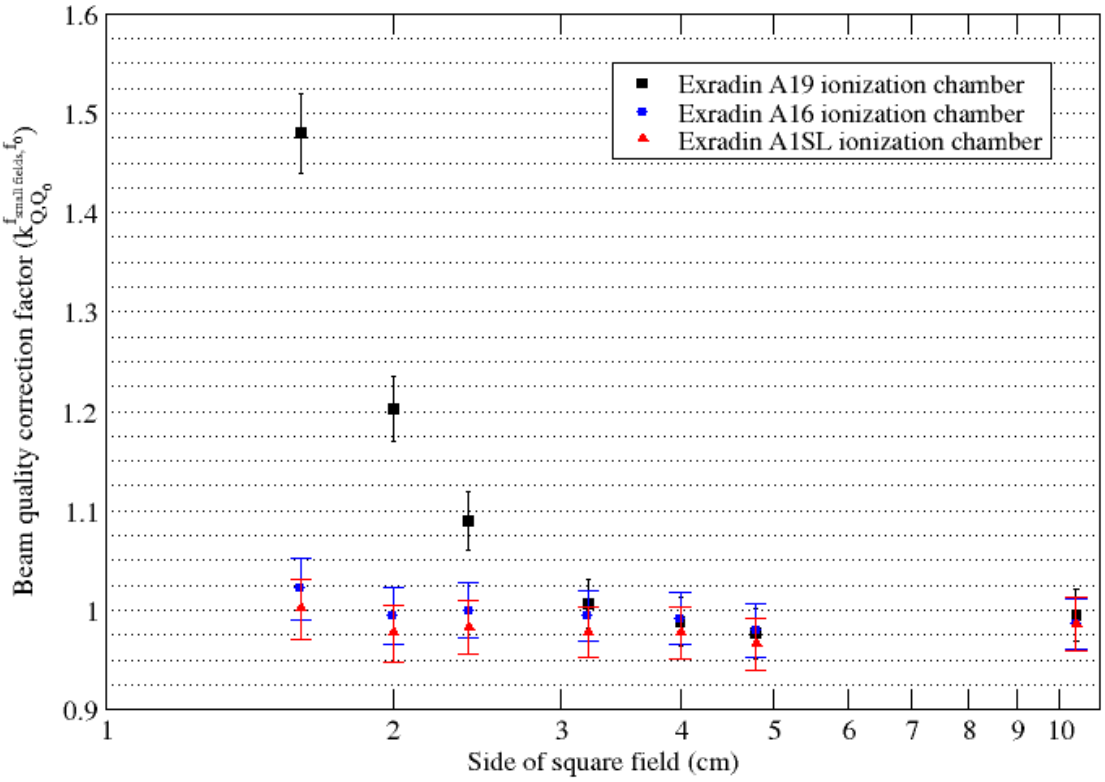

Figure 4.2: The markers are TLD-determined small field beam quality correction factors for an Exradin A19 Farmer-type ionization chamber (0.65 cm^3 collecting volume), Exradin A1SL ionization chamber (0.057 cm^3 collecting volume), and Exradin A16 ionization chamber (0.007 cm^3 collecting volume). Error bars correspond to the first standard deviation of the measurements reproducibility.

Table 4.1: Dose in static fields obtained using NIST alanine pellet. Difference from 40 Gy less than 2% are considered inconsequential because UPMC existing TG-51 beam calibration values were used to determine dose delivered. This is a result of TG-51 beam calibration values not being altered during routine QA unless a measured dose discrepancy of more than 2% is found

Alanine pellet No.	Field size [cm^2]	Dose measured by NIST [Gy]	Difference from 40 Gy [%]
1	1.6 x 1.6	38.03	-4.9
2	1.6 x 1.6	38.51	-3.7
3	1.6 x 1.6	38.35	-4.1
4	3.2 x 3.2	39.23	-1.9
5	3.2 x 3.2	39.35	-1.6
6	4.8 x 4.8	39.37	-1.6

4.5 In-phantom measurements of beam quality correction factor of static and composite fields

4.5.1 Methods

TLD, alanine, and ionization chamber measurements in photon fields from a linac and ^{60}Co unit were made to track the beam quality correction factor, $k^{f_{\text{small fields}},f_0}_{Q_{\text{small fields}},Q_0}$, from that of the standard NIST-traceable ^{60}Co absorbed dose to water to that of the f_{msr} and f_{pcsr} as outlined in the proposed formalism. Additionally, alanine- and TLD-determined $s_{c,p}$ and ionization chamber OFs were calculated in the same conditions using Equations (2.11) and (2.12). Beam quality correction factors were determined using Equation (4.2) for three ionization chambers ($M^{f_0}_{Q_0}$, $M^{f_{\text{small fields}}}_{Q_{\text{small fields}}}$); TLD and alanine were used to determined absorbed dose to water in the small ($D^{f_{\text{small fields}}}_{w,Q_{\text{small fields}}}$) and NIST-traceable ^{60}Co ($D^{f_0}_{w,Q_0}$) reference fields. The standard deviation (σ) for the beam quality correction factor was calculated by adding in quadrature the reproducibility uncertainty in the ionization chamber and TLD- or alanine-determined absorbed dose to water measurements.

The beam quality correction factor was measured at multiple steps in the calibration coefficient transfer process. This transfer process starts at the ^{60}Co standard reference condition for absorbed dose to water calibrations of 5 cm depth in water for a $(10\,\text{x}\,10)$ cm^2 field and ends with the ionization chamber in phantom in a composite field, f_{pcsr}. Figure 4.4 depicts the sequences of steps used in determining the beam quality correction factors from the ADCL ^{60}Co standard reference conditions (step 1 in Figure 4.4) to the proposed formalism's f_{pcsr} reference conditions (step 6 in Figure 4.4). One calibration condition variable was altered at each step, and the corresponding beam quality conversion factor was determined. Beam quality

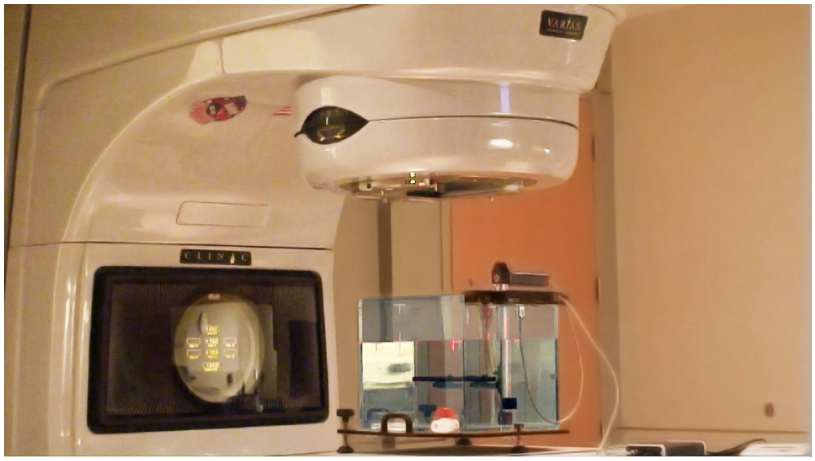

Figure 4.3: Ionization chamber dose measurements of irradiated by the Varian Linac in TG-51 reference conditions

correction factors were measured for several different sequences of steps that transfer the calibration coefficient from f_0 to the proposed formalism's f_{pcsr} reference conditions. Table 4.2 and 4.3 present in detail the different calibration conditions used during each step of the calibration coefficient transfer in which the beam quality correction factors were measured. Step 3d in Figure 4.4 corresponds to the TG-51 broad beam reference conditions (Figure 4.3), allowing for comparison of the beam quality correction factors found in this work with the TG-51 published Monte Carlo determined beam quality correction factors. Static field and composite field measurements were performed in a specially developed cylindrical PMMA phantom (Standard Imaging, Inc., Middleton, WI) as shown in Figure 4.5. PMMA was determined to be the optimal material for construction of the phantom used in this work based on its ease of use, homogeneity, and the manufacturing consistency of its physical composition. The cylindrical phantom has a diameter of 10 cm and length of 10 cm. Interchangeable inserts are available for positioning an array of TLDs, a single alanine pellet, a stack of three pieces of film, or ionization chambers. In-water TLD and alanine measurements were performed in the water tight VW holder shown

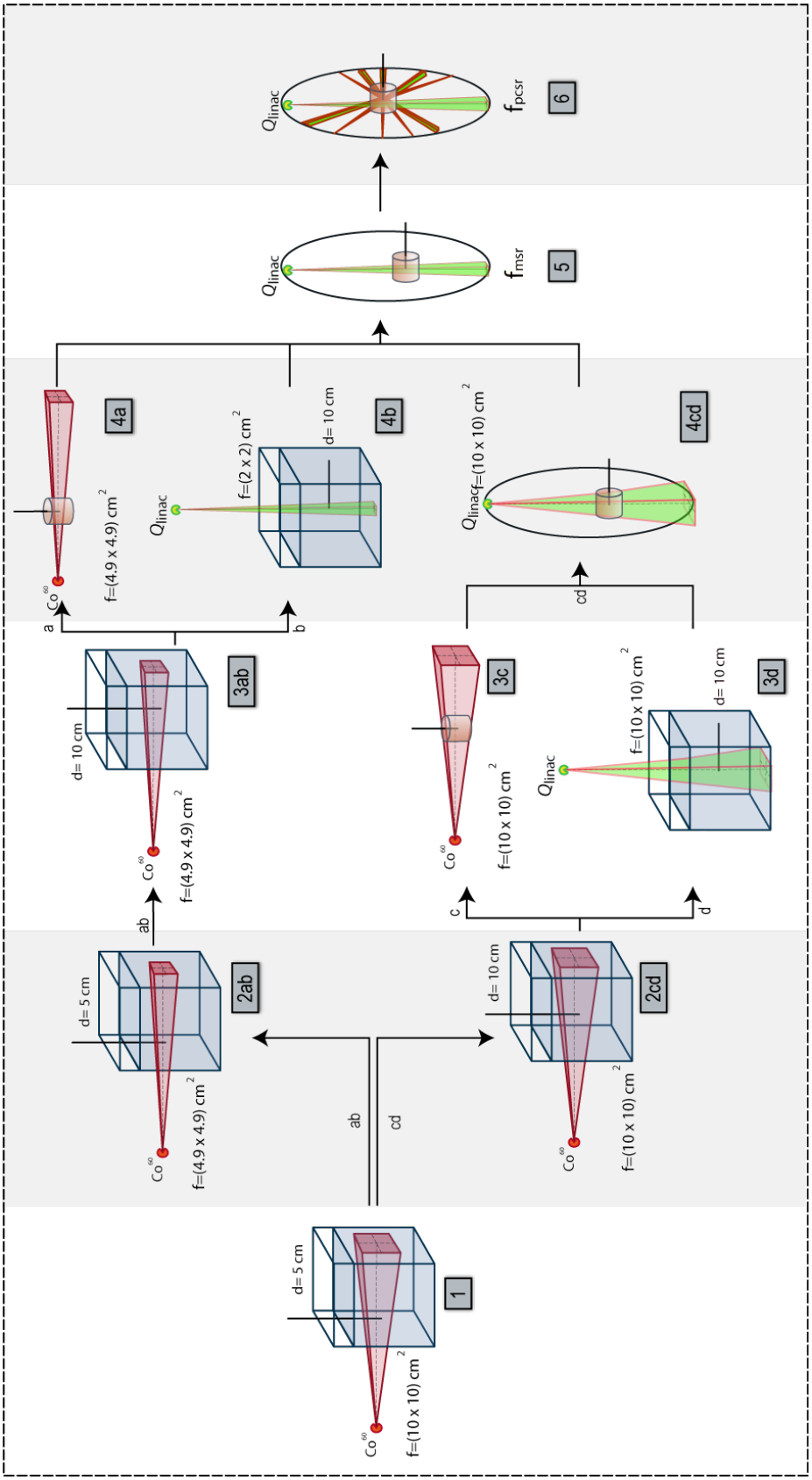

Figure 4.4: Flowchart of ionization chamber calibration transfer from ^{60}Co reference field (step 1) to plan-class specific reference field (f_{pcsr}) (step 6). Tables 4.2 and 4.3 describe the calibration conditions in more detail. a,b,c, and d represent the four possible pathways displayed in this figure.

in Figure 3.9. A VW holder was modified to be able to accommodate one alanine pellet positioned along the central axis.

A composite small field treatment, as discussed in the proposed formalism (f_{pcsr}), was created using the Pinnacle^3 (Philips, Fitchburg, WI) treatment planning system and was designed to produce a uniform dose to a three-dimensional volume that was sufficiently larger than the dimensions of the ionization chamber. The treatment plan used in this work mimicked a typical head and neck treatment with one treatment volume and one organ at risk representing the spinal cord. It was planned using inverse treatment planning optimization and was comprised of five IMRT fields. Dynamic multileaf collimation was used to define the field shape and modulation of each field, intensity distributions are shown in Figure 4.6. The resulting dose distribution calculated by Pinnacle is shown in Figure 4.7 and provides a uniform dose over the detector volume.

4.5.2 Results and discussion

Total scatter factor ($s_{c,p}$) measurements using alanine and TLD fell within one standard deviation of the output factor (OF) measurements for the Exradin A19, A1SL, and A16 ionization chambers for field size above $(2\,\mathrm{x}\,2)$ cm^2 (Figure 4.8). Deviations between $s_{c,p}$ and OF at the $(2\,\mathrm{x}\,2)$ cm^2 field sizes increased with increasing chamber volume, with a max deviation of approximately 20% found for the OF measurements using the Farmer-type A19. The Exradin A19, A1SL, and A16 OF measurements in the composite field reference conditions agreed, indicating a lack of volume dependance for the composite reference condition (f_{pcsr}). The alanine- and TLD-determined $s_{c,p}$ values agreed with each other, but the ionization chamber OF measurements disagree with the $s_{c,p}$ values by approximately 4%. The disagreement

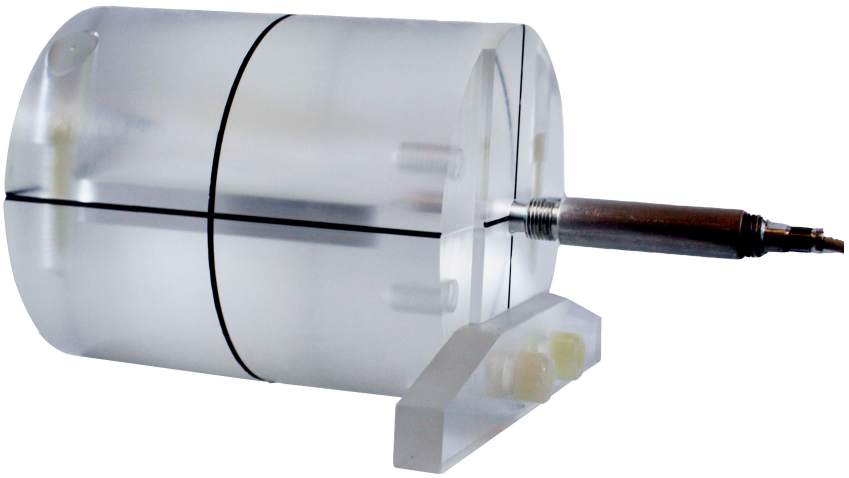

Figure 4.5: Acrylic phantom with a diameter of 10 cm and a length of 10 cm used in the measurement of beam quality correction factors. Inserts are available to accommodate a variety of detectors including TLDs, alanine, film, and ionization chambers (Standard Imaging, Inc., Middleton, WI).

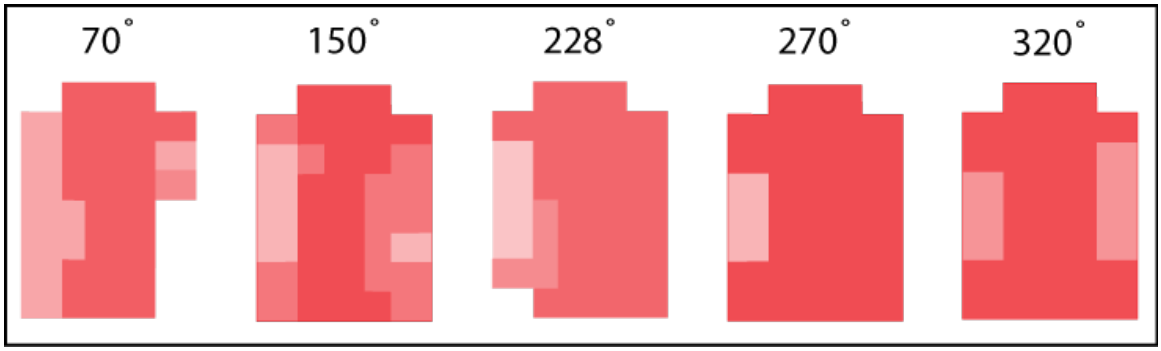

Figure 4.6: MLC intensity distributions defined by the number of MU delivered at each leaf position. The darker red indicates more dose was delivered in that region of the MLC defined field.

between the $s_{c,p}$ and OF indicates a change in beam quality and subsequently the detector response (Section 2.5.7). Interestingly, the magnitude of the beam quality response is independent of ionization chamber type and size. This indicates that the f_{pcsr} has the potential to reduce or remove ionization chamber volume dependancies (Section 2.5.4), but beam quality dependancies are present and must be corrected using beam quality correction factor (Derivation 2.5).

TLD-determined beam quality correction factors for the calibration conditions investigated (Figure 4.4) ranged from 0.97 to 1.30 and had associated standard deviations from 1% to 3% (Table 4.2). The alanine-determined beam quality correction factors ranged from 0.996 to 1.293 (Table 4.3) The trends were similar to those observed with TLD. The alanine-determined absorbed dose to water expressed greater measurement reproducibility than the TLD-determined values, with the alanine-determined beam quality correction factors expressing a standard deviation for 0.5% to 0.9% (Table 4.3).

The TLD-determined beam quality correction factors found in the ^{60}Co beam quality remained within one standard deviation of the normalization ionization chamber response found in the standard ^{60}Co reference conditions (Table 4.2, top half).

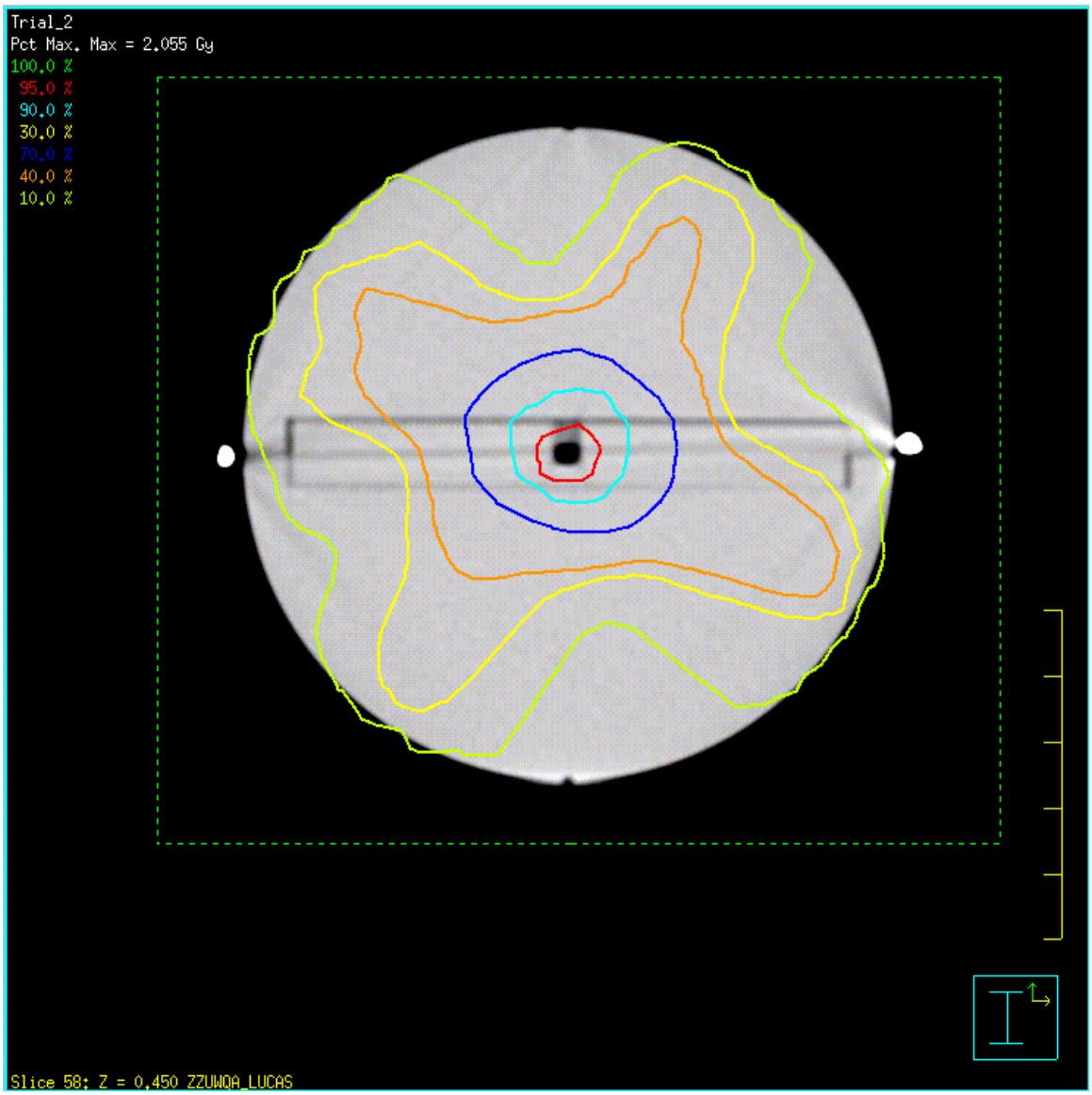

Figure 4.7: Pinnacle calculated dose distribution for the f_{pcsr} in the Lucas cylindrical phantom. Provides a uniform dose over the detector volume with a dose uniformity constraint set to 2%.

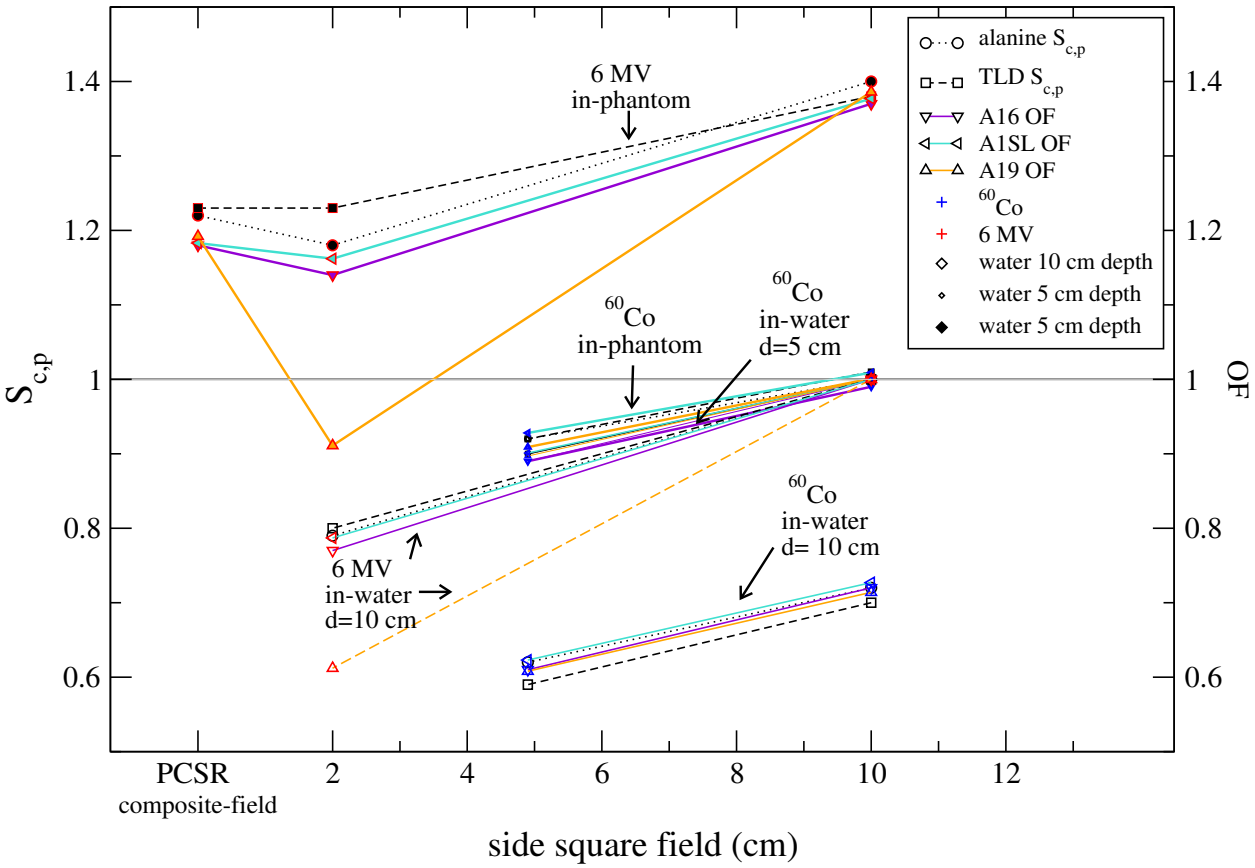

Figure 4.8: Total scatter factors measured using alanine and TLD (black lines) and output factor measurements (colored lines) for the Exradin A19 Farmer-type ionization chamber (0.65 cm^3 collecting volume), Exradin A1SL ionization chamber (0.057 cm^3 collecting volume), and Exradin A16 ionization chamber (0.007 cm^3 collecting volume) as a function of field size. Measurements in the ^{60}Co and linac beam qualities are normalized to the ADCL ^{60}Co calibration conditions and TG-51 reference conditions, respectively.

Any slight variations in the beam quality correction factor from unity may be attributed to beam hardening in the phantom or additional scatter from the phantom for the ^{60}Co conditions. The TLD-determined beam quality correction factor found in the standard TG-51 CoP broad beam reference conditions were equivalent to the published k_Q values (Table 4.2, step 3d). The majority of the TLD-determined beam quality correction factors found in the linac produced 6 MV beam quality fell within one standard deviation of the k_Q values used in the standard CoPs (Table 4.2, bottom half). The largest beam quality correction factors value was for the Exradin A19 Farmer-type ionization chamber in which the value increased to 1.30 for a field size of $(2\,\mathrm{x}\,2)$ cm^2 (Table 4.2, steps 4cd and 5). This is likely due to loss of lateral CPE and an averaging of the resultant inhomogeneous charged particle fluence over the detector volume (Section 2.5.1). These results are similar to what was observed in the static field results for the $(2.4\,\mathrm{x}\,2.4)$ cm^2 field (Section 4.4.2).

The alanine-determined absorbed dose to water yielded smaller standard deviations and beam quality correction factors which differed by more than one standard deviation compared to the TLD-determined beam quality correction factors (table 4.3). The beam quality correction factors varied from 0.996 to 1.028, with a substantial increase of approximately 1.293 for the A19 Farmer-type ionization chamber at the field sizes of $(2\,\mathrm{x}\,2)$ cm^2, which was similar to what is observed with the TLD-determined beam quality correction factors (Table 4.3, step 4.3 and 5). The alanine measured beam quality correction factors in the TG-51 reference conditions (table 4.3, step 3.3) were equal to the published TG-51 k_Q values for the ionization chambers within one standard deviation. The alanine-determined beam quality correction factor measured in-phantom (PMMA) and in-water were equal within one standard deviation of the measurements, if all other conditions variable were equivalent. This demonstrated that altering the phantom material from water

to PMMA does not effects the stopping power ratios and beam quality within the alanine's precision (~0.2%). The in-phantom measurement of (2 x 2) cm^2 6 MV field (Table 4.3 step 5), representing an arbitrary f_{msr} condition, yielded statistically significant alanine-determined beam quality correction factors which differed by more than one standard deviation from the published TG-51 k_Q values for all three ionization chambers.

The Exradin A19 Farmer-type ionization chamber's beam quality correction factor was approximately 30% larger than the smaller Exradin A16 and A1SL chambers in the (2 x 2) cm^2 static field. However, in the f_{pcsr} composite field made up of multiple beamlets smaller than (2 x 2) cm^2, the Exradin A19 Farmer-type ionization chamber's beam quality correction factor was within one standard deviation of the smaller Exradin A1SL and A16 ionization chambers' beam quality correction factors. Each individual beamlet in the f_{pcsr} may not exhibit lateral CPE, especially for the case of the larger A19 farmer-type chamber, but the f_{pcsr} was designed to provide a uniform dose distribution over the ionization chambers volume resulting in a cumulative CPE condition and remedying the volume averaging issues by blurring the charged particle inhomogeneous dose distributions over the detector volume.

While the f_{pcsr} has demonstrated its potential to reduce or remove ionization chamber volume dependancies, the measured beam quality correction factors were not equal to the standard CoP's k_Q indicating a change in beam quality in the f_{pcsr} relative to the standard CoP broad beam conditions. The TLD- and alanine-determined beam quality correction factors in the f_{pcsr} were approximately 1.03 for all three chambers (Table 4.3 and 4.3, step 6) and differed by more than one standard deviation from the published TG-51 k_Q values. The differences are due to variations in the beam quality and the 3% beam quality correction factor for the f_{pcsr} may be the result of modulating the field which increased the scatter contribution leading to a lower

effective energy. While the Exradin A19 Farmer-type beam quality correction factor decreased as a result of decreased volume averaging, the smaller Exradin A16 and A1SL ionization chambers displayed a 0.4% and 2.2% increase in the beam quality correction factor from the (2×2) cm^2 static field conditions.

4.6 Uncertainty analysis

Sources of uncertainty for the TLD and alanine determined beam quality correction factors included TLD/alanine measurement reproducibility, energy dependence, positioning, and ionization chamber reproducibility.

4.6.1 UWMRRC TLD

The TLD-100 chips were found to have an average reproducibility standard deviation of around 1.5%. The energy dependence correction factor applied to the TLD measurements was 0.97 and had an associated uncertainty of 1.5% at k=1. The expanded relative uncertainty for the TLD-determined beam quality correction factors is approximately 4% at k=2 (table 4.4). The TLD reproducibility differs for each calibration condition as it is the average of the standard deviation of the corrected readings of the TLDs irradiated in the 6 MV photon calibration condition and the corresponding ^{60}Co readings.

An evaluation of uncertainties associated with position and volume averaging encountered when using the ionization chambers and TLDs was performed by repositioning the ionization chamber before and after the alanine and TLD exposures. There was no observable difference for repeated ionization chamber positioning and measurements. The uncertainties associated with position of the TLD was evaluated

Table 4.2: Measured beam quality correction factors for the Exradin A19, A1SL, and A16 ionization chambers. TLDs were used to determine absorbed dose to water. All results were normalized to the standard UWADCL ^{60}Co calibration conditions. Presented uncertainties correspond to the first standard deviation. Depth values are labeled "na" for measurements not made in water.

Calibration conditions					A16		A1SL		A19	
Sequential Step	Energy	Field Size (cm^2)	SSD/Depth (cm/cm)	Medium	$k_{Q_{\text{small fields}},Q_0}^{f_{\text{small fields}},f_0}$	σ	$k_{Q_{\text{small fields}},Q_0}^{f_{\text{small fields}},f_0}$	σ	$k_{Q_{\text{small fields}},Q_0}^{f_{\text{small fields}},f_0}$	σ
1	^{60}Co	10 x 10	100/5	water	1.00	0.02	1.00	0.02	1.00	0.02
2ab	^{60}Co	4.9 x 4.9	100/5	water	1.00	0.03	0.99	0.03	1.00	0.03
2cd	^{60}Co	10 x 10	100/10	water	0.97	0.03	0.96	0.03	0.98	0.03
3ab	^{60}Co	4.9 x 4.9	100/10	water	0.97	0.02	0.95	0.02	0.97	0.02
3c	^{60}Co	10 x 10	100/na	phantom	1.02	0.03	1.00	0.03	1.01	0.03
4a	^{60}Co	4.9 x 4.9	100/na	phantom	1.02	0.04	0.99	0.04	1.01	0.04
TG-51 published k_Q values					*0.996*		*0.995*		*0.997*	
3d	6 MV	10 x 10	100/10	water	0.99	0.02	0.99	0.02	0.99	0.02
4b	6 MV	10 x 10	100/na	phantom	1.00	0.02	0.99	0.02	0.99	0.02
4cd	6 MV	2 x 2	100/10	water	1.02	0.05	1.00	0.05	1.29	0.05
5	6 MV	2 x 2	100/na	phantom	1.06	0.04	1.04	0.04	1.33	0.04
6	6 MV	f_{PCSR}	100/na	phantom	1.03	0.03	1.03	0.03	1.02	0.03

Table 4.3: Measured beam quality correction factor for the Exradin A19, A1SL, and A16 ionization chambers. Alanine provided by NPL was used to determine absorbed dose to water. All results were normalized to the standard UWADCL ^{60}Co calibration conditions. Presented uncertainties correspond to the first standard deviation. Depth values are labeled "na" for measurements not made in water.

Calibration conditions					A16		A1SL		A19	
Sequential Step	Energy	Field Size (cm^2)	SSD/Depth (cm/cm)	Medium	$k_{Q_{\text{small fields}},Q_0}^{f_{\text{small fields}},f_0}$	σ	$k_{Q_{\text{small fields}},Q_0}^{f_{\text{small fields}},f_0}$	σ	$k_{Q_{\text{small fields}},Q_0}^{f_{\text{small fields}},f_0}$	σ
1	^{60}Co	10 x 10	100/5	water	1.000	0.007	1.000	0.007	1.000	0.007
2ab	^{60}Co	4.9 x 4.9	100/5	water	1.009	0.008	0.999	0.008	1.004	0.008
2cd	^{60}Co	10 x 10	100/10	water	0.998	0.009	0.990	0.009	1.009	0.009
3ab	^{60}Co	4.9 x 4.9	100/10	water	1.026	0.005	1.000	0.005	1.026	0.005
3c	^{60}Co	10 x 10	100/na	phantom	1.015	0.007	0.994	0.007	1.001	0.007
4a	^{60}Co	4.9 x 4.9	100/na	phantom	1.028	0.005	0.991	0.005	1.012	0.005
TG-51 published k_Q values					*0.996*		*0.995*		*0.997*	
3d	6 MV	10 x 10	100/10	water	0.996	0.006	0.996	0.006	0.998	0.006
4b	6 MV	10 x 10	100/na	phantom	1.015	0.005	1.010	0.005	1.005	0.005
4cd	6 MV	2 x 2	100/10	water	1.019	0.006	1.005	0.006	1.293	0.006
5	6 MV	2 x 2	100/na	phantom	1.025	0.006	1.008	0.006	1.288	0.006
6	6 MV	f_{PCSR}	100/na	phantom	1.029	0.005	1.030	0.005	1.023	0.005

by performing the TLD measurements multiple times (n $\geq$ 5) for each calibration condition. Each measurement contained 5 TLDs in a cross shape occupying an approximately (1x1) cm^2 square perpendicular and centered on the beams central axis. There were no observable differences outside the TLDs reproducibility uncertainty, except for the (2 x 2) cm^2. This positioning uncertainty is incorporated into the measured reproducibility uncertainty. An uncertainty of 0.1% is applied for any slight volume averaging across a single chip that is masked by the TLDs high reproducibility uncertainty.

4.6.2 Alanine

NPL

NPL states their precision of a single dosimeter measurement to be better than $\pm$1% at k=1 for doses between 5 Gy and 10 Gy for their therapeutic dose monitoring service.[88,69] This work found an average reproducibility standard deviation ranging from 0.2% to 0.8% for the different calibration conditions for the NPL alanine absorbed dose to water measurements. The conservative value of 0.8% was used for this uncertainty analysis. The energy dependence correction factors applied to the alanine dosimeters had an associated uncertainty of 0.7% at k=1. The expanded relative uncertainty is approximately 2% at k=2 (Table 4.5).

NIST

The alanine pellets provided by NIST were found to have an average reproducibility standard deviation of approximately 5%. In past published work, NIST states a total absorbed dose uncertainty of 1.7% at 2σ for their alanine dosimeters exposures in the (30-50) Gy range.[28,29,66,67] However, no additional uncertainty estimates

Table 4.5: NPL alanine uncertainty budget.

	Type A (%)	Type B (%)
Alanine reproducibility	0.8	
Alanine positioning		0.1
NPL reported energy dependence		0.7
A and B quadratic sum	0.8	0.72
quadratic Sum k=1	1.1	
Expanded to k=2	2.2	

or explanations can be made for the difference in the observed 5% reproducibility uncertainty and NISTs lower published expanded uncertainty values, as NIST did not provide the readout methodology or associated uncertainty used in the measurements for this work.

Table 4.4: TLD uncertainty budget.

	Type A (%)	Type B (%)
TLD reproducibility	1.5	
TLD positioning		0.1
Energy dependence		1.5
A and B quadratic sum		1.9
quadratic Sum k=1	2.1	
Expanded to k=2	4.2	

4.7 Conclusions

The experimentally derived beam quality correction factors provide a comparison of the proposed formalism's calibration conditions with the secondary University of Wisconsin Accredited Dosimetry Calibration Laboratory's (UWADCL) ^{60}Co standard reference conditions in which the ionization chamber calibration coefficient is obtained. This work provides an increased understanding of how the calibration coefficient from an ADCL can be applied to the proposed small and nonstandard field formalism using beam quality correction factors. This work evaluated the feasibility of the proposed small and nonstandard field calibration protocol of the joint IAEA and AAPM working group to reduce the tolerance criterion of IMRT calibrations to that of the standard CoP larger reference field tolerances of less than 2%. The f_{pcsr} has the potential to reduce or remove ionization chamber volume dependencies (Section 2.5.4), but beam quality dependencies are present and must be corrected using beam quality correction factor (Derivation 2.5). In order to perform calibrations at this level, new beam quality correction factors will need to be provided for the f_{msr} and f_{pcsr} calibration conditions as their beam qualities differed from the standard CoP beam quality correction factors. In addition the f_{pcsr} needs to be evaluated further and the effects of modulation well characterized. The methodology developed for this work can also help to guide future research of other small field radiotherapy modalities and the measurements of even smaller field sizes. In addition, this work can be used for experimental verification for future Monte Carlo models used to simulate small and non standard field beam quality correction factors.

Chapter 5

Small Field Monte Carlo Methods

5.1 Introduction

As discussed in Section 2.5, determining dose in non-equilibrium conditions using cavity theory is challenging since all the parameters in the cavity theory dose equation are energy and spectrum dependent (Equation (2.1)).[23,1] Monte Carlo simulations are a good alternative to cavity theory for studying small field effects on energy spectra, because the simulations rely only on the energy imparted and not CPE calculations to determine dose.

Monte Carlo methods have been used in previous works to determine beam quality correction factors for ionization chambers in broad beam conditions.[100,3,7] Wulff *et al.*[100] found agreement with MC-determined and experimentally-determined beam quality correction factors within 0.5% for the standard CoPs reference conditions. They also found agreement within the uncertainty of MC-determined beam quality correction factors with TRS-398 k_Q values.[100,3,7,59,99] Additionally, Monte Carlo methods, benchmarked against calorimetry measurements, are used to determine standard broad beam CoP beam quality correction factors.

Beam quality correction factor accuracy is dependent on the validity of the Monte Carlo models. Accurate models for small and nonstandard fields are difficult to produce due to spectral variations in charged-particle fluence. Compared to ionization chamber beam quality correction factor simulation in broad beam geometries, small and nonstandard field Monte Carlo models require more complex geometries to obtain an accurate representation for their complex charged particle dose distribution, resulting beam quality correction factors could be large, and simulations are more sensitive to variations in the models source and geometry parameters. In addition, experimentally verifying the models is difficult due to the unknown level variation in their spectra and limitations of available detectors. Both measurements and simulations are difficult in small and nonstandard fields since the variability of the charged particle spectrum is dependent on multiple correlated variables. Measurements and Monte Carlo methods for small and nonstandard field dosimetry have drawbacks and a future solution will likely rely on a mix of the two techniques to be able to reduce the uncertainty in a meaningful way.

5.2 Monte Carlo code

A source of uncertainty for Monte Carlo calculations is in the photon and electron cross sections and the resulting stopping power ratios of the materials that comprise the ionization chambers. Based on the cross section uncertainty used in EGSnrc, ionization chamber simulations have been shown to pass the fano cavity test at 0.1%.[46,47,95] Due to its relatively low cross section uncertainty and advanced electron transport algorithms, the EGSnrc Monte Carlo code will be used in this work.[17]

The EGSnrc C++ user codes "cavity" and the more advanced "egs_chamber", are capable of performing Monte Carlo calculations of ionization chamber response

and ionization chamber determined beam profiles are used to model the ionization chambers.[100,99]BEAMnrc is a user code used to model radiotherapy accelerators and is based on the EGSnrc code. A linear accelerator was modeled using the BEAMnrc code to calculate phase space files, which can then be used as the input source in egs_chamber to model ionization chamber response.

5.3 Beam quality correction factor methods

Beam quality correction factor simulations require an accurate source model to account for the variations in the charged particle fluence spectrum. In addition, highly detailed and accurate models of the ionization chambers are required to account for the perturbation effects and changes in the mass attenuation coefficient across the chamber cavity due to the variable charged particle spectrum incident across the detector volume. Figure 5.1 illustrates the simulations method for obtaining the perturbation factors included in simulated beam quality correction factor ($k_{Q_r,Q_0}^{f_{\mathrm{fr}},f_{Q_0}}$) values shown in Equation Total scatter factors and output factors in the computational derivation of $k_{Q_r,Q_0}^{f_{\mathrm{fr}},f_{Q_0}}$.

$$k_{Q_r,Q_0}^{f_{\mathrm{fr}},f_{Q_0}} = \left[\left[\frac{\overline{L}}{\rho}\right]_a^w P_{\mathrm{fl}}\ P_{\mathrm{stem}}\ P_{\mathrm{cel}}\ P_{\mathrm{wall}} \right]_{\mathrm{Q_0}}^{Q_r} \tag{2.15}$$

The ionization chamber perturbation factors P_{stem}, P_{cel}, and P_{wall} account for the effects of the detectors components physical presence on the attenuation and scatter on the charged particle fluence for the stem central electrode and wall, respectively. The fluence perturbation factor (P_{fl}) accounts for the detector medium nonequivalence to water. This difference in composition can significantly alter the low-energy charged particle fluence and the photoelectric dose contribution. The

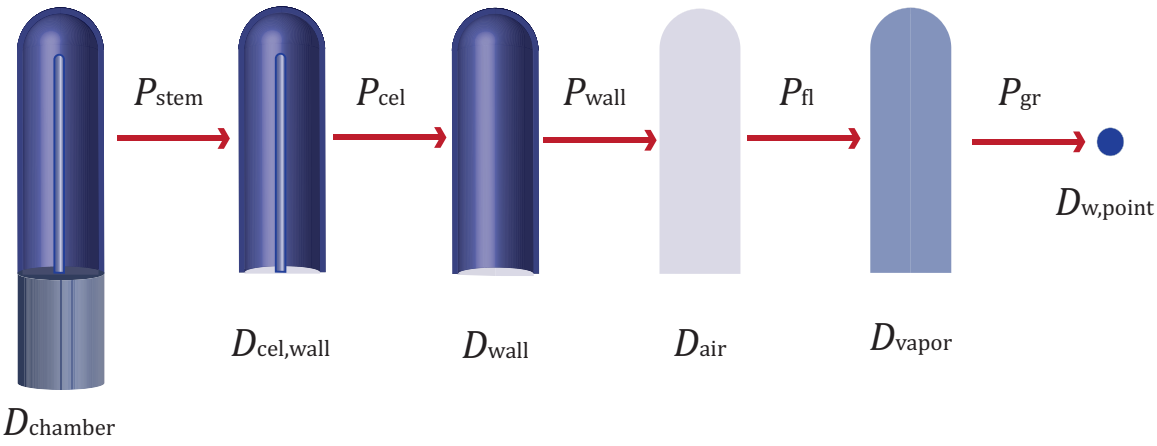

Figure 5.1: Ionization chamber perturbation factors

gradient correction factor (P_{gr}) accounts for averaging of the charged particle fluence energy deposition over the sensitive volume and is extremely important for small and nonstandard fields lacking CPE. P_{gr} can be orders of magnitude larger for small fields compared to the broad beam reference conditions and depends on beam quality, field size, and chamber volume as this work experimentally demonstrated in Chapter 4.

The size and composition of the detector components must be known explicitly for these factors to be determined accurately. In addition, for a generalized ionization chamber make-specific beam quality correction factor to be used in a small and nonstandard field protocol, the manufacturing tolerances must be strict as variations in small and nonstandard field reference conditions could effect the beam quality correction factor. The ionization chamber geometry will have a larger effect on the beam quality correction factor value for a variable charged particle fluence in a small or nonstandard field lacking CPE compared to the homogeneous broad beam CPE charged particle fluence. Additionally, all factors are dependent on the accuracy of the incident charged particle spectrum and therefore require a complete and experimentally verified source model of the inhomogeneous charged particle spectrum characteristic of small or nonstandard field lacking CPE. These

models require a complex geometry to obtain an accurate charged particle fluence that is representative of the spectrum variability across the field for small and nonstandard fields. Standard broad beam beam quality correction factors can be accurately simulated using point source models to create the uniform CPE charged particle fluence and accurate beam quality correction factor are less difficult to simulate.[99]

A linac and a ^{60}Co teletherapy unit was modeled in detail using BEAMnrc. The generated phase space files for the linac and ^{60}Co teletherapy unit contain the energy, position, direction, charge and history variable for every particle exiting downstream from the primary collimator. These files are used in conjunction with the egs_chamber ionization chamber models to obtain the desired beam quality correction factors.

5.4 Source models

The Monte Carlo codes BEAMnrc/DOSXYZnrc were used to create models for a linac and a ^{60}Co teletherapy unit. Linear accelerator component construction differs by manufacturer, but those components indicated in the generic model shown in Figure 5.2[96] are what is generally required in a complete Monte Carlo model.

In this study, a model was made for 6 MV photon beams produced from a Varian linear accelerator with Millennium™ 120 multileaf collimator. The Varian 6 MV linac was modeled from proprietary schematics and included the Bremstrauhlung target, primary collimator, beryllium window, flattening filter, monitor chamber, mirror, dynamic jaws, Varian dynamic Millennium™ MLCs, and light reticle (Figure 5.3 and 5.5).

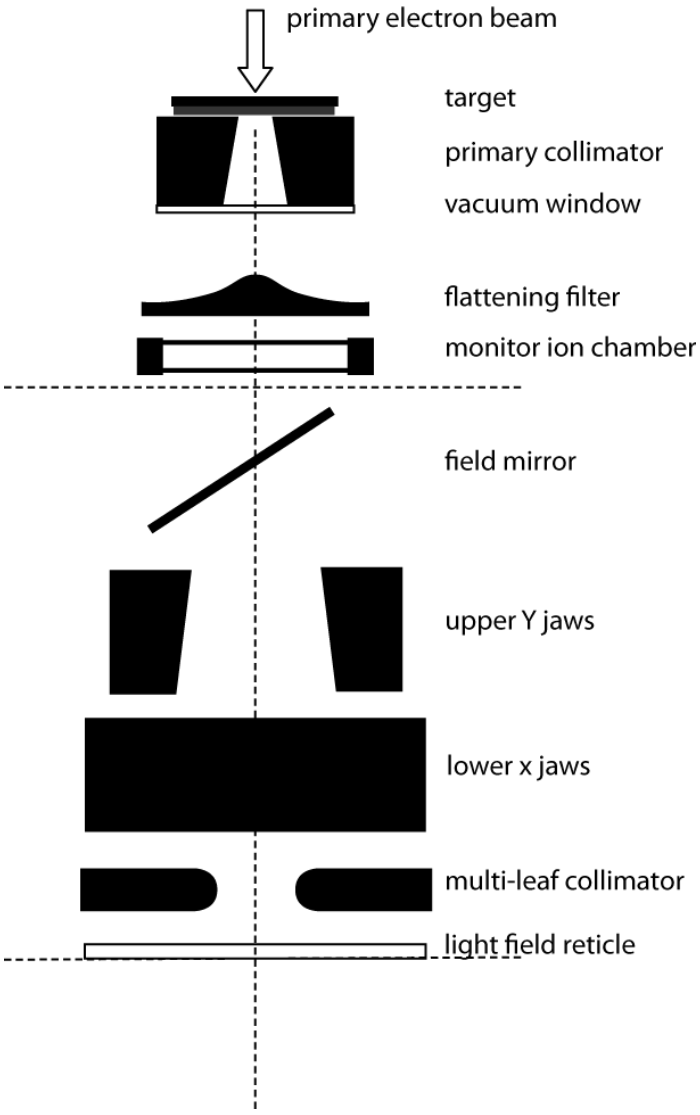

Figure 5.2: Generic linac geometry for Monte Carlo models

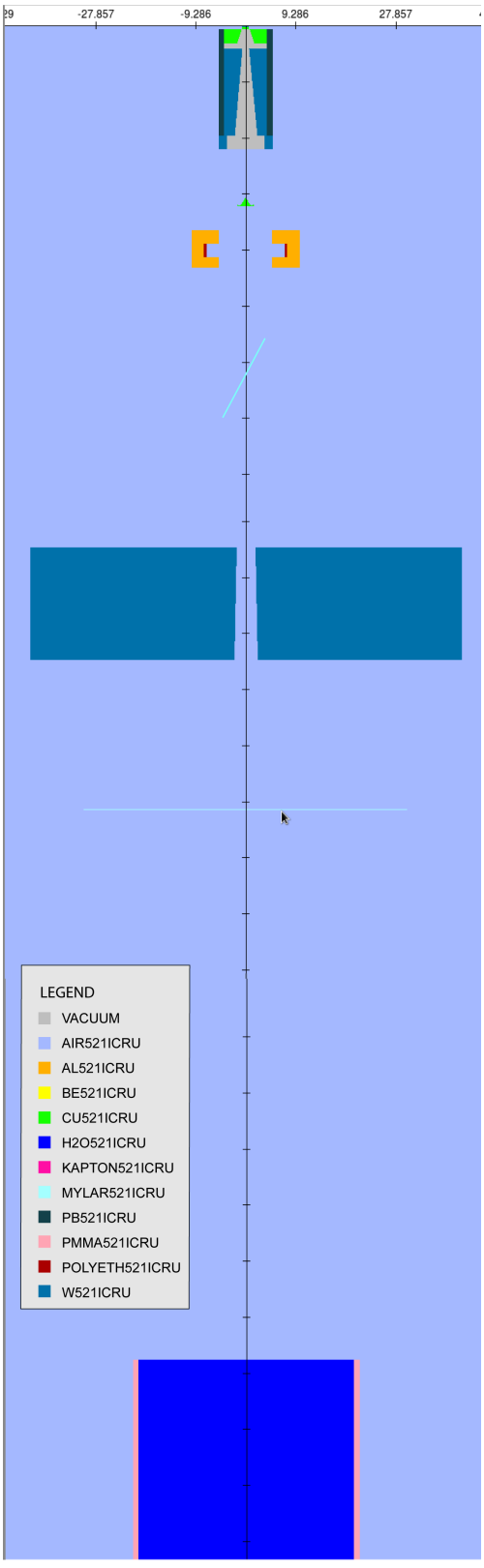

Figure 5.3: Schematic drawing of linac components modeled in the BEAMnrc full linac head MC simulations.[96]

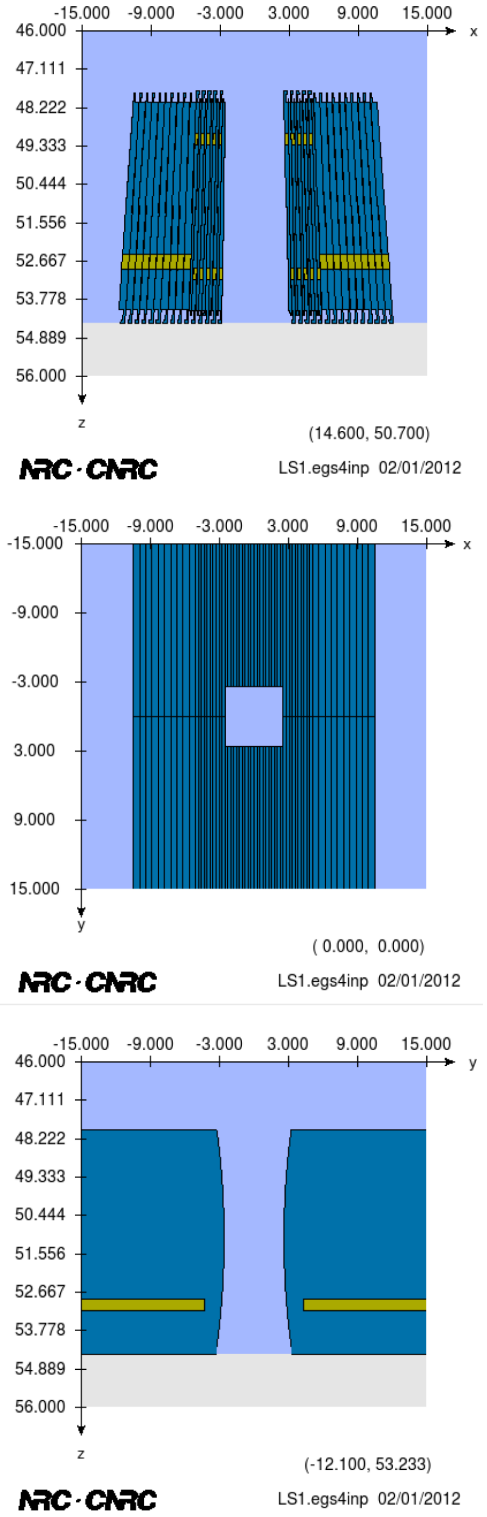

Figure 5.4: Rendering of Varian Millennium™ 120 leaf MLC.

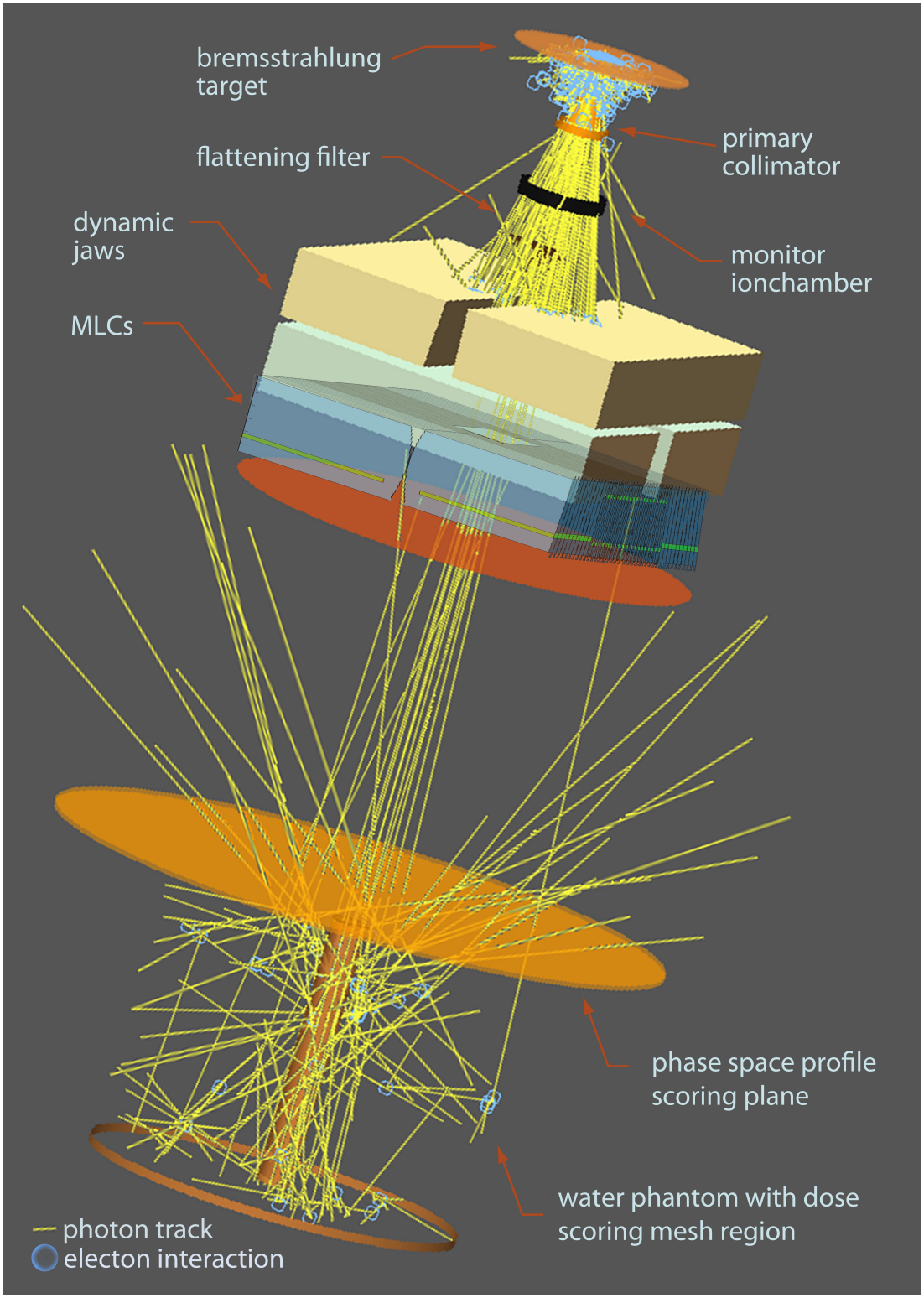

Figure 5.5: Rendering of the Varian linac BEAMnrc model for a (10x10) cm2 field simulation. With 120 dynamic MLCs . The orange disk represents the phase space scoring planes.

The Bremstrauhlung target was defined as a 0.0889 cm thick slab of tungsten (W) followed by 0.1575 cm thick slabs of copper (Cu). The front slab was set as the source location (Z=0 cm). Electrons were followed target down to kinetic energies of 10 keV (total energies of 0.521 MeV) and photons were followed down to energies of 1 keV. The copper flattening filter was modeled using 20 concave and convex conical layers with a maximum radius of 5 cm. Dose deposited in the monitor chamber due to backscatter from the jaws and MLCs was tracked in the model.

The Varian dynamic Millennium™ MLC model is comprised of 120 movable tungsten leaf pairs, which move perpendicularly to the beam central axis and has variable leaf widths. The finer, 5 mm wide leaves (40 pairs), are located in the centre of the field area, and followed by 1 cm wide leaves (20 pairs) (Figure 5.4). The Varian dynamic Millennium™MLC and dynamic jaws have the option of being programmed using simple text files to create a dynamically delivered radiation plan.

The linac source was modeled as a cylindrical electron beam with a Gaussian intensity distribution incident on the surface of the bremsstrahlung target. The starting incident electron energy and radial intensity distribution were adjusted to produce the best match between Monte Carlo calculated and measured dose distributions for a $(20 \times 20)\,\mathrm{mm}^2$, $(30 \times 30)\,\mathrm{mm}^2$, $(40 \times 40)\,\mathrm{mm}^2$, and $(100 \times 100)\,\mathrm{mm}^2$ field, defined by the Jaws and MLCs. The incident electron energy and radial intensity distribution were the only two parameters adjusted in the beam simulation. The resultant incident Gaussian radial intensity electron distribution had a FWHM of 0.1177 cm and a mono-energetic energy of 6.1 MeV for the nominal 6 MV linac beam (Figure 5.6).

The Theratronics T1000 ^{60}Co teletherapy unit at the UWADCL will also be modeled based on work from previous UWMRRC students J. Smilowitz and L. Bartol.[92,11] The ^{60}Co teletherapy unit consists of a 2 cm diameter source capsule

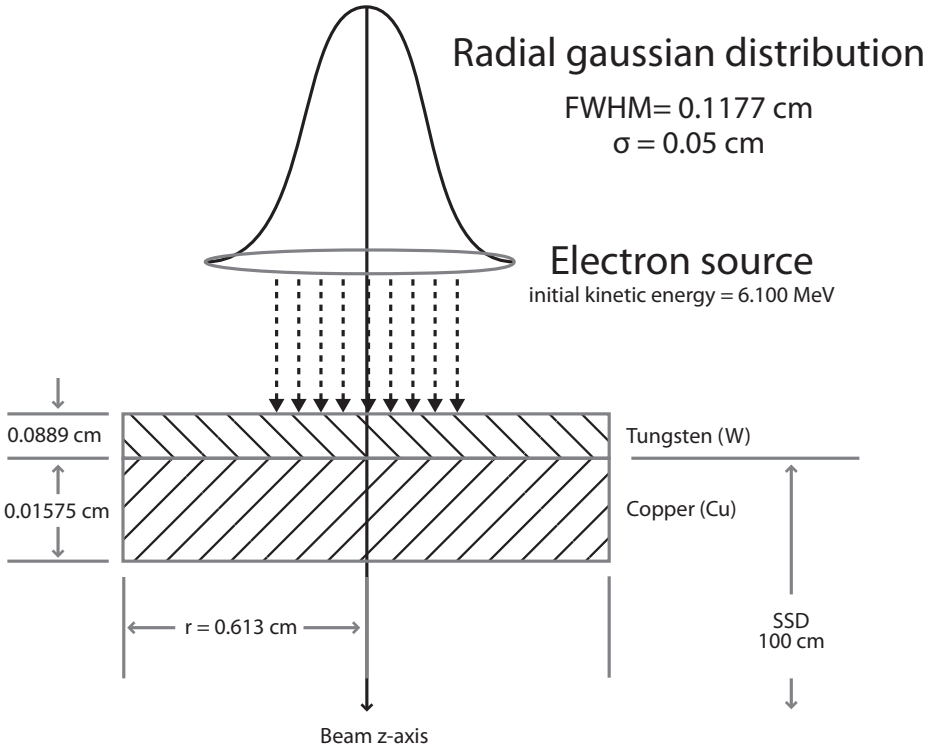

Figure 5.6: Electron source with gaussian intensity distribution

which contains radioactive ^{60}Co pellets, a stationary primary collimator, an outer set of adjustable trimmer bars, which defines the various field sizes of the therapy beam, and an outer shield for radiation protection. The Co-60 pellet source strength was ~ 5 kCi.

The Monte Carlo linac model set the energy thresholds for secondary particle creation and energy cutoffs to AE = ECUT = 0.100 MeV, AP = PCUT = 0.010 MeV for beam simulations and AE = ECUT = 0.521 MeV, AP = PCUT = 0.010 MeV for absorbed dose calculations in the water phantom. The phase-space file for each field shaped by Jaws and MLC was scored at an SSD of 100 and the linac or ^{60}Co head exit window.

5.5 Ionization chambers

Ionization chamber geometries were modeled with the C++ class library egspp for the EGSnrc code system.[48] Models of each ionization chamber, based on manufacturer specifications and include the different regions and materials such as the collector, guard, collector-guard insulator, high-voltage insulator, thrust washer, strain relief, stem, and shell. Four different models of ionization chambers were modeled: a Standard Imaging Exradin A19, a Standard Imaging Exradin A1SL, a Standard Imaging Exradin A16, and a PTW pinpoint chamber. The advanced user code egs_chamber and its variance reduction techniques were used.

5.6 Experimental benchmarking

The 6 MV linac model created from proprietary schematics provided by Varian was benchmarked against the Varian linac located at the UW Carbone Cancer Center (UWCCC). Figure 5.11 and 5.12 are examples of the comparison between measured and Monte Carlo calculated scatter ratios as a function of field size shaped by the MLC with X–Y jaws set to the corresponding calculated field size. The detector used for measurements was an Exradin A1SL ionization chamber. The PDDs were scaled by their calculated scatter ratios normalized to the $(10 \times 10)\,\mathrm{cm}^2$ field. Good agreement was shown between the Monte Carlo models and the measured PDDs.

5.7 UWMRRC Monte Carlo data base and programing

Many Monte Carlo simulations were performed for this dissertation on small and nonstandard dosimetry and represent only a fraction of the amount required to

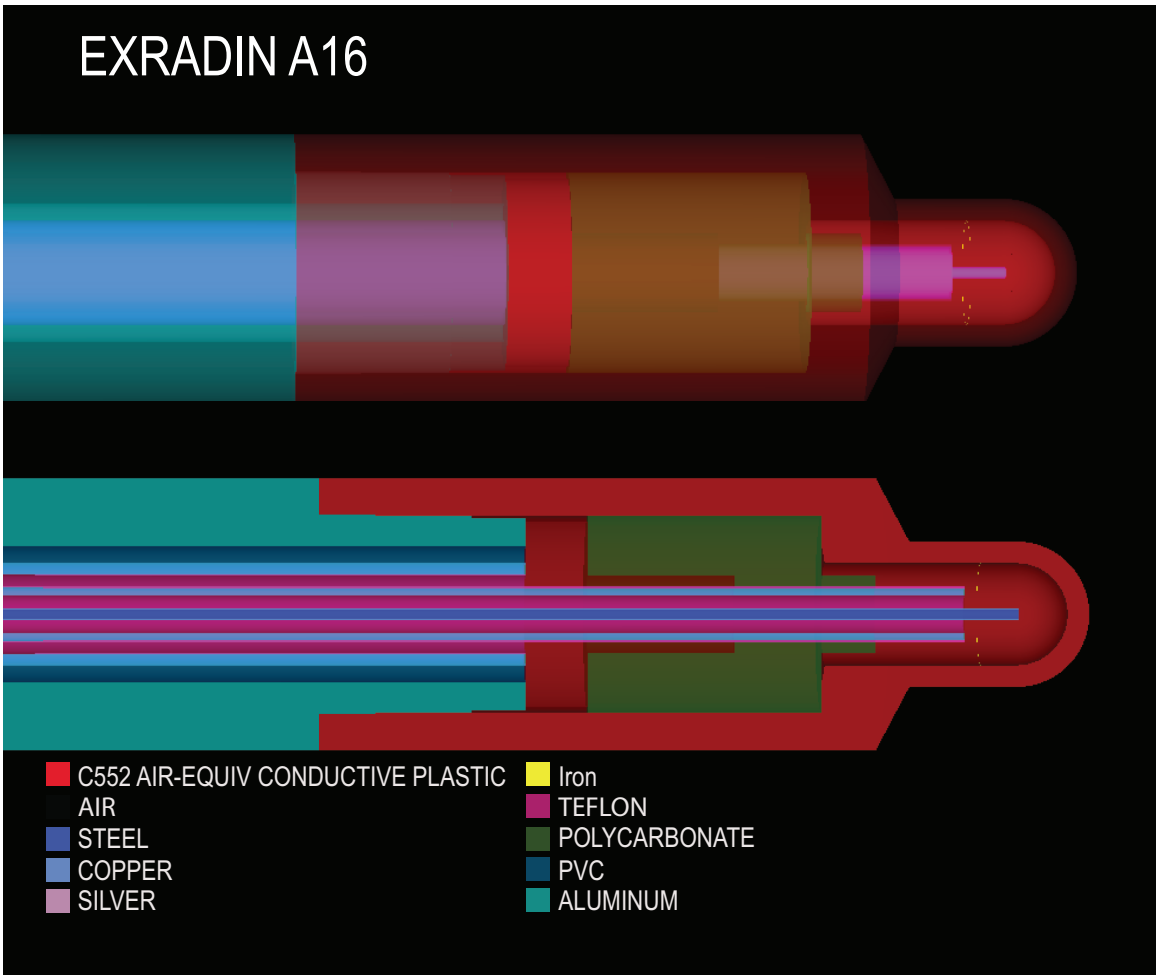

Figure 5.7: Exradin A16 ionization chamber model rendering with variance reduction region.

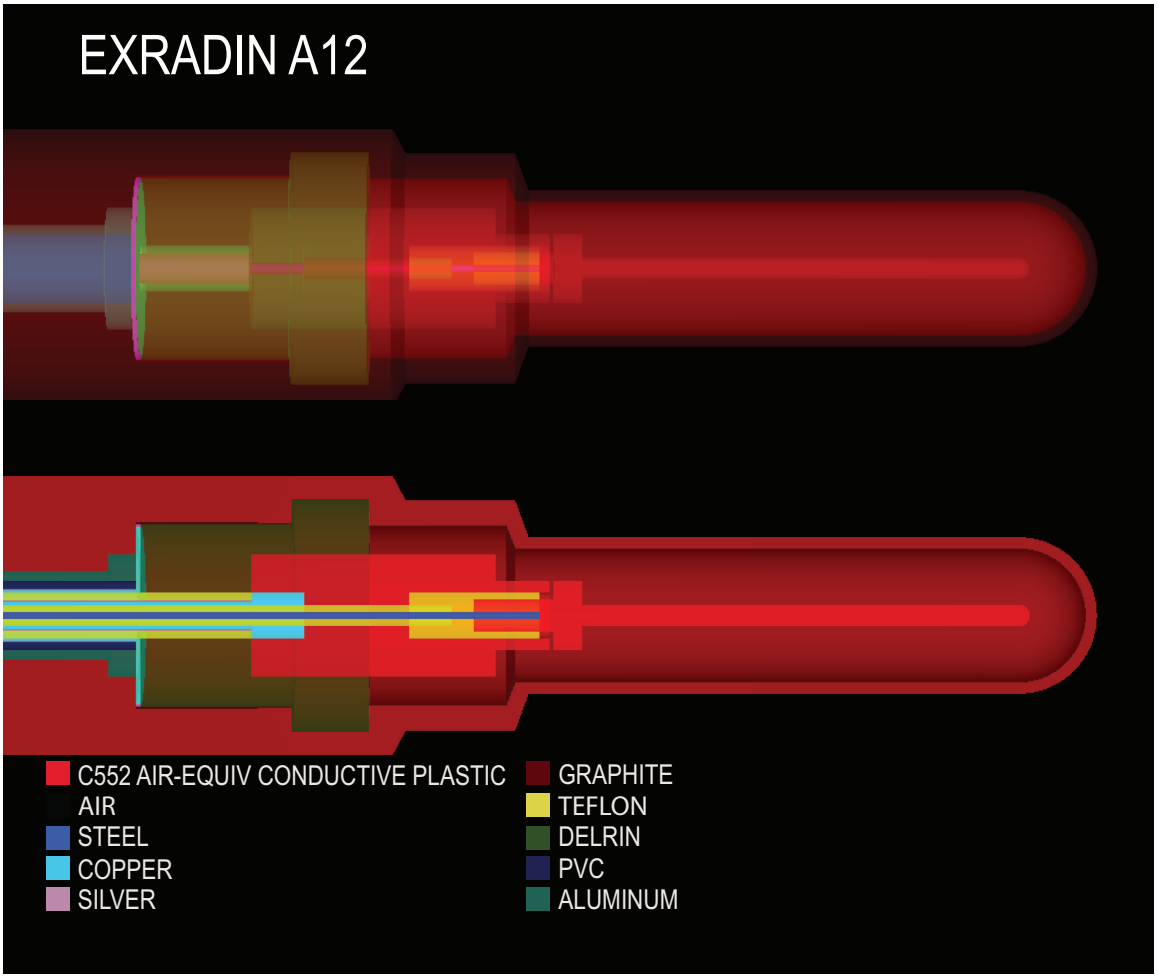

Figure 5.8: Exradin A1SL ionization chamber model rendering with variance reduction region.

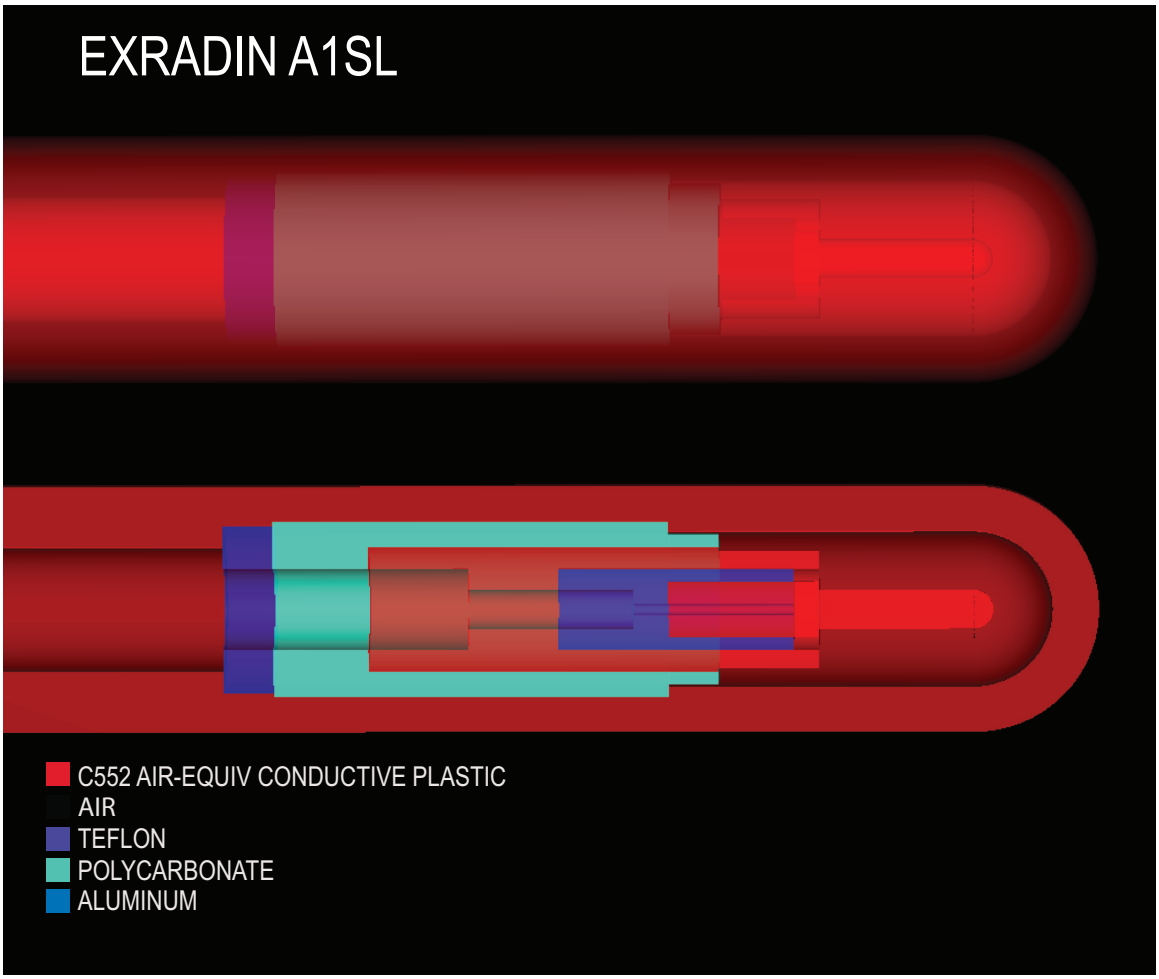

Figure 5.9: Exradin A1SL ionization chamber model rendering with variance reduction region.

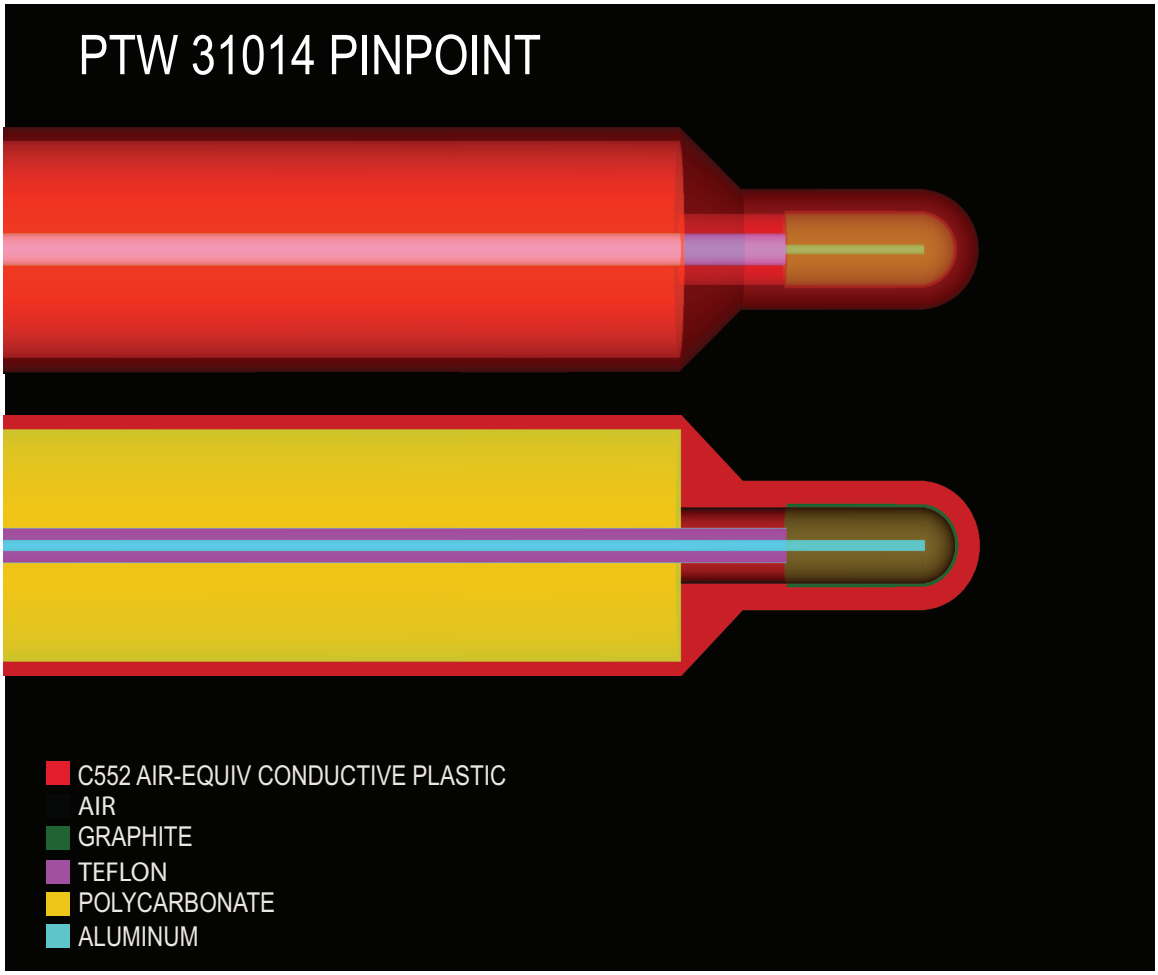

Figure 5.10: Simplified model of PTW 31014 PinPoint micro ionization chamber. Uncertainty in simulations was found to be large due to lack of proprietary schematics.

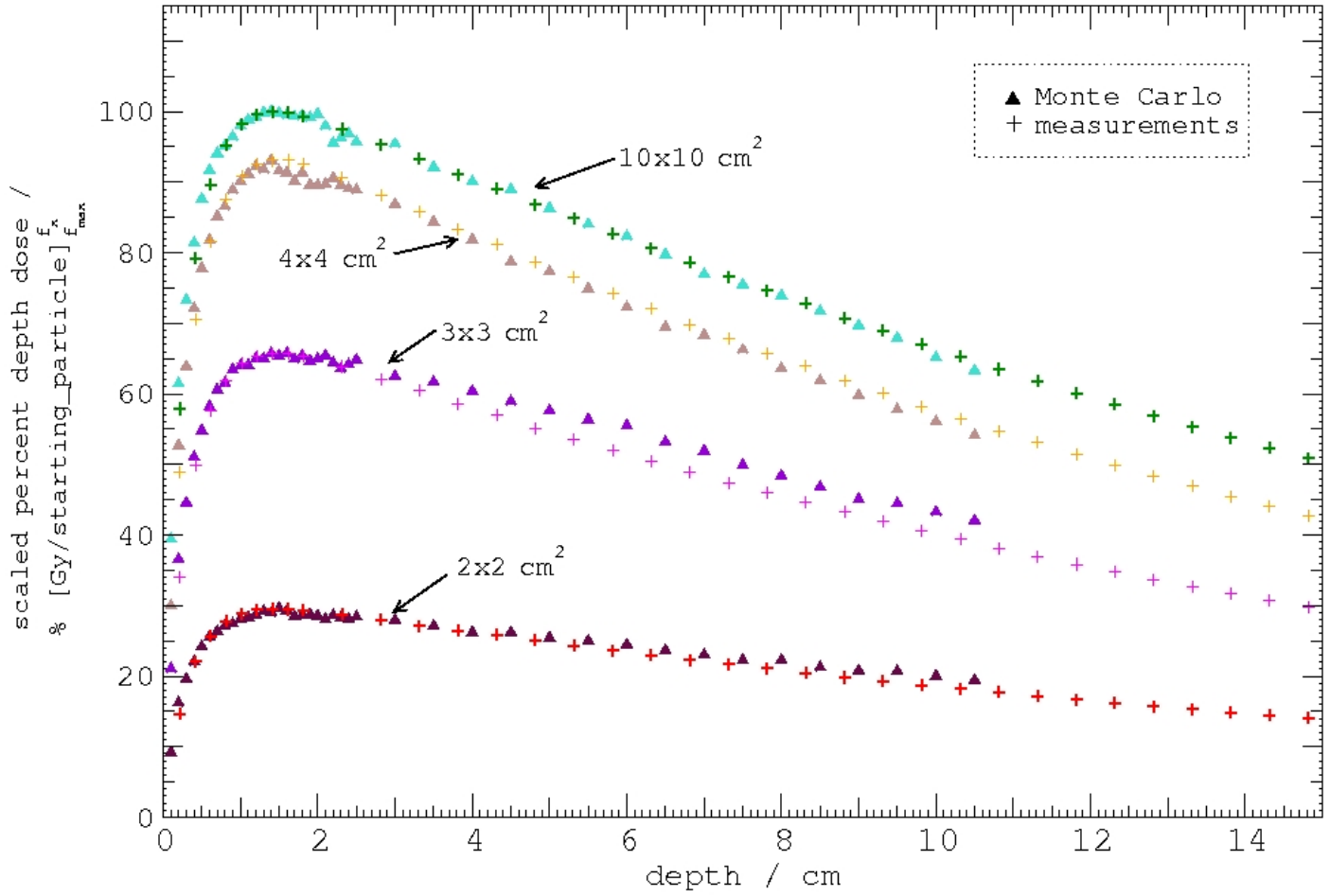

Figure 5.11: An example of the Monte Carlo benchmarking against measurement data: simulated and measured PDD curves for four field sizes. Comparison between the Monte Carlo calculated and measured central-axis depth– dose curves for a field size of (a) $(20 \times 20)\,\mathrm{mm}^2$, (b) $(30 \times 30)\,\mathrm{mm}^2$, (c) $(40 \times 40)\,\mathrm{mm}^2$, and (d) $(100 \times 100)\,\mathrm{mm}^2$, defined by the Jaws and MLCs for a 6 MV beam at SSD = 100 cm. PDDs are scaled to number of starting particles in Monte Carlo simulation and by their calculated scatter ratios normalized to the $(10 \times 10)\,\mathrm{cm}^2$ field.

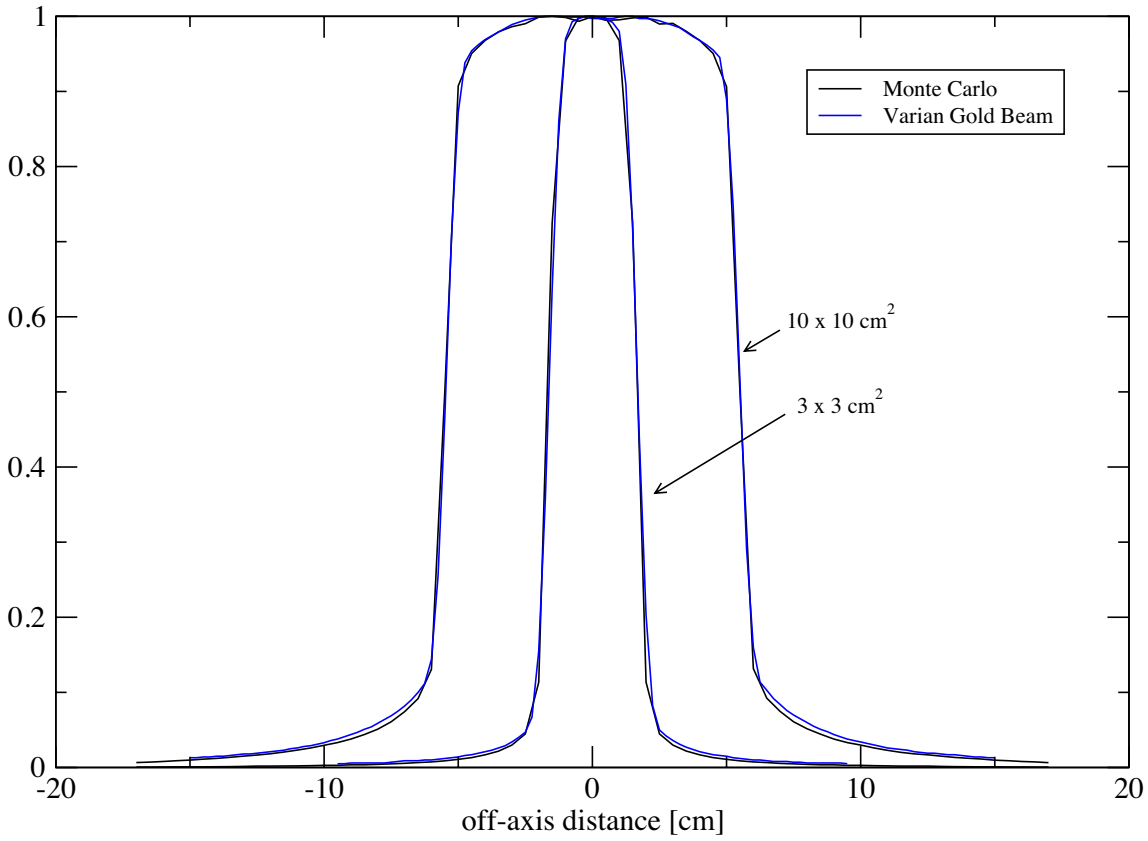

Figure 5.12: An example of the Monte Carlo benchmarking against measurement data: simulated and measured Profiles curves for a $(30 \times 30)\,\mathrm{mm}^2$ and $(100 \times 100)\,\mathrm{mm}^2$ field. Fields are defined by the Jaws and MLCs for a 6 MV beam at SSD = 100 cm.

perform a comprehensive Monte Carlo study on small and nonstandard fields. Manually processing large amounts of Monte Carlo generated data was found to be impractical and led to various errors. The need for quality control when performing data evaluation has led to program development for the automatic processing of Monte Carlo simulation input and output data related to the specific applications used in this work.

Due to the infancy of the proposed formalism and the lack of a practical definition for a f_{pcsr}, it was determined that directly applicable simulations relating to the proposed formalism would not be performed until the f_{pcsr} is defined. The large amount of Monte Carlo simulation and procedures used in this work require a structured and manipulatable data format for future implementation. This organizational need evolved into the development of a Monte Carlo database framework for the UWMRRC.

The programing for automatic processing of Monte Carlo simulation input/output data and the database framework developed for use in this work was expanded upon to accommodate the large research program at the UWMRRC. This expansion forms the basic framework for the new UWMRRCs Monte Carlo Database and aims to incorporate all future and retrospectively add all past Monte Carlo data acquisitions at the UWMRRC.

The purpose of the UWMRRC Monte Carlo Data Base is to increase Monte Carlo simulation quality control and resource efficiency through development of a Monte Carlo Database framework for automatic processing and organization of Monte Carlo simulation input/output data for all Monte Carlo simulations for UWMRRC research projects, including small and nonstandard field dosimetry.

5.7.1 Framework

The current database framework is displayed in Figure 5.13. The program is currently written in Python coding language and uses a command line interface. The framework is based upon a universal variable library (Variables.properties) and headers written into the databases items. Future and past models and simulations are labeled using user defined variables from a list of universal variables allowing for a congruent and searchable database.

The database functionality is expanded by allowing future models to be created using a template input and a corresponding template properties file that contains a set of values corresponding to one or more universal variables. These templates can then use batch input files declaring multiple values for the template variables, which will automatically generate a set of input files. In addition, the simulations can then be automatically analyzed based on the variable values defined by the user in the batch file. The current database structure includes universal variables for Linac, Cobalt-60, and Orthovoltage x-ray source options; static field and composite field treatment options; water, solid water, acrylic, and air phantom options; and ionization chambers, TLD, alanine, and water detector options.

5.8 Conclusions

Monte Carlo models and a database were developed for small and nonstandard beam quality correction factor determination. Monte Carlo models for a linac and a ^{60}Co teletherapy unit were created using BEAMnrc. Four ionization chambers were modeled in the advanced EGSnrc user code egs_chamber. This Monte Carlo work

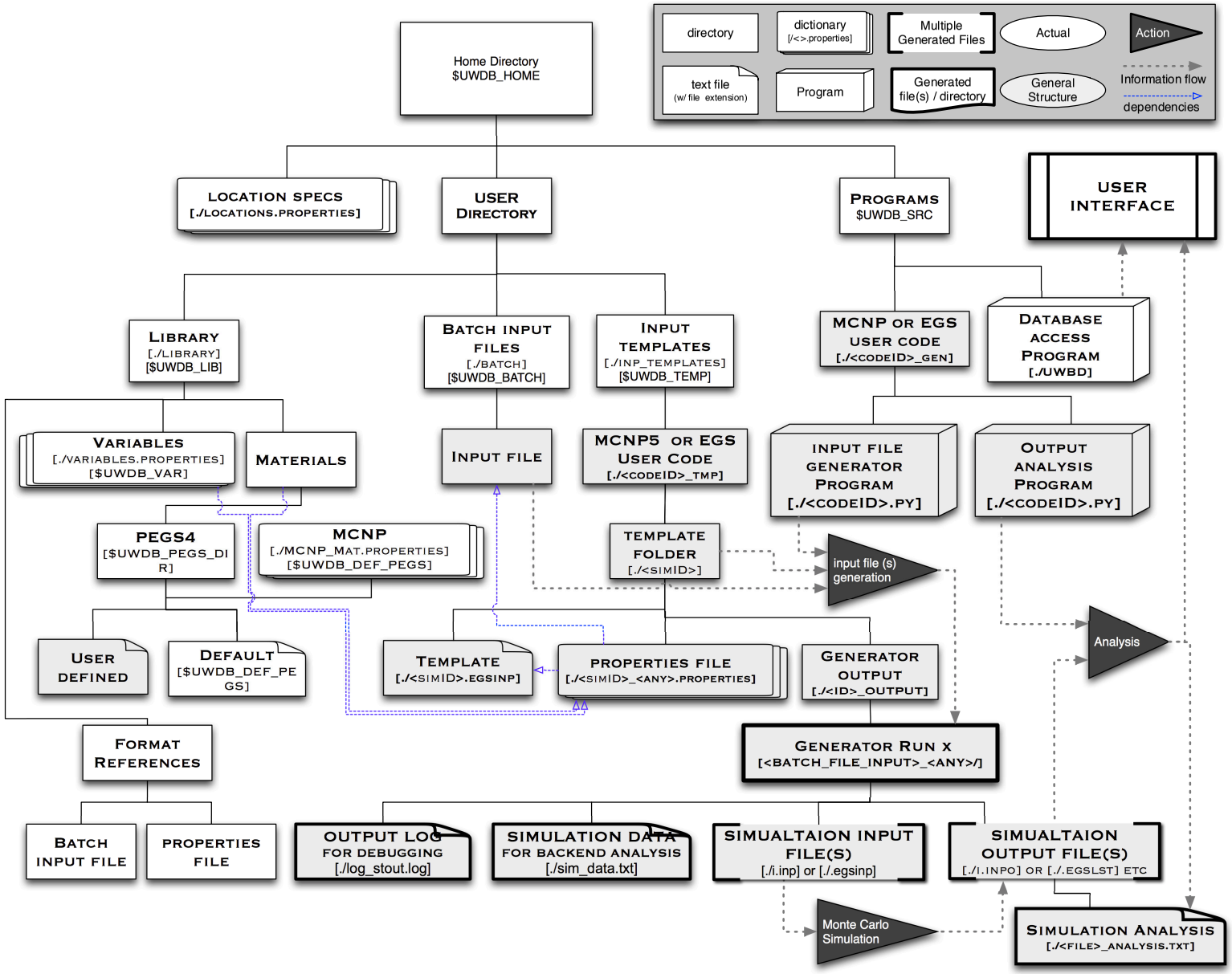

Figure 5.13: Framework structure

can be used as a basis for future research for the dosimetry of fields lacking CPE as well as all Monte Carlo research at the UWMRRC.

Chapter 6

Conclusions and Future Work

Advancements in radiation therapy treatment techniques have led to the utilization of small and nonstandard fields to achieve precise dose-conformality and has enabled the possibility for margin reduction. Biological optimization through hypo-fractionated treatment schedules has increased the dose per fraction for SRS and SBRT treatments. The use of decreased margins and escalated dose per fraction increases the magnitude of negative repercussions due to miscalibration and necessitates strict QA protocols and improved dosimetry for the small and nonstandard fields used in these advanced treatment modalities. Current absorbed dose to water extrapolation methods from standard CoPs broad beam reference conditions to clinical small fields involve output factor measurements using ionization chambers, diodes, or radiochromic film. Often, minimally corrected detector output factors determined by film, diodes, or a small volume ionization chambers are considered equivalent to $s_{c,p}$. Using these detectors' output factors in small and nonstandard fields with a currently available standard CoP provided beam quality correction factor could result in incorrect estimations of $s_{c,p}$ and dose due to the spectral variations. This error is then amplified due to detector beam quality dependencies associated with measurements in the field-edge regions and conditions where the broadened penumbra occupies a significant portions of the total field size.

The IAEA and AAPM have proposed a new protocol for the dosimetry of small and nonstandard fields that addresses these issues and creates a standardized formalism. The international proposed formalism aims to create new and expanded beam quality specification definitions for small and nonstandard fields, with related detector specific correction and perturbation factors, which provide ionization chamber based reference calibrations at the same level of accuracy as present standard CoP of approximately ±2%. The proposed formalism suggests new beam quality correction factors for the new and expanded beam quality specification definitions be determined with Monte Carlo simulations or a dosimeter traceable to a primary standard of absorbed dose to water. The proposed formalism introduces two calibration methods for performing reference dosimetry of small and nonstandard fields. The first method involves small, static-field reference geometries, while the second involves composite-field reference geometries.

This dissertation designed and demonstrated a viable methodology for transferring ionization chamber calibration coefficients from a primary or secondary standard laboratory to hypothetical clinical small and nonstandard reference fields in accordance with emerging dosimetry formalisms. It was accomplished through the characterization of two solid state dosimetry systems for the transfer of absorbed dose to water standards to the end user beam, and used a detailed calibration coefficient transfer pathway designed to maintain metrological traceability. The two solid state dosimetry systems included a TLD system characterized as part of this dissertation and an alanine system provided by NPL.

The TLD-100 dosimetry system was fully characterized for high energy photon and electron beam absorbed dose to water determination referenced to a NIST-traceable energy correction factor standard. The main portion of the characterization determined the energy correction factor for TLD-100 (LiF:Mg,Ti) chips. The exper-

imentally determined energy correction factors relative to ^{60}Co were found to be 0.973, 0.960, 0.959, and 0.955 for 6, 10, 15, and 23 MV photon beams, respectively. The energy correction factors for electron beams was found to be 0.94, 0.95, 0.97, 0.95, and 0.95 for 6, 9, 12, 15, and 18 MeV energies, respectively. Monte Carlo simulations showed similar energy correction values to those found experimentally for electron beam qualities. Monte Carlo simulations showed no energy correction values for the different photon beam qualities, while the experimentally determined energy correction values showed the energy correction factor trending toward the value of one with decreasing photon energy displaying a difference in response due to an increase in the photoelectric effect at lower energies. In addition to the measurements of absorbed dose to water in small and nonstandard fields, the TLD system can also be used as a secondary calibration method for high energy electron beams to verify standard TG-51 calibration methods.

Beam quality correction factors for three ionization chambers were experimentally derived and provide a comparison of the proposed formalism's calibration conditions with the secondary University of Wisconsin Accredited Dosimetry Calibration Laboratory's (UWADCL) ^{60}Co standard reference conditions in which the ionization chamber calibration coefficient was obtained. TLD-determined beam quality correction factors for the calibration conditions investigated (Figure 4.4) ranged from 0.97 to 1.30 and had associated standard deviations from 1% to 3% (Table 4.2). The alanine-determined beam quality correction factors ranged from 0.996 to 1.293 (Table 4.3). The composite field f_{pcsr} demonstrated its potential to reduce or remove ionization chamber volume dependancies, but, as expected, the related measured beam quality correction factor were not equal to the standard CoP's k_Q indicating a change in beam quality in the f_{pcsr} relative to the standard CoP broad beam conditions. The TLD- and alanine-determined beam quality correction factors

in the f_{pcsr} were approximately 1.03 for all three chambers and (Table 4.3 and 4.3, step 6) differed by more than one standard deviation from the published TG-51 k_Q values. The differences are due to variations in the beam quality, and the 3% beam quality correction factor for the f_{pcsr} may be the result of modulating the field which increased the forward scatter contribution leading to a slightly lower effective energy.

This work provides an increased understanding of how the calibration coefficient from an ADCL can be applied to the proposed small and nonstandard field formalism using beam quality correction factors. The f_{pcsr} has the potential to reduce or remove ionization chamber volume dependancies, but beam quality dependencies are present and must be corrected using a beam quality correction factor. In order to perform calibrations at the 2% uncertainty level, new beam quality correction factors will need to be provided for the f_{msr} and f_{pcsr} calibration conditions as their beam qualities differ from the the standard CoP beam quality correction factors. With new beam quality correction factors, it is feasible that the proposed formalism could reduce the tolerance criterion of IMRT calibrations to that of the standard CoP larger reference field tolerances of less than 2%. The f_{pcsr} needs to be evaluated further and the effects of modulation need further characterization. The methodology developed for this work can help to guide future research of other small field radiotherapy modalities and measurements of even smaller field sizes.

Monte Carlo models and a database were developed for small and nonstandard beam quality correction factor determination. Monte Carlo models for a linac and a ^{60}Co teletherapy unit were created using BEAMnrc. Four ionization chambers were modeled in the advanced EGSnrc user code egs_chamber. This Monte Carlo work can be used as a basis for future research for the dosimetry of fields lacking CPE as well as all Monte Carlo research at the UWMRRC. In addition, the measurements performed in this work can be used for experimental verification for future Monte

Carlo models used to simulate small and non standard field beam quality correction factors.

The f_{pcsr} needs to be more refined and future work could involve Monte Carlo investigation with verified models of the behavior of possible f_{pcsr} and their beam quality correction factors. To determine the beam quality correction factor, four Monte Carlo simulations must be performed: two simulations to calculate dose to water for the ^{60}Co and $Q_{\text{small field}}$ beam qualities, and two simulations to calculate dose to the air occupied by the ionization chamber for the ^{60}Co and $Q_{\text{small field}}$ beam qualities. Calculating dose to air requires a detailed model of the ionization chamber, which this work provides, and accurate simulation of secondary charged particles created in the wall. Phase space files created by the linac and ^{60}Co models in BEAMnrc could be used as the source spectra incident on the ionization chambers. The Monte Carlo models will need to be benchmarked against NIST-traceable standards through iterative modifications to the chambers and source models' until simulation of the NIST-traceable measurements matched the measured values within its uncertainty for each f_{pcsr}. This work provides a methodology for experimental verification and models for many small and nonstandard field Monte Carlo simulations.

The reference conditions in which the calibration coefficient was obtained were analyzed through detailed transfer pathways. It was discussed that standards laboratories could provide a direct calibration coefficient $N_{D,w}^{Q_{\text{msr}}}$ for an ionization chamber in the f_{msr} or $N_{D,w}^{Q_{\text{PCSR}}}$ for the f_{PCSR}. The calibrations coefficients would ideally be directly traceable to calorimetry determined dose to water in the f_{msr} or f_{PCSR}, and beam quality correction factors would not be required for calibration. As discussed in Section 2.6.1, this is not a feasible solution due to the limited availability of water calorimeters. An intermediate step would be to perform calibrations on a NIST-traceable ^{60}Co unit in phantom instead of in water. As a result, a clinic would

obtain a new calibration coefficient $N_{D,w}^{Q_0,\text{in phantom}}$ from an in-phantom calibration in ^{60}Co, in addition to their standard $N_{D,w}^{^{60}Co}$ calibration coefficient to be used with standard CoPs broad beam reference conditions. In-phantom calibration coefficients would remove any material correction component in the beam quality correction factor. This work demonstrated that obtaining the calibration coefficient in reference conditions closer to the small field formalism's reference conditions did not produce any substantial reduction (<1%) in uncertainty. This solution also has the potential to increase the work load at the clinics as well as the standards and secondary standards laboratories. As a result, this work recommends that the standard ^{60}Co reference conditions for determination of the calibration coefficient is still applicable with the addition of the appropriate beam quality correction factor for the users f_{msr} and f_{pcsr} calibration conditions.

Future work could include a study to see if there is any benefit in the related reproducibility uncertainty of calibrating in phantom compared to the standard in-water calibration protocol by simulating the different tolerances for variables of the phantom and set-up and whether the phantom used in the proposed formalism should be water filled or a solid plastic. Phantoms consisting of water or different solid materials could be simulated using Monte Carlo and experimentally verified by comparison to the PMMA phantom used in this work. The variables simulated could include perturbation of the beam and the inhomogeneity known to be associated with different materials and its effect on the calculation of the beam quality correction factors. In addition, the outer dimensions could be tested using Monte Carlo to determine how stringent the manufacturing process must be to obtain an acceptable uncertainty.

There is still more work that must be performed in order for the IAEA and AAPM's proposed new protocol for the dosimetry of small and nonstandard fields

to be implemented. This work has shown that it is possible to provide ionization chamber based transfer calibrations at the same level of accuracy as present standard CoP of approximately $\pm 2\%$ using the standard ^{60}Co calibration coefficient and new beam quality correction factor in the proposed formalism f_{msr} and f_{pcsr} calibration conditions.

References

[1] AAPM American Association of Physicists in Medicine, Task Group 21. A protocol for the determination of absorbed dose from high energy photon and electron beams. *Medical Physics*, 10:741–771, 1983.

[2] R. Alfonso, P. Andreo, R. Capote, M. Saiful Huq, W. Kilby, P. Kjall, T. R. Mackie, H. Palmans, K. Rosser, J. Seuntjens, W. Ullrich, and S. Vatnitsky. Medical physics letter: A new formalism for reference dosimetry of small and nonstandard fields. *Medical Physics*, 35:5179–5186, 2008.

[3] Peter R. Almond, Peter J. Biggs, B. M. Coursey, W. F. Hanson, M. Saiful Huq, Ravinder Nath, and D. W. O. Rogers. AAPM's TG-51 protocol for clinical reference dosimetry of high energy photon and electron beams. *Medical Physics*, 26(9):1847–1870, September 1999.

[4] P. Andreo. Improved calculations of stopping-power ratios and their correlation with the quality of therapeutic photon beams. In *Measurement Assurance in Dosimetry Vienna IAEA*, page 335, 1994.

[5] P. Andreo. On the beam quality specification of high-energy photons for radiotherapy dosimetry. *Medical Physics*, 27(3):434–440, 2000.

[6] P. Andreo, D.T. Burns, K. Hohlfeld, M. S. Huq, T. Kanai, F. Laitano, V. G. Smyth, and S. Vynckier. Absorbed dose determination in external beam radiotherapy: An international code of practice for dosimetry based on

standards of absorbed dose to water. Technical Report Series, No. 398 in Press, IAEA, Vienna, 2000.

[7] P. Andreo, M. Saiful Huq, M. Westermark, H. Song, A. Tilikidis, and K. Shortt. Protocols for the dosimetry of high-energy photon and electron beams: a comparison of the IAEA TRS-398 and previous international codes of practice. *Physics in Medicine and Biology*, 47:3033–3053, 2002.

[8] M. Anton, R. P. Kapsch, M. Krystek, and F. Renner. Response of the alanine/ESR dosimetry system to MV x-rays relative to ^{60}Co radiation. *Physics in Medicine and Biology*, 53:2753–2770, 2008.

[9] Frank H. Attix. *Introduction to Radiological Physics and Radiation Dosimetry*. John Wiley and Sons, Inc., New York, 1986.

[10] M. Barberio, P. Barone, V. Pingitore, and A. Bonanno. UV luminescence from LiF/carbon nanotube microcomposites. *Superlattices and Microstructures*, 52(6):1053 – 1061, 2012.

[11] L. Bartol. *Energy Fluence Dosiemtry of High-Energy Photon Beams*. PhD thesis, University of Wisconsin - Madison, 2010.

[12] ES Bergstrand, KR Shortt, CK Ross, and EO Hole. An investigation of the photon energy dependence of the EPR alanine dosimetry system. *Physics in Medicine and Biology*, 48:1753–1771, 2003.

[13] SA Bhide and CM Nutting. Recent advancements in radiotherapy. *BMC Medicine*, 8:25, 2010.

[14] Walt Bogdanich. As technology surges, radiation safeguards lag. *The New York Times*, page A1, 2010.

[15] Walt Bogdanich. Radiation offers new cures, and ways to do harm. *The New York Times*, page A1, 2010.

[16] Hugo Boucharda, Jan Seuntjens, Jean-Francois Carrier, and Iwan Kawrakow. Ionization chamber gradient effects in nonstandard beam configurations. *Medical Physics*, 36:4654, 2009.

[17] Roberto Capote, Francisco Sanchez-Doblado, Antonio Leal, Juan Ignacio Lagares, Rafael Arrans, and Gunther H. Hartmann. An EGSnrc Monte Carlo study of the microionization chamber for reference dosimetry of narrow irregular IMRT beamlets. *Medical Physics*, 31:2416, 2004.

[18] F. Chen, C.F.O. Graeff, and O. Baffa. Response of L-alanine and 2-methylalanine minidosimeters for K-band (24 ghz) EPR dosimetry. *Nuc Instru Methods*, 264:277–281, 2007.

[19] O. Chibani and C.M. Ma. Photonuclear dose calculations for high-energy photon beams from Siemens and Varian linacs. *Medical Physics*, 30:1990–2000, 2003.

[20] K.S. Chung, J.I. Lee, and J.L. Kim. A computer program for the deconvolution of the thermoluminescence glow curves by employing the interactive trap model. *Radiation Measurements*, 47(9):766–769, 2012. Proceedings of the 13th International Conference on Luminescence and Electron Spin Resonance Dating, on 14 July, 2011.

[21] Philip P. Connell and Samuel Hellman. Advances in radiotherapy and implications for the next century: A historical perspective. *Cancer Res*, 69:383–392, 2009.

[22] Morgan Cox. The Harshaw chemical company: As seen via one great series of stories. *Radiation Protection Management*, 21:9–17, 2004.

[23] Indra J. Das, George X. Ding, and Anders Ahnesjo. Small fields: Nonequilibrium radiation dosimetry. *Medical Physics*, 35:206, 2008.

[24] Indra J. Das, M.Beverly Downes, Alireza Kassaee, and Z. Tochner. Choice of radiation detector in dosimetry of stereotactic radiosurgery-radiotherapy. *Journal of Radiosurgery*, 3:177–186, 2000.

[25] S. D. Davis, C. K. Ross, P. N. Mobit, L. Van der Zwan, W. J. Chase, and K. R. Shortt. The response of LiF thermoluminescence dosemeters to photon beams in the energy range from 30 kV x rays to ^{60}Co gamma rays. *Radiat. Prot. Dosim.*, 106:33–43, 2003.

[26] Marc Derosier and David Schauer. Electron paramagnetic resonance (epr) biodosimetry. *Nuclear Instruments And Methods*, 184:219–228, 2001.

[27] Desrosiers, M.F. Desrosiers, S.L. Cooper, J.M. Puhl, A.L. McBain, and G.W. Calvert. A study of the alanine dosimeter irradiation temperature coefficient in the -77 to +50 °c range. *Radiat. Phys. Chem.*, 71:363–368, 2004.

[28] M. F. Desrosiers, J. M. Puhl, , and S. L. Cooper. An absorbed-dose/dose-rate dependence for the alanine-EPR dosimetry system and its implications in high-dose ionizing radiation metrology. *Journal of Research of the National Institute of Standards and Technology*, 2:113, 2008.

[29] S. Duane, D. Nicholas, H. Palmans, B. Schaeken, J. Sephton, P. Sharpe, R. Thomas, M. Tomsej, D. Verellen, and S. Vynckie. Dosimetry audit for tomotherapy using alanine/EPR. *Medical Physics*, 33:2093, 2006.

[30] Simon Duane. Application(s) of alanine. In *Radiotherapy Standards User Group,*, 2007.

[31] A. DuSautoy. UK photon-beam primary standard graphite calorimeter. Technical report, NPL Calorimetry Workshop, Teddington, Middlesex, United Kingdom, October 1994.

[32] A R DuSautoy. The uk primary standard calorimeter for photon-beam absorbed dose measurement. *Physics in Medicine and Biology*, 41:137–151, 1996.

[33] Paolo Francescon, Stefania Cora, and Carlo Cavedon. Total scatter factors of small beams: A multidetector and Monte Carlo study. *Medical Physics*, 35:504, 2008.

[34] Feliciano Garcia-Vicentea, Maria Jose Bejarb, Leopoldo Pereza, and Juan J. Torresa. Clinical impact of the detector size effect in 3D-CRT. *Radiotherapy and Oncology*, 74:315–322, 2005.

[35] V Grégoire and TR Mackie. State of the art on dose prescription, reporting and recording in intensity-modulated radiation therapy (icru report no. 83). *Cancer/Radiothérapie*, 15(6):555–559, 2011.

[36] J.W. Hansen and K.J. Olsen. Predicting decay in free-radical concentration in L-*a*-alanine following high-let radiation exposures. *International Journal of Radiation Applications and Instrumantation*, 40:935–939, 1989.

[37] Robert B. Hayes, Edwin H. Haskell, Albrecht Wieser, Alexander A. Romanyukha, Byron L. Hardy, and Jeffrey K. Barrus. Assessment of an alanine EPR dosimetry technique with enhanced precision and accuracy. *Nuclear Instruments and Methods in Physics Research Section A: Accelerators, Spectrometers, Detectors and Associated Equipment*, 440(2):453 – 461, 2000.

[38] Y S Horowitz. Theory of thermoluminesence gamma dose response: The unified interaction model. *Nuc Instru Methods*, 184:68–84, 2001.

[39] Y.S. Horowitz. The theoretical and microdosimetric basis of thermoluminescence and applications to dosimetry. *Physicists in Medicine and Biology*, 26(4):765–824, 1981.

[40] YS Horowitz and M Moscovitch. Highlights and pitfalls of 20 years of application of computerised glow curve analysis to thermoluminescence research and dosimetry. *Radiation Protection Dosimetry*, pages 1–22, 2012.

[41] Y.S. Horowitz, L. Oster, H. Datz, and M. Margaliot. Some dosimetric characteristics of the high temperature TL in LiF:Mg,Ti (TLD-100). *Radiation Measurements*, 43(26):203–207, 2008. Proceedings of the 15th Solid State Dosimetry (SSD15).

[42] A. Horsfield, J.R. Morton, and D.H. Whiffen. The electron spin resonance spectrum of $CH_3CHCOOH$ at 77^oK in l-*a*-alanine. *Molecular Physics*, 4:425–431, 1961.

[43] JCPM. International vocabulary of metrology - basic and general concepts and associated terms, 2012.

[44] S. Junell and L. DeWerd. Determination of the energy correction factor for TLD-100 in 6 and 10 MV photon beams relative to ^{60}Co. *(abstract) Medical Physics*, 35:2780–2781, 2008.

[45] Mikio Katayama. Electron spin resonance of gamma-irradiated single crystals of acetyl-d,l-alanine and chloroacetyl-d,l-alanine. *Journal of Molecular Spectroscopy*, 9(0):429 – 435, 1962.

[46] I. Kawrakow. Accurate condensed history Monte Carlo simulation of electron transport. i. EGSnrc, the new EGS4 version. *Medical Physics*, 27:485, 2000.

[47] I. Kawrakow. Electron impact ionization cross sections for EGSnrc. *(abstract) Medical Physics*, 29:1230, 2002.

[48] Iwan Kawrakow. On the effective point of measurement in megavoltage photon beams. *Medical Physics*, 33(6):1829, 2006.

[49] Kirby. Mailable TLD system for photon and electron therapy beams. *Int. J. Radiation Oncology Biol. Phy.*, 12:261–265, 1985.

[50] Glenn F. Knoll. *Radiation Detection and Measurement*. John Wiley and Sons, New York, second edition, 1989.

[51] A R Lakshmanan, B Chandra, and R C Bhatt. On the role of z centres and competing nonluminescent centres in the sensitisation and supralinearity mechanism of LiF TLD-100 phosphor. *Journal of Physics D: Applied Physics*, 15(8):1501, 1982.

[52] S. Lelie, P. Meijnders, D. Van den Weyngaert, H. Janssens, D. Verellen, and B. Schaekena. Alanine/EPR dosimetry applied to the verification of a total body irradiation protocol and treatment planning dose calculation using a humanoid phantom. *Medical Physics*, 37:6292–6299, 2012.

[53] Qing Liang, Stephen D. Davis, Yigal S. Horowitz, and Larry A. DeWerd. Investigation of the relative TL response for low-energy x-rays relative to ^{60}Co for TLD-100. *Radiation Measurements*, 46(12):1453 – 1456, 2011. Proceedings of the 16th Solid State Dosimetry Conference, September 19-24, Sydney, Australia.

[54] Daniel A. Low, Jean M. Moran, James F. Dempsey, Lei Dong, and Mark Oldham. Dosimetry tools and techniques for IMRT. *Medical Physics*, 38:1313, 2011.

[55] Thomas Rockwell Mackie. Chapter 19: Dosimetry for IMRT. AAPM Summer School, 2009.

[56] S Mahajna and Y S Horowitz. The unified interaction model applied to the gamma ray induced supralinearity and sensitization of peak 5 in LiF:Mg,Ti (TLD-100). *Journal of Physics: Applied Physics*, 30(18):2603, 1997.

[57] A.C. McEwan. Corrections for scattered photons in free-air ionisation chambers. *Physics in Medicine and Biology*, 27(3):375–386, July 1982.

[58] Malcolm McEwen. Updating reference dosimetry a decade after TG-51. In *CE Presentation at AAPM Annual Meeting*. AAPM, July 2010.

[59] Malcolm R. McEwen. Measurement of ionization chamber absorbed dose K_Q factors in megavoltage photon beams. *Medical Physics*, 37:2179, 2010.

[60] P. H. McGinley and J. C. Landry. Neutron contamination of x-ray beams produced by the varian clinac 1800. *Physics in Medicine and Biology*, 34:777–783, 1989.

[61] R Minniti, J Shobe, SM Seltzer, H Chen-Mayer, and SR Domen. Absorbed dose to water calibration of ionization chambers in a ^{60}Co gamma-ray beam. Technical report, NIST, 2005.

[62] P. N. Mobit, P. Mayles, and A. E. Nahum. The quality dependence of LiF TLD in megavoltage photon beams: Monte Carlo simulation and experiments. *Physics in Medicine and Biology*, 41:387–398, 1996.

[63] Paul N Mobit, Alan E Nahum, and Philip Mayles. A Monte Carlo study of the quality dependence factors of common TLD materials in photon and electron beams. *Physics in Medicine and Biology*, 43(8):2015, 1998.

[64] M. Moscovitch and Y.S. Horowitz. Thermoluminescent materials for medical applications: LiF:Mg,Ti and LiF:Mg,Cu,P. *Radiation Measurements*, 41, Supplement 1(0):S71 – S77, 2006. The 2nd Summer School on Solid State Dosimetry: Concepts and Trends in Medical Dosimetry.

[65] B. R. Muir and D. W. O. Rogers. The central electrode correction factor for high-z electrodes in small ionization chambers. *Medical Physics*, 38(2):1081–1088, 2011.

[66] Vitaly Nagy. Accuracy considerations in EPR dosimetry. *Applied Radiation and Isotopes*, 52(5):1039 – 1050, 2000.

[67] Vitaly Nagy, James M Puhl, and Marc F Desrosiers. Advancements in accuracy of the alanine dosimetry system. Part 2. the influence of the irradiation temperature. *Radiation Physics and Chemistry*, 57(1):1–9, 2000.

[68] Vitaly Yu Nagy and Marc F Desrosiers. Complex time dependence of the EPR signal of irradiated l-*a*-alanine. *Applied Radiation and Isotopes*, 47(8):789–793, 1996.

[69] NPL website. http://www.npl.co.uk/ionising-radiation/dosimetry/products-and-services/alanine-reference-dosimetry-services-for-radiotherapy, 2009.

[70] A. A. Nunn, S. D. Davis, J. A. Micka, and L. A. DeWerd. LiF:Mg,Ti TLD response as a function of photon energy for moderately filtered x-ray spectra in the range of 20-250 kVp relative to ^{60}Co. *Medical Physics*, 35:1859–1869, 2008.

[71] Sara Olsson and Eva S. Bergstrand. Calibration of alanine dosimeters. Technical report, ISRN, 2001.

[72] B. Rasmussen, S. Davis, J. Micka, and L. A. Dewerd. Determination of the LiF:Mg,Ti TLD energy response correction factor for ^{125}I brachytherapy sources. *Medical Physics*, 34:2612, 2007.

[73] B Paul Ravindran, Lee Fairclough, and Satish M Jaywant. Phantom dosimetry for conformal stereotactic radiotherapy with a head and neck localizer frame. *Physics in Medicine and Biology*, 46(7):1975, 2001.

[74] D. Regulla. From dating to biophysics: 20 years of progress in applied ESR spectroscopy. *Appl. Radiat. Isot.*, 52:1023–1030, 2000.

[75] D.F. Regulla and U. Deffner. Dosimetry by ESR spectroscopy of alanine. *Int. J. Radiat. Isot.*, 33:1101, 1982.

[76] D. Rogers and J. Cygler. Clinical dosimetry measurements in radiotherapy. In *Proceedings of the American Association of Physicists in Medicine Summer School*, 2009.

[77] D. W. O. Rogers. Fundamentals of high energy x-ray and electron dosimetry protocols. In J. Purdy, editor, *Advances in Radiation Oncology Physics, Medical Physics Monograph 19*, pages 181–223. AAPM, New York, 1992.

[78] Sheldon M. Ross. *A First Course in Probability*. Prentice Hall, Upper Saddle River, New Jersy 07458, fifth edition, 1998.

[79] Dirk De Ruysscher, M. Mark Lodge, Bleddyn Jones, Michael Brada, Alastair Munro, Thomas Jefferson, and Madelon Pijls-Johannesma. Charged particles in radiotherapy: A 5-year update of a systematic review. *Radiotherapy and Oncology*, 103(1):5 – 7, 2012.

[80] Einar Sagstuen, Eli O. Hole, Solvi R. Haugedal, and William H. Nelson. Alanine radicals: Structure determination by EPR and ENDOR of single crystals x-irradiated at 295°K. *The Journal of Physical Chemistry*, 101(50):9763–9772, 1997.

[81] F. Sanchez-Doblado, P. Andreo, R. Capote, A. Leal, M. Perucha, R. Arrans, L. Nunez, E. Mainegra, J. I. Lagares, and E. Carrasco. Ionization chamber dosimetry of small photon fields a Monte Carlo study on stopping-power ratios for radiosurgery and IMRT beams. *Physics in Medicine and Biology*, 48:2081, 2003.

[82] F Sanchez-Doblado, GH Hartmann, J Pena, JV Rosello, G Russiello, and DM Gonzalez-Castano. A new method for output factor determination in MLC shaped narrow beams. *Physica Medica*, 23:58–66, 2007.

[83] David A. Schauera, Akinori Iwasakib, Alexander A. Romanyukhaa, Harold M. Swartzb, and Sandro Onoric. Electron paramagnetic resonance (EPR) in medical dosimetry. *Radiation Measurements*, 41:S117–S123, 2007.

[84] Edmund Schule. Messtechnische kontrollen fur therapiedosimeter and von vergleichsmessungen mit TLDs. Guest seminar - Dept. of Radiological Physics Hospial of the Canton Basel (Switzerland) PTW-Freiburg, April 2002.

[85] P. H. G. Sharpe, K. Rajendran, and J. P. Sephton. Progress towards an alanine/ESR therapy level reference dosimetry service at NPL. *Appl Rad Isot*, 47:1171–1175, 1996.

[86] Peter Sharpe and John Sephton. An automated system for the measurement of alanine/EPR dosimeters. *Appl Rad Isot*, 52:1185–1188, 2000.

[87] Peter HG Sharpe and David T Burns. The relative response of Fricke, dichromate and alanine dosimeters to ^{60}Co and high energy electron beam radiations. *Radiation Physics and Chemistry*, 46(46, Part 2):1273–1277, 1995.

[88] P.H.G. Sharpe, A.Miller, J.P.Sephton, C.A.Gouldstone, M.Bailey, and J.Helt-Hansen. The effect of irradiation temperatures between ambient and 80°c on the response of alanine dosimeters. *Radiation Physics and Chemistry*, 78:473 – 475, 2009.

[89] P.H.G. Sharpe, J.P. Sephton, and C.A. Gouldstone. The behaviour of alanine dosimeters at temperatures between 100 and 300^{o}k. *Radiation Physics and Chemistry*, 78:477 – 479, 2009. 15th International Meeting on Radiation Processing.

[90] D. Sheikh-Bagheri and D. Rogers. Monte Carlo calculation of nine megavoltage photon beam spectra using BEAM code. *Medical Physics*, 29:391–402, 2002.

[91] Ken Shortt, Carl Ross, Jan Seuntjens, Frank Delaunay, Aimé Ostrowsky, Philippe Gross, and Eric Leroy. Comparison of dosimetric standards of Canada and France for photons at ^{60}Co and higher energies. *Physics in Medicine and Biology*, 46(8):2119, 2001.

[92] J. B. Smilowitz, R. Jeraj, G. H. Olivera, L. A. DeWerd, and T. R. Mackie. Monte Carlo model of an accredited dosimetry calibration laboratory Cobalt-60 unit. In *Proceedings of Recent developments in accurate radiation dosimetry: International Workshop*, page in press. Medical Physics Publishing, 2001.

[93] RC Tailor, JF Aguirre, and WF Hanson. RPC experience with TLD for output and energy monitoring of radiaiton therapy beams. Technical report, RPC, 1999.

[94] M. Taylor, T. Kron, and R. Franich. A contemporary review of stereotactic radiotherapy: Inherent dosimetric complexities and the potential for detriment. *Acta Oncologica*, 50:483, 2011.

[95] F. Verhaegen. Evaluation of the EGSnrc Monte Carlo code for interface dosimetry near high-z media exposed to kiloVolt and Co-60 photons. *Phys Med Biol*, 47:1691–1705, 2002.

[96] Frank Verhaegen and Jan Seuntjens. Monte Carlo modelling of external radiotherapy photon beams. *Physics in Medicine and Biology*, 48:R107–R164, 2003.

[97] Einar Waldeland and Eirik Malinen. Review of the dose-to-water energy dependence of alanine and lithium formate EPR dosimeters and lif tl-dosimeters. *Radiation Measurements*, 46:945–951, 2011. EPRBioDose 2010 International Conference.

[98] C.J. Wong, T. Ackerly, C. He, W. Patterson, C.E. Powell, G. Qiao, D.H. Solomon, and M. Geso R. Meder. Small field size dose-profile measurements using gel dosimeters, gafchromic films and micro-thermoluminescent dosimeters. *Radiation Measurements*, 44:249–256, 2009.

[99] J. Wulff, J. T. Heverhagen, and K. Zink. Monte-Carlo-based perturbation and beam quality correction factors for thimble ionization chambers in high-energy photon beams. *Phys Med Biol*, 53:2823–2836, 2008.

[100] J. Wulff, K. Zink, and I. Karwrakow. Efficiency improvements for ion chamber calculations in high energy photon beams. *Medical Physics*, 35(4):1328, 2008.

[101] P. Zaránd. Effect of thermal and dosimetric history on the accuracy of LiF:Mg,Ti and CaSO4:Dy. *Radiation Protection Dosimetry*, 66(1-4):279–282, 1996.

[102] G G Zeng, M R McEwen, D W O Rogers, and N V Klassen. An experimental and Monte Carlo investigation of the energy dependence of alanine/EPR dosimetry: I. clinical x-ray beams. *Physics in Medicine and Biology*, 49(2):257, 2004.

[103] T. C. Zhu and B. E. Bjarngard. The head-scatter factor for small field sizes. *Medical Physics*, 21:65–68, 1994.